

Heavy Ion Collisions: Achievements and Challenges

Edward Shuryak

*Department of Physics and Astronomy, Stony Brook University,
Stony Brook, New York 11794-3800, USA*

(Dated: October 29, 2015)

A decade ago brief summary of the field could be formulated as a discovery of strongly-coupled Quark-Gluon-Plasma, sQGP, making a very good liquid with surprisingly small viscosity. Since 2010 we have LHC program, which added a lot to our understanding, and now there seems to be a need to consolidate what we learned and formulate a list of issues to be studied next. Hydrodynamical perturbations, leading to higher harmonics of angular correlations, are identified as long-lived sound waves. Recently studied reactions involving sounds include phonon decays into two (“loop viscosity”), phonon+magnetic field into photons/dileptons (sono-magneto-luminescence), and two phonons into a gravity wave, a penetrating probe of the Big Bang. The mainstream issues in the field now include a quest to study transition between pp, pA and heavy ion AA collisions, with an aim to locate “the smallest drops” of the sQGP displaying collective/hydrodynamics behavior. The issues related to out-of-equilibrium stage of the collisions, and mechanisms of the equilibration, in weak and strong coupling, are also hotly debated.

I. A WIDER PICTURE

Before we immerse ourselves in recent discoveries and puzzles of heavy ion physics itself, one perhaps should look in a wider field of “strong interaction physics”. Its definitions have many different meanings, ranging from a narrow one, (i) hadronic and nuclear physics phenomena based on its fundamental theory, QCD; to much wider one (ii) aiming at understanding of all gauge theories, including QCD-like and supersymmetric ones, and even including dualities of those to string/gravity theories. We will keep mostly to the former end, with only some sections venturing to the latter definition.

QCD-like theories at finite temperature and density has a number of regimes and phases. Due to asymptotic freedom, the simplest of them to understand is the high T (or μ or both) limit, known as *weakly coupled* Quark-Gluon Plasma (wQGP). Well developed tools of the manybody theory – perturbative diagrams and their re-summations – were used to show its main features, the electric screening and formation of finite-mass quasiparticles. This is where the name “plasma” came from [1]. For early reviews on high-T QCD see [2, 3].

Prior to RHIC era, it was generally assumed that wQGP regime extends down to the phase transition region, $T > T_c$. Lattice-based thermodynamic quantities showed relatively small (20% or less) deviation from those for non-interacting quarks and gluons. Many if not most theorist were skeptical, thinking that RHIC program aimed at “production of new form of matter” would basically fail. Perturbative equilibration estimates indicated unrealistically long time. Models predicted “firework of minijets” rather than collective effects.

Yet strong hydrodynamical flows were observed at RHIC from the first months, supplemented by strong jet quenching. All of that was later confirmed at the LHC, which provided even much more accurate data on many details. For example, as we will discuss below, there are

unmistakable signs that the excitation modes of the matter produces is basically the sound modes. The systematics of those lead to viscosity value which is remarkably small, more than an order of magnitude smaller than that predicted originally by the perturbative theory. So, the window in which matter produced at RHIC/LHC is, $T_c < T < 2T_c$, was renamed into a “*strongly coupled QGP*”, sQGP for short.

So, which physical phenomena take place there and why? What exactly happens as T decreases from the wQCD to sQGP domain? The growing coupling induces two different kinds of phenomena.

(i) One preserves the basic picture of quark and gluon quasiparticles and plasma-related phenomena, with gradual change of parameters consistent with smooth *logarithmic* running $g^2 \sim 1/\log(T/\Lambda)$. While in the wQCD domain the electric screening (Debye) mass are small compared to their energy, $M_E/T = O(g) \ll 1$, in sQGP domain one learned from lattice simulations that those are not small, $M_E/T = 2 - 3 > 1$. So, while expansions in such ratio used in the wQGP in this domain are invalid, perhaps an extrapolation using the running coupling may still hold, at least qualitatively. Similar arguments were put forward for the quasiparticle masses, thermodynamical and kinetic quantities as well, with variable rate of success depending on the quantity under consideration.

(ii) Moreover, there are other type of phenomena, which depend on the coupling *exponentially*, leading to much stronger *power* dependences on the temperature

$$\exp\left(-\frac{\text{const}}{g^2(T)}\right) \sim \left(\frac{\Lambda}{T}\right)^{\text{power}} \quad (1)$$

Those come from gauge field configurations – semiclassical solitons – which are qualitatively distinct from perturbative quarks and gluons. One such example is the (Euclidean 4-dimensional) topological solitons called *instantons*. Their physics is tunneling through certain barriers into “valleys” of topologically distinct gauge

field configurations. Perturbative theory, an expansion around zero fields, knows little about existence of such valleys. (Except in a very subtle way, via divergences of its series. There is recent progress in this direction, known as a *resurgence theory*, which however still focuses on quantum mechanical and low-dimensional scalar theories rather than gauge theories. See for recent update in the talks at [7].)

Discussion of the instanton theory will take us too far from our main direction, so I only mention its two major breakthroughs. In 1980-1990's it has been shown how instantons *break the chiral symmetries*, the $U_A(1)$ explicitly and $SU(N_f)$ spontaneously, via collectivization of fermionic zero modes, for a review see [5]. Recently it morphed into plasma made of instanton constituents, Lee-Li-Kraan-van Baal (LLKvB) *instanton-dyons*, or instanton-monopoles. It has been shown that those, if dense enough, can naturally enforce *both* confinement and chiral symmetry breaking. For recent discussion see talks at [6].

Another – still very puzzling – set of effects, predicted by the Operator Product Expansion (OPE), are related with “higher twist effects” and VEVs of various operators appearing in the QCD sum rule framework. The so called *renormalons* are supposed to induce effects with various integer powers of the scale, e.g. T . In the gauge theory we still do not know which solitons, if any, are related to them, but in simpler theories there was recent progress: see again [7].

An extremely important notion of the theory is that of *electric-magnetic duality*. Asymptotically free gauge theories, QCD-like or supersymmetric ones, have weak “electric” coupling in the UV, but in the IR they generically flow to strong coupling. “Magnetic” objects, such as color-magnetic monopoles, are expected to become lighter and more numerous along this process. The key observation I tirelessly emphasize is the good old *Dirac condition*. If one wants simultaneously describe objects with electric and magnetic charges (e and g in his old notations/normalization) singularities of the gauge potential of the form of the Dirac strings are unavoidable. The requirement that should be pure gauge artifacts and thus invisible leads to

$$\frac{2eg}{\hbar c} = 1 \quad (2)$$

(or in general an integer in the r.h.s.). Thus e and g must run in unison, in the opposite directions. Thus one expects in the infrared limit of gauge theories to find the so called *dual description* based on magnetic degrees of freedom, which are light and weakly coupled. The question is whether one can construct a Lagrangian of this dual theory, and also if/when one can/needs to use it.

(One great example of the kind is provided by celebrated $\mathcal{N}=2$ supersymmetric Seiberg-Witten theory: near certain special points of the Higgs VEV the monopoles are nearly massless and weakly interacting:

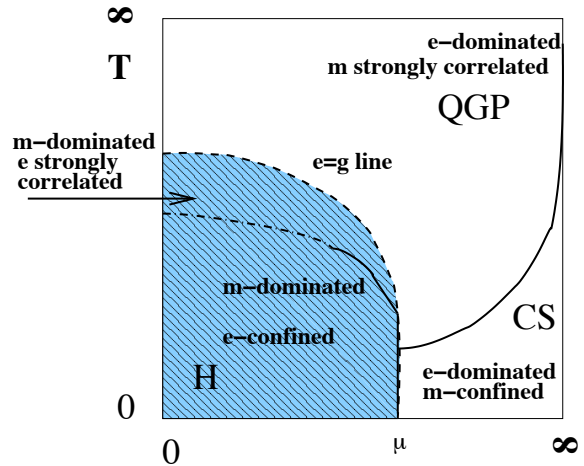


FIG. 1: A schematic phase diagram on a (compactified) plane of temperature and baryonic chemical potential $T - \mu$, from [8]. The (blue) shaded region shows magnetically dominated region $g < e$, which includes the e-confined hadronic phase as well as postconfined part of the QGP domain. Light region includes electrically dominated part of QGP and also color superconductivity (CS) region, which has e-charged diquark condensates and therefore obviously m-confined. The dashed line called $e=g$ line is the line of electric-magnetic equilibrium. The solid lines indicate true phase transitions, while the dash-dotted line is a deconfinement cross-over line.

the magnetic theory is then scalar QED. Its beta function, as expected, has the opposite sign to that of the electric theory. Even greater example is $\mathcal{N}=4$ theory: it is electric-magnetic selfdual, so the beta function is equal to minus itself and thus is identically zero.)

Returning to QCD, one can summarize the picture of the so called “magnetic scenario” by a schematic plot shown in Fig. 1, from [8]. At the top – the high T domain – and at the right – the high density domain – one finds weakly coupled or “electrically dominated” regimes, or wQGP. On the contrary, near the origin of the plot, in vacuum, the electric fields are, subdominant and confined into the flux tubes. The vacuum is filled by the magnetically charged condensate, known as “dual superconductor”. The region in between (relevant for matter produced at RHIC/LHC) is close to the “equilibrium line”, marked by $e = g$ on the plot. (People for whom couplings are too abstract, can for example define it by an equality of the electric and magnetic screening masses.) In this region both electric and magnetic coupling are equal and thus $\alpha_{electric} = \alpha_{magnetic} = 1$: so neither the electric nor magnetic formulations of the theory are simple.

Do we have any evidences for a presence or importance for heavy ion physics of “magnetic” objects? Here are some arguments for that based on lattice studies and phenomenology, more or less in historical order:

(i) In the RHIC/LHC region $T_c < T < 2T_c$ the VEV of the Polyakov line $\langle P \rangle$ is substantially different from 1. Hidaka and Pisarski [9] argued that $\langle P \rangle$ must be incorporated into density of thermal quarks and gluons, and thus suppress their contributions. They called such matter “semi-QGP” emphasizing that say half of their degrees of freedom are actually operational.

And yet, the lattice data insist that the thermal energy density remains close to the T^4 trend nearly all the way to T_c . “Magnetic scenario” [8] may explain this puzzle by introducing extra contributions of the magnetic quasi-particles. (They are not subject to $\langle P \rangle$ suppression because they lack the electric charge.)

(ii) Lattice monopoles so far defined are gauge dependent. And yet, they were found to behave as physical particles. Their motion definitely shows Bose-Einstein condensation at $T < T_c$ [10]. Their spatial correlation functions are very much plasma-like. Even more striking is the observation [11] revealing magnetic coupling which *grows* with T . Moreover, it is indeed an inverse of the asymptotic freedom curve.

(iii) Plasmas with electric and magnetic charges show unusual transport properties [8]: Lorenz force enhances collision rate and reduce viscosity. Quantum gluon-monopole scattering leads to large transport cross section [12], providing small viscosity in the range close to that observed at RHIC/LHC.

(iv) high density of (non-condensed) monopoles near T_c affect electric flux tubed, and perhaps explain [122] lattice observations of high tension in the potential energy (not free energy) of the heavy-quark potentials. We will discuss those in section X.

(v) Last but not least, high density of monopoles near T_c seem to be directly relevant for jet quenching. This issue- a very important part of heavy ion physics - we will discuss in section XI.

(Completing this brief introduction to monopoles, it is impossible not to mention the remaining unresolved issues. Theories with adjoint scalar fields – such as e.g. celebrated $\mathcal{N}=2$ Seiberg-Witten theory – naturally have particle-like monopole solutions. Yet in QCD-like theories without scalars it has to be dynamically generated, not yet explained. So far lattice definitions of monopoles are gauge-dependent. A good news is that most if not all of monopole physics can be taken care of via the instanton-dyons we mentioned above: in this case the role of the adjoint “Higgs” is played by the time component of the gauge potential A_4 . It is real on the Euclidean lattice, but would get i in Minkowski continuation: so it cannot be directly a “particle” in ordinary sense.)

Another famous duality is AdS/CFT gauge-string duality [14], basically used at large number of colors as a gauge-gravity duality. It directly relates equilibrated QGP at strong coupling to a certain black hole solutions in 5 dimensions, with the plasma temperature being its Hawking temperature, and the QGP entropy being its Bekenstein entropy. In section VII we will discuss recent studies of out-of-equilibrium settings, in which black

hole is dynamically generated. Holographic models of the AdS/QCD types also lead to new views on the QCD strings, Reggeons and Pomerons: see section VIII C.

This brief introduction shows that heavy ion physics did acquired a lot of outreach into many other areas of physics.

II. THE MAIN ISSUES IN QCD AND HEAVY ION PHYSICS

Like any other rapidly developing field, heavy ion physics has has “growth problems”. Quark Matter conferences (and their proceedings) provide regular snapshots of the field’s development. Yet those provide poor service for young people or outsiders who want to understand what is going on. The talk time is always severely limited, so naturally only the latest results are reported. They are kaleidoscopic set of compressed answers to questions which were never formulated, as there is no time for that. Discussion session are becoming extremely short (or non-existing), and never recorded. Furthermore, large conferences have multiple parallel sessions, and it is hard to follow more than one subfield.

Traditionally the “second pillar” of any field consists of books, reviews, lecture notes. Those formulate the basic questions and the the lessons learned. They also provide a list of “challenges”, the questions which need to be answered next. With ongoing RHIC program and the now maturing LHC heavy ion program, it is perhaps time for a review. Looking through the talks at the latest Quark Matter conferences, I feel a relative weakness of the theory, compared to overwhelming amount of data from RHIC and LHC. and decided it is time to do it. This review certainly is not complete, many important directions/achievements are not covered. Jet quenching is nearly missing. Fluctuations in the gauge topology, related to chiral magnetic effect, are not discussed: it needs to be developed further before some summary emerges. It is a subjective overview of the field, focusing on big picture, questions and trends rather than specific results.

(On a personal note: the first review I wrote [2], on finite temperature QCD proclaiming a search for QGP as a new goal for community, was written due to an advice given to me by Evgeny Feinberg. Let me also mention here Gerry Brown: long before I met him I benefited from his vision, in founding Physics Reports devoted to such reviews of subfields. The instanton review in RMP of 1996 [5] is in fact my most cited paper. In 2004, when the sQGP paradigm of “a perfect liquid” has been born, many people wrote summary papers. My most extensive version was the second part of my book [4].)

Let me start with few “super-questions” (and comments on them), which are common to the whole strong interaction physics, extending well beyond the boundaries of the heavy ion field.

I.Can one locate the “soft-to-hard” boundary,

in whatever observables under consideration, where the transition from weak to strong coupling regimes take place?

II. Can one locate the ‘micro-to-macro’ boundary, where the transition from large mean-free-path (ballistic) to small one (hydrodynamic) regimes happen? In particular, where in the observable discussed one finds a transition from effects due to single-parton distributions to those due to collective explosion?

III. Can we experimentally identify signals of the QCD phase transition, in particular locate the “softest” and the QCD critical point?

Brief comments on them are:

(Ia) Since 1970’s the “golden” test of pQCD at large momenta transfer was deep inelastic scattering (DIS), as well as hard exclusive processes, e.g. the pion and nucleon formfactors. Unlike jets in DIS, the latter have colorless final state, they can in principle be accurately measured, and thus promised to test the pQCD predictions due to the specific lowest order diagrams. And yet, to the highest $Q^2 \sim 4 GeV^2$ measured so far, neither of them had been found to reach quantitative agreement with the pQCD predictions, because even at such Q the non-perturbative effects still dominate.

Closer to our field is the “mini-jet” issue. While the identified jets have rather large momenta, say $p_{\perp} > 20 GeV$ or so, it is widely assumed that the parton description is good down to much smaller momenta. How much smaller? Following DGLAP evolution toward small Q^2 all the way to $\sim 1 GeV^2$ one eventually reach a negative gluon density. Many other arguments tell us that at this scale, $1 GeV$, pQCD cannot be used. At which scale Q_{min} one has to stop is defined by the “higher twist effects”, not yet studied quantitatively. Thus we are still left with uncomfortably large gap, between 1 and $20 GeV$.

(Ib) The elementary process fundamental for our field is the pp scattering. Its total cross section and elastic amplitude is described by the so called Pomeron phenomenology. Elastic amplitude is function of the momentum transfer $t = -q^2$ and its Bessel-Fourier transform is the so called profile function $F(b)$ depending on the impact parameter b . Small b is understood via perturbative BFKL Pomeron, while large b via some string-exchange models. In this case the experimental data actually do indicate sharp transition between these regimes. Recently an attempt to understand both regimes in a single model has been quite successful, in the so called AdS/QCD framework. Furthermore, it has been suggested that the critical b is related to critical temperature T_c of the phase transition in the gauge theory: we will discuss this in section VIII C.

Ic. Proceeding from elastic to inelastic collisions, under which conditions we should describe the initial snapshots of hadrons and nuclei in terms of perturbative partons (quarks and gluons) or non-perturbative effective objects (strings, constituent quarks, etc)? As we will discuss, hydro sound modes survive till freezeout, and thus

this make these initial snapshots visible to the detectors. Therefore, one can now estimate at least the number of such “objects”.

(IIa) Furthermore, now we have a variety of cases – AA, pA and pp collisions with widely variable multiplicities. All of them show collective phenomena – radial, elliptic and even triangular flows -at high enough multiplicity. Pushing such observables down in multiplicity is a current frontier. One would like to find some regime changes there, experimentally and theoretically. No sharp changes are so far detected. People apply microscopic theory at one end of the pA and pp collisions and macroscopic theory (thermo and hydrodynamics) at another, checking to what extent one can justify them, but this process is far from converged so far.

(IIb) Where exactly is the boundary between the micro and macro theories? Textbook answer is that one can compare the micro or “mean free path” scale l to the size of the system

$$L \gg l \quad (3)$$

and if the l/L ratio is small one can use the macroscopic theories. Given a very small phenomenological viscosity $\eta/s \sim .2$ one formally get a mean free path smaller than interparticle distance. Does it actually make sense? Testing the sounds with the shortest wavelengths we can see, or the exploding systems with the smallest sizes, one seem to conclude that in fact it does!

III. SOUNDS ON TOP OF THE “LITTLE BANG”

A. Introductory comments on hydrodynamics

Since the start of the RHIC era in 2000, it has become soon apparent that the data on particle spectra (the radial flow) and the elliptic flow confirm nicely predictions of hydrodynamics, supplemented by hadronic cascade at freezeout [16–18]. All relevant dependences – as a function of p_{\perp} , centrality, particle mass, rapidity and collision energy – were checked and found to be in good agreement. Since the famous 2004 RBRC workshop in Brookhaven, with theory and experiment summaries collected in Nucl.Phys.A750, the statements that QGP “is a near-perfect liquid” which does flow hydrodynamically has been endlessly repeated. QGP is recognized to be in the strongly coupled regime, now called sQGP, and hundreds of theoretical papers are written, developing dynamics at strong coupling. Several second-order hydro+cascade models had been developed in the last decay, which do an excellent job in describing the data. The interested readers should look at recent reviews such as [34]: we will take this to be a “well established domain”. (Of course, the data are constantly getting more impressive with time: let me mention e.g. the elliptic flow v_2 of the deuterons recently measured by ALICE and shown at QM2015.)

The interest has now been shifted to understanding the *limits* of the hydro description. Of course, the exact boundary depends on which version of it is implied. In the simplest case, when one thinks of ideal hydro plus viscous corrections, this happens when the viscosity times the velocity gradients is as large as the main terms. Now, there can be two different reasons why this correction gets large: (i) either the fluid is not good, viscosity-to-entropy ration η/s is not small, or (ii) the gradients are too large. Studies of the former have recently been done using anisotropic hydro and exact solution of Boltzmann equation in Gubser setting, as well as by the so called anisotropic hydrodynamics: we will discuss those in section IV C. The latter situations can be approached via the so called *higher order hydrodynamics*. Gradient resummation was in particular attempted by Lublinsky and myself: we will discuss those in section VII E. In all of these cases, an improved hydrodynamics is supposed to shift its initiation time somewhat earlier, or promise to treat somewhat smaller systems. Yet, while the “out-of-equilibrium” initial stage get reduced, of course it can never be eliminated. The distinction between the “initial” and “equilibrated” stages is a matter of definition: but physical outputs – e.g. the total amount of entropy produced – should ideally be independent of that. Unfortunately, in practice we are still far from this ideal scenario: studies of entropy generation at an initial stage is still in its infancy.

Few other issues remains open till now, related with the boundary of hydrodynamical description.

One is the boundary at high p_t . When the first RHIC data came, it has been gratifying to see that agreement with hydro-based spectra went down more than order of magnitude and reached $p_t \sim 1 \text{ GeV}$. The it has been extended much further, till $p_\perp \sim 3 \text{ GeV}$. This region includes more than 99.9% of all secondaries! Indeed, only few – out of thousands – particles in a heavy ion collision do come from hard tails of the spectra.

As the regime changes at $p_\perp \sim 3 \text{ GeV}$, one needs to understand why. One important point is that particles at high p_t come from an edge of the fireball, at which the magnitude of the hydro flow is maximal. Using the saddle point method for Cooper-Frye integral [19] one can see that the region from which such particles come shrinks, as p_t grows. (We will return to this point in connection to high multiplicity pp collisions and HBT radii, see section V E.) Eventually this region shrinks to a single hydro cell (defined by the mean free path), and then hydro description needs to be modified. Teaney [20] introduced the viscosity effect in the cell, and noticed that due to extra derivative these effects should be enhanced at the edge. They also should have extra power of p_t , he argued, and the deviation should be downwards, as indeed is observed in harmonic flows. Still, physics in the window $4 < p_\perp < 20 \text{ GeV}$, between the hydro-dominated and clearly jet-dominated regions is not yet understood.

The second issue is the relative role of sQGP and hadronic stages in the expansion and flows. At AGS/SPS

energy domain one clearly had to understand both quantitatively: otherwise the results got wrong. For example, the paper [59] was all about the sequential freezeout of different kinds of secondaries, and how it was seen in radial flow. It has been fairly important for radial flow at RHIC: yet elliptic and other harmonics of flow were formed earlier and the hadronic stage were less important.

The last 4 years had provided further confirmation of the *hydro paradigm* at LHC. One of the benefits is that, even for radial flow, the main acceleration is done in the sQGP phase, to such an extent that one can neglect the sequential freezeout and related complications. Let me just provide one example of how well it works, from ALICE.

Out of all individual properties of the secondary hadron, only one – its mass – is important for hydro models. All one needs to know is that putting an object of mass m into a flow with velocity v , the momentum will be mv . Nice demonstration that it is indeed so can be made by direct comparison of the spectra for a pair of hadrons with the same mass, with otherwise completely different quantum numbers, cross sections etc. The classic example is p and ϕ : those can hardly be more different, the former is non-strange baryon, the latter is a strange-antistrange meson, etc. And yet, as e.g. ALICE measurements shows, their spectra are – with impressive precision – identical, up to $p_T \sim 4 \text{ GeV}/c$. The very fact that $p/\pi, \phi/\pi$ ratios can increase by two orders of magnitude and reach $O(1)$ at such p_t is by itself a dramatic hydro effect, never seen in generic (non-high-multiplicity) pp collisions.

I think it puts to rest many non-flow explanations of the particle spectra in AA collisions.

Among those I count a widely popularized idea of the so called “quark scaling” of the elliptic and other flows, that suggests that if a hadron is made of n quarks then its flow harmonics should be proportional to n , $v_m^{(h)} \sim n v_m^{(q)}$, with some the “quark” $v_m^{(q)}$. The logic behind this idea [151] comes from the expression (82) of that paper which assumes that the quark distribution function in the phase space is “factorized”

$$w(R; p) = w_i(R; p)[1 + 2v_2^a(p_\perp)\cos(2\phi)]. \quad (4)$$

Note that the bracket does not depend on the location R . So, the authors assume v_2 to originate from some anisotropic momentum distribution in *every local hydro cell*. This assumption is in direct contradiction to the flow picture, which instead postulate that each cell has an equilibrium (=isotropic) distribution of particles [162] Anisotropic flows are due to different *number of cells* moving in different directions. This n -parton structure cannot possibly matter: a hadron can be made of 2, zero or 22 partons: all you need to know is its mass.

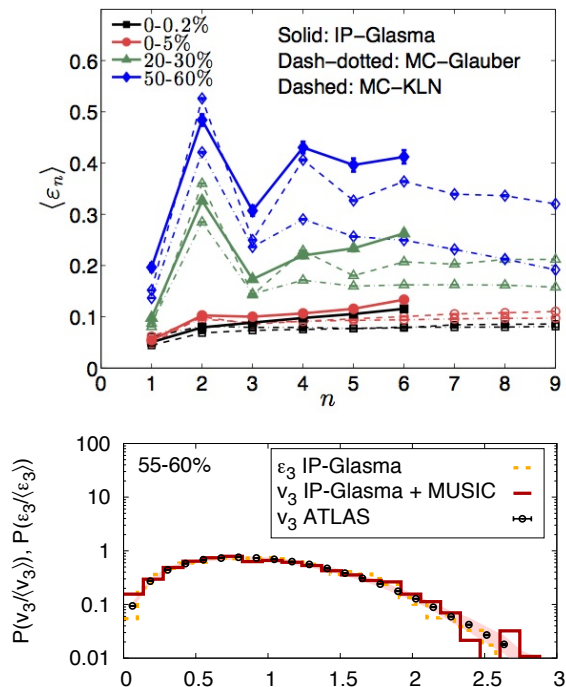


FIG. 2: (a) From [34]: average deformations $\langle \epsilon_n \rangle = \langle \cos(n\phi) \rangle$ for various centralities using models indicated in the figure. (b) From [23]. Data points correspond to the event-by-event distribution of v_3 measured by the ATLAS collaboration, compared to the distributions of initial eccentricities in the IP-Glasma model and the distributions of v_3 from fluid dynamic evolution with IP-Glasma initial conditions.

B. Hydrodynamical response to perturbations

Now, assuming that the *average pattern of the fireball explosion* has been well established, we are going to perturb it. The fluctuations and their correlations is thus the next topic of our discussion.

There are two schools doing this. One uses the so called event-by-event hydro, with ensemble of initial conditions defined by some model. Yet I will argue that practically all one learned from such expensive studies can also be understood from a much simpler approach, in which one adds small and elementary perturbations on top of smooth average fireball, and solve for the complete spectrum of excitations. Using an analogy, instead of beating the drums strongly, with both hands and all fingers, one may first touch it gently with a drumstick, at different locations, recording the spectra and intensities of the sounds produced. Eventually, one may understand not only its spectrum, but also all the relevant modes of excitations. The one can work out linear and nonlinear superpositions of those elementary modes.

(The reader should understand that by no means the latter approach undermines good work which the latter does. People developing stable hydro codes and ensem-

bles of initial conditions, averaging hydro results over thousands of configurations with complicated shapes. All that works spectacularly well: the v_n moments of the flow perturbations in azimuthal angle ϕ as a function of transverse momentum, particle type and centrality $v_n(p_t, m, Np)$ are all reproduced. Hardly any further convincing of that is now needed: multiple versions of the plots proving that are shown at all conferences and perhaps seen by a reader: so I will not discuss this and take it for granted as well.)

Now is the time of synthesis of all that information. In order to summarize what we have learned from fluctuation/correlation studies one needs to go back to the data and to the results of hydro calculation and separate their essence from unimportant complications. Some simple pocket formula fits to analytic expressions, revealing the systematics of physical effects in question, can be very useful at this stage, and we will discuss them below.

But before we dip into details, let me formulate the main answers, using my drum analogy. First of all, we did learned that perturbations on top of the little bang basically behave as sounds propagating on the drum. The main phenomenon is the viscous damping, and the value of sQGP viscosity is the main physics output of these studies. Different time evolution of different modes is the next issue: unlike the usual drum, the little bang is not static but exploding: therefore oscillating behavior is superimposed with time dependence of the amplitudes. Different excitations are excited if the drum is struck at different places: similarly here, and we only start understanding the excitation modes themselves.

Let me continue where these calculations typically start: from angular deformations of the initial state. In Fig.2(a) one finds the dependence of the mean harmonics (eccentricities)

$$\epsilon_n = \langle \cos(n\phi) \rangle \quad (5)$$

where n is integer and ϕ is the azimuthal angle. The angular brackets mean average over events, usually for certain centrality bin (indicated in the upper left corner as a fraction of the total cross section, which scale as bdb). The one 0-0.2% is called the ultra-central collisions, $b \approx 0$, and 50 – 60% are some peripheral collisions. The first obvious comment to this plot is that $n = 2, 4$ harmonics are special: they have some peaks for peripheral bins, due to collision geometry. However other harmonics, and in fact, *all* harmonics for the central bins, are basically independent on n and centrality. What that tells us is that statistically independent “elementary perturbations” have small angular size $\delta\phi \ll 2\pi$, so one basically deals with an angular Fourier transform of the delta function.

The next observation is that the deformations gets smaller toward the central collisions, to just few percent level. This is also natural: larger fireballs have more particles and thus they fluctuate less, in relative terms. In

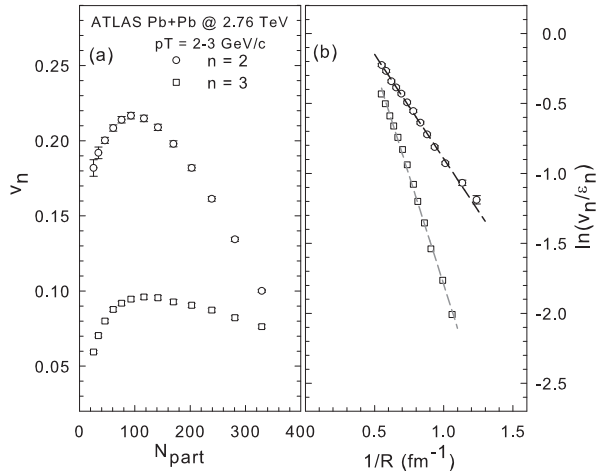


FIG. 3: (a) Atlas data, from Ref. [35], for v_2, v_3 vs. N_{part} : (b) $\ln(v_n/\epsilon_n)$ vs. $1/R$ for the same data

fact one expect

$$\langle \epsilon_n \rangle \sim \frac{1}{\sqrt{N_{cells}}} \quad (6)$$

where $N_{cells} = A_{cell}/A_{fireball}$ is the number of statistically independent cells in the transverse plane. (What exactly is a cell is not simple and we will discuss it below in the section on the initial state. Depending on the model it changes from a fraction to few fm^2 .)

Models of the initial state give not only the average deformation but also their distributions and correlations. Going a bit ahead of myself, let me note that, remarkably, the experimentally observed distributions over eccentricities of *particle momenta distributions* $P(v_n)$ appears to directly reflect distributions of angular anisotropies $P(\epsilon_n)$ at the initial time, see e.g. ϵ_3, v_3 distributions in Fig.2(b). (Thus, apparently no noise is generated by the hydro evolution, from the initial state ϵ_n to the final state v_n : why is it so we will discuss below.)

C. Acoustic systematics: the viscous damping

There is a qualitative difference between the radial flow and higher angular harmonics. While the former monotonously grows with time, driven by the outward pressure gradient with a fixed sign, the latter are basically sounds, or a (damped) oscillators. Therefore the signal observed should, on general grounds, be the product of the two factors: (i) the amplitude reduction factor due to viscous damping and (ii) the *phase* factor containing the oscillation at the freezeout. (We will discuss the effects of the phase in the next section.)

Let us start with the “acoustic systematics” which includes only the viscous damping factor. It provides good

qualitative account of the data and hydro calculations into a simple expression, reproducing dependence on the viscosity value η , the size of the system R and the harmonic number n in question. Let us motivate it as follows. We had already mentioned “naive” macro and micro scales (3): now we define it a bit better by inserting the famous viscosity-to-entropy ratio $\eta/s = lT$,

$$\frac{l}{L} = \frac{\eta}{s} \frac{1}{LT} \quad (7)$$

This “true micro-to-macro ratio”, corresponding to the mean free path in kinetic theory, defines the minimal size of a hydro cell.

One effect of viscosity on sounds is the damping of their amplitude. The so called “acoustic damping” formula, suggested by Staig and myself [47], is given by

$$\frac{v_n}{\epsilon_n} \sim \exp \left[-Cn^2 \left(\frac{\eta}{s} \right) \left(\frac{1}{TR} \right) \right] \quad (8)$$

where C is some constant. The number n appears squared because the damping includes square of the gradient, or momentum of the wave. So, we have the following predictions: (i) the viscous damping is exponential in n^2 ; (ii) the exponent contains the product of two small factors, η/s and $1/TR$, (iii) the exponent contains $1/R$ which should be understood as the *largest* gradient in the system, often modelled as $1/R = 1/R_x + 1/R_y$.

Extensive comparison of this expression with the AA data, from central to peripheral, has been done in Ref. [35] from which we borrow Fig.3 and Fig.4. The Fig.3 (a) shows the well known centrality dependence of the elliptic and triangular flows. v_2 is small for central collisions due to smallness of ϵ_2 , and also small at very peripheral bin because viscosity is large at small systems. Fig.3

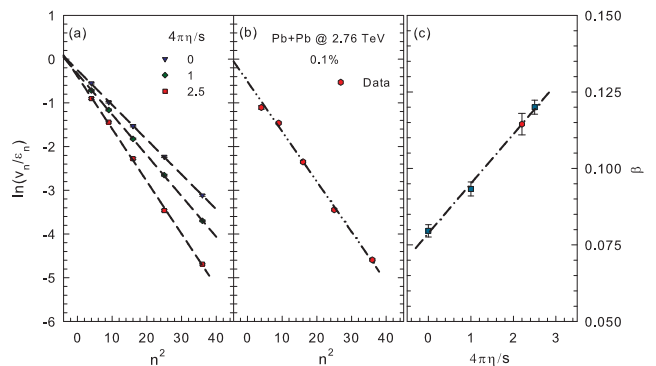


FIG. 4: (a) Atlas data, from Ref. [35], $\ln(v_n/\epsilon_n)$ vs. n^2 from viscous hydrodynamical calculations for three values of specific shear viscosity as indicated. (b) $\ln(v_n/\epsilon_n)$ vs. n^2 for Pb+Pb data. The p_\perp -integrated v_n results in (a) and (b) are from ATLAS 0.1% central Pb+Pb collisions at sNN = 2.76 TeV; the curves are linear fits. (c) exponent vs. viscosity-to-entropy ratio $4\pi/s$ for curves shown in (a) and (b).

(b) shows the $\ln(v_n/\epsilon_n)$, which according to the formula is the exponent. As a function of the inverse system's size $1/R$ both elliptic and triangular flows show perfectly linear behavior. Further issues – the n^2 dependence as well as linear dependences of the $\log(v_m/\epsilon_m)$ on viscosity value – are also very well reproduced, see Fig.4. Note that this expression works all the way to rather peripheral AA collisions with $R \sim 1 fm$ and multiplicities comparable to those in the highest pA binds. It also seem to work till the largest n so far measured.

So, the acoustic damping provides correct systematics of the harmonic strength. This increases our confidence that – in spite of somewhat different geometry – the perturbations observed are actually just a form of a sound waves.

Since we will be interested not only in large AA systems but also in new – pA and pp – much smaller fireballs, one may use the systematics to compare it with the new data. Or, using it, one can estimate how many flow harmonics can be observed in these cases. For central PbPb at LHC collisions with

$$\frac{1}{TR} = \mathcal{O}(1/10) \quad (9)$$

its product of η/s is $\mathcal{O}(10^{-2})$. So one can immediately see from this expression why harmonics up to $n = \mathcal{O}(10)$ can be observed. Proceeding to smaller systems by keeping a similar initial temperature $T_i \sim 400 MeV \sim 1/(0.5 fm)$ but a smaller size R , results in a macro-to-micro parameter that is no longer small, or $1/TR \sim 0.5, 1$, respectively. For a usual liquid/gas, with $\eta/s > 1$, there would not be any small parameter left and one would have to conclude that hydrodynamics is inapplicable for such a small system. However, since the quark-gluon plasma is an exceptionally good liquid with a very small η/s , one can still observe harmonics up to $m = \mathcal{O}(\sqrt{10}) \sim 3$. And indeed, v_2, v_3 have been observed in the first round of measurements (for latest data see Fig.17).

D. The Green function: waves from a point perturbation

The problem appears very complicated: events have multiple shapes, described by multidimensional probability distributions $P(\epsilon_2, \epsilon_3\dots)$. Except that it is not. All those shapes are however mostly a statistical noise. The reason is as follows: rows of nucleons sitting at different locations in the transverse plane cannot possibly know about each other fluctuations at the collision moment, so they must be statistically independent. An “elementary excitation” is just one delta-function in the transverse plane (in reality, of the size of a nucleon), on top of a smooth average fireball. In other words, the first thing to do is to calculate the Green function of the linearized hydro equations.

A particular model of the initial state expressing locality and statistical independence of “bumps” has been

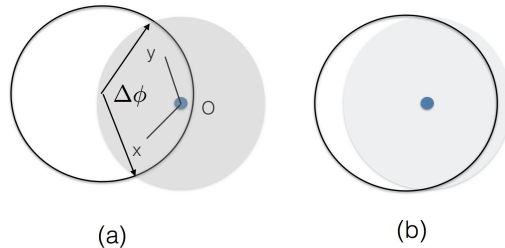


FIG. 5: The perturbation is shown by small blue circle at point O: its time evolution to points x and y is described by the Green function of linearized hydrodynamics shown by two lines. Perturbed region – shown by grey circle – is inside the sound horizon. The sound wave effect is maximal at the intersection points of this area with the fireball boundary: $\Delta\phi$ angle is the value at which the peak in two-body correlation function is to be found. Shifting the location of the perturbation, from (a) to (b), result in a rather small shift in $\Delta\phi$.

formulated in [24]: the correlator of fluctuations is given by the Poisson local expression

$$\langle \delta n(x)\delta n(y) \rangle = \bar{n}(x)\delta^2(x-y) \quad (10)$$

where $\bar{n}(x)$ is the average matter distribution. The immediate consequence of this model is that, for the central collisions on which we now for simplicity focus, ϵ_m are the same for all $m < m_{max} = \mathcal{O}(10)$ (till the bump size gets resolved).

In order to calculate perturbation at later time one needs to calculate the Green functions, from the original location O to observation points x and y as shown in Fig.5(a). That has been first done in [36], analytically for Gubser flow. One finds that the main contributions come from two points in Fig.5, where the “sound circle” intersects the fireball boundary. In a single-body angular distributions those two points correspond to two excesses of particles at the corresponding two directions. Let us call the angle between them $\Delta\phi$: at Fig.5(a) it is about 120° or 2 rad. This is because the freesout time times speed of sound $R_h = c_s\tau_{freezeout}$ happens to be close to the radius of the fireball.

The correlation function calculated in [36], is shown in Fig. 6(a). One its feature is a peak at zero $\delta\phi = 0$: it is generated if both observed particles come from the same intersection point. If two particles come from different points, one finds two peaks, at $\Delta\phi = \pm 2$ rads. (As shown in Fig.5, if one shifts the position of perturbation from (a) to (b), the peak angle $\Delta\phi$ changes toward its maximal value, π radian, or $1/2$ of the circle.)

This calculation has been presented at the first day of Anecy Quark Matter *before* the experimental data. The ATLAS correlation function (for the “super-central bin”, with the fraction of the total cross section 0-1%) is shown in Fig. 6(b). The agreement of the shape is not perfect – because a model is with conformal QGP and a bit different shape – but all predicted elements of its

shape are indeed observed.

While there is no need to use Fourier harmonics – I insist that the correlation function itself teaches us more than harmonics, separately studied – one can certainly do so. Note that for ultra-central collisions we now discuss the largest harmonics is v_3 (the blue curve in Fig. 6(b)) and not v_2 (the green one). Since starting deformations ϵ_n are basically the same for all n , the difference must come from hydro, and it does: we just explained it above, using notion of sound horizon. Alternative explanation can be done in terms of the freezeout phases of the harmonics $\phi_{freezeout}^n$.

A related arguments are quite famous in the theory of Big Bang perturbations. All harmonics get excited at the same time by Big Bang – hydro velocities at time zero are assumed to be zero for all harmonics – and are frozen at the same time. The acquired phases depend on n – harmonics with a larger n oscillate more rapidly. Binary correlator is proportional to $\cos^2(\phi_{freezeout}^n)$ and harmonics with the optimal phases close to $\pi/2$ or $3\pi/2$ values show maxima, with minima in between. Planck collaboration data on harmonics power spectrum of the cosmic microwave Big Bang perturbations, shown in Fig. 9, do display a number of such maxima/minima.

Our calculation had shown such oscillations clearly, with the first peak between $n = 3, 4$ (see Fig.), the next should be at $n=9$, with the minimum predicted to be around 7, see Fig.8(a). More sophisticated event-by-event hydro calculation by Rose et al [25] does not reproduce oscillations around the smooth sound damping trend, see Fig.8(b). One may think that averaging over many bumps in multiple configurations may indeed average out the freeze out phase factor.

Yet the ultra-central ATLAS data shown in Fig.8(a), and even the CMS central bin data in Fig.8(b) (which include a bit larger impact parameters and thus feed more geometry-related contribution to v_2) one can still see clear deviation from smooth damping curve $\sim \exp(-n^2 * const)$. Note that the v_3 is higher than in all hydro output shown, while v_6 is lower. Let me conclude this discussion with a note that while certain oscillatory deviations from “acoustic systematics” are there in the experimental data, their origin and even qualitative reproduction by the hydro models remains uncertain.

Let me conclude this section with brief discussion of the following issue. The “flow harmonics”, solutions of linearized equations on top of the average smooth hydro solution should possess a complete spectrum of perturbations, whose time evolutions are different from each other. The perturbations of course depend not only on the angle ϕ , as $e^{im\phi}$, but of course on other coordinates r, η as well.

For Gubser setting (see appendix) one can use comoving coordinates ρ, θ, ϕ, η and dependence on *all* coordinates separate nicely, with known analytic expressions for harmonics and their time evolution. The flow in transverse plane is conveniently combined into a single angular momentum harmonics $Y_l(\theta, \phi)$, combining azimuthal an-

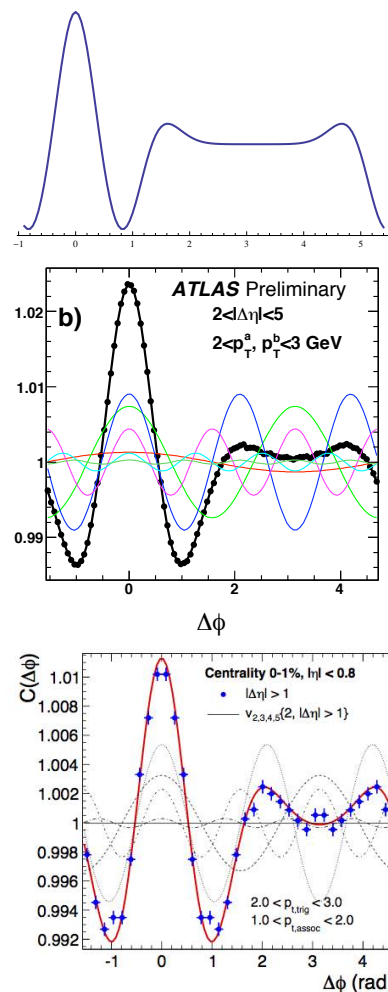


FIG. 6: (a) Calculated two-pion distribution as a function of azimuthal angle difference $\Delta\phi$, for viscosity-to-entropy ratios $\eta/s = 0.134$, from [36]. (b) from ATLAS [32], (c) from ALICE [33]: All for ultra-central collisions.

gle and r . Another simple eigenfunctions are plane waves with some momenta k in the rapidity direction η .

Can one define similar set of independent harmonics for a generic non-Gubser setting? And, even more importantly, can those be observed? A nice step in this direction has been recently made by Mazeliauskas and Teaney [50]. Using experimental data (and of course hydro calculations) they define such “subleading harmonics”. Instead of describing how they do it, here is just one picture from that work, for triangular flow, indicating a difference between the leading and subleading flows: unlike the former, the latter gets a sign change along the radial direction.

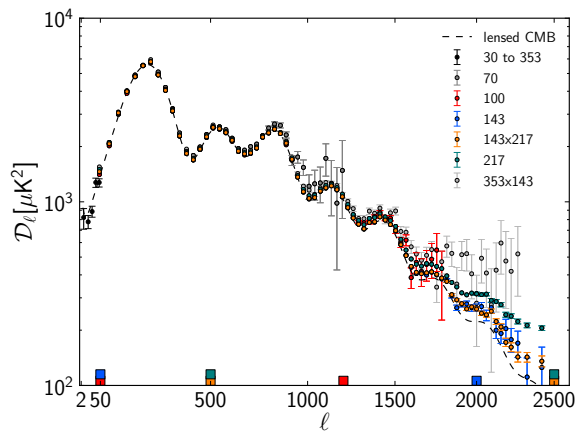


FIG. 7: Power spectrum of cosmic microwave background radiation measured by Planck collaboration [93].

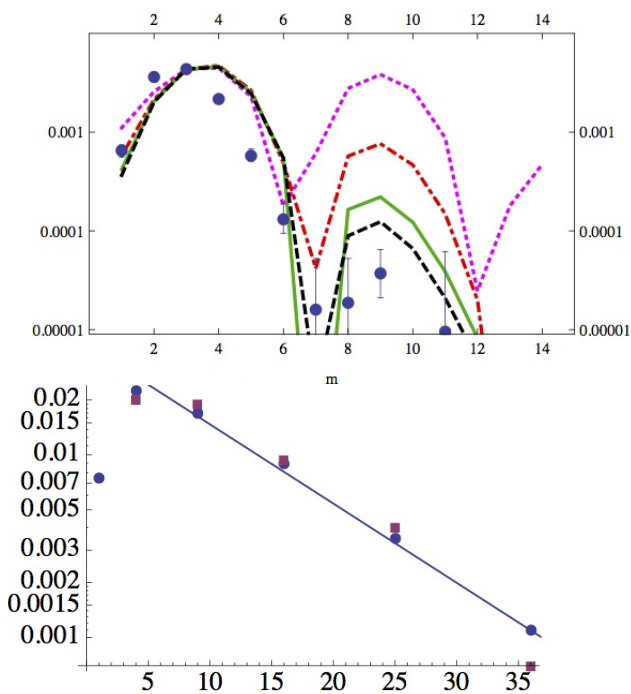


FIG. 8: (a) The lines are hydro calculations of the correlation function harmonics, v_m^2 , based on a Green function from a point source [36] for four values of viscosity $4\pi\eta/s = 0, 1, 1.68, 2$ (top to bottom at the right). The closed circles are the Atlas data for the ultra-central bin. (b) v_n^2 plotted vs n^2 . Blue closed circles are calculation of via viscous even-by-event hydrodynamics [25], “IP Glasma+Music”, with $\eta/s = 0.14$. The straight line, shown to guide the eye, demonstrate that “acoustic systematics” does in fact describe the results of this heavy calculation quite accurately. The CMS data for the 0-1% centrality bin, shown by the red squares, in fact display larger deviations, perhaps an oscillatory ones.

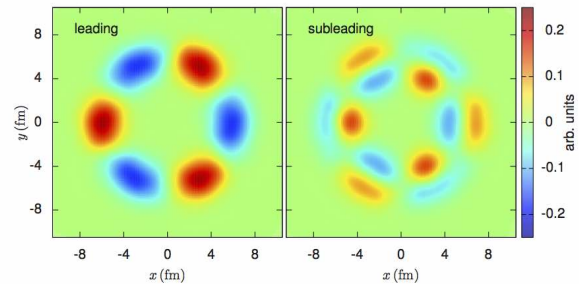


FIG. 9: The leading (left) and subleading (right) harmonics of triangular flow, from [50].

E. Non-linear effects for harmonics

We argued above that one can view perturbations as superposition of uncorrelated local (delta-function-like) sources. We then further argued that only those close to the fireball surface are visible. How many of them are there? For central collisions the circumference of the fireball $2\pi R_A \approx 40 \text{ fm}$. The correlation length is perhaps the typical impact parameter in NN collisions, which at LHC energies is $b \sim \sqrt{\sigma/\pi} \sim 1.6 \text{ fm}$. Their ratio suggest existence of about

$$N_{sources} \approx \frac{2\pi R_A}{b} \approx 25 \quad (11)$$

cells on the fireball surface which fluctuate independently, up or down from the mean value. Glauber initial conditions indeed have about a dozen sound-producing “bumps”.

The absolute scale of modulation in the experimental correlators are of the order of a percent in magnitude, see e.g. Fig.6(b). Of course, it comes from incoherent sum over the single bumps, so one should divide by their number and get the individual correlation from a bump to be of $O(10^{-3})$ in magnitude. It however is quadratic in the wave amplitude: taking the square root of it we get sound amplitudes to be of the order of $1/30$ or so.

Summarizing: the picture looks like that from about a dozen stones thrown into the pond. While the sound circle visibly interfere, they do not really interact with each other, since the amplitude is too small.

Yet the conclusion that since individual sounds are weak, the linear theory is completely correct, is premature. Even when the amplitude of the sound is small, they can produce large effects at the large p_t end. Indeed at $p_t \sim 3 \text{ GeV}$ the elliptic flow reach values which makes angular distribution 100% asymmetric. This happens because a weak sound may sit “on the shoulders of the giants”, the explosions themselves.

Similarly, the non-linear effects of flows at comparable large p_t are non-negligible and were in fact observed. For example v_4 is getting a contribution proportional to ϵ_2^2 , v_6 from ϵ_3^2 , etc. Detailed studies of such effects one can

find in [31], including an interesting case of v_1 coming from $\epsilon_2 * \epsilon_3$.

These nonlinear effects come *not* from nonlinear terms in the hydro equation, but from an expansion of the Cooper-Fry exponent $\exp(p^\mu u_\mu/T)$ in powers of the perturbation. Obviously they become more important at high p_t . Furthermore, one can see that linear terms should be linear in p_t , the non-linear we mentioned should be quadratic $\sim p_t^2$, etc, see more in [31].

F. Event-by-event v_n fluctuations/correlations

At the beginning of this section we had already emphasized that the main source of the v_n fluctuations is that of the original perturbations ϵ_n themselves, see e.g. Fig. 2(b). Now we return to the question: *Why does the ratio v_n/ϵ_n , evaluated by hydro, has such a small spread?* While the practitioners of the event-by-event hydrodynamics use huge variety of the initial configurations, it turns out that just one number – ϵ_n – insufficient to characterize them. Even adopting the simplest model advocated above – that the perturbations come from point-like sources – it is nontrivial that their event-by-event fluctuations of strength and locations do not create any spread in the ratio v_n/ϵ_n . (Or, using my drum analogy, why does it sound the same, if hit in different locations?)

Trying to understand this, let us come back to Fig.5. The source located at the fireball edge, fig.(a), leads to correlations which are at $\Delta\phi \approx 2rad$, as we emphasized above. Projected on harmonics, it will excite $m = 3$ mostly, as 2 rad is about 1/3 of 2π . When the source moves inward, fig.(b), the perturbations move to the opposite points of the fireball $\Delta\phi = \pi$, and the leading excitation becomes elliptic $m = 2$. Estimates show that in the latter case the correlation weakens. The observed shape of the correlator, for ultra-central collisions does have a *minimum* at $\Delta\phi = \pi$, supports that. As the source moves further toward the fireball center (not shown in Fig.5), the whole fireball becomes included inside the sound horizon. The angular correlation dilutes to all angles and its contributions to harmonics gets negligible. In summary: the sources located near the boundary of the fireball are mostly responsible for the harmonics we see. All of them thus generate the same angular shape of the correlator. What remains is the overall strength, a single parameter captured in the ϵ_n magnitude.

Harmonic correlations is a rapidly developing field. Those can be divided to correlations sensitive to relative phases of the harmonics and those which are not. An example of the later is

$$SC(m, n) = \langle v_m^2 v_n^2 \rangle - \langle v_m^2 \rangle \langle v_n^2 \rangle \quad (12)$$

on which Alice provided good data at QM 2015 for $SC(4, 2)$ and $SC(3, 2)$. In particular it is observed that $SC(4, 2) > 0$ but $SC(3, 2) < 0$, which is qualitatively reproduced in hydro. Now, in order to explain these data, one needs first to have the initial state model which is

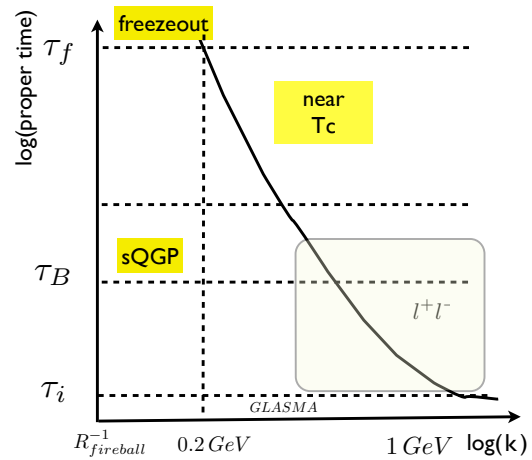


FIG. 10: The log-log plane proper time τ – sound momentum k . The solid curve indicates the amplitude damping by a factor e : only small- k sounds thus survive till freeze out. The shadowed region on the right corresponds to that in which sonomagnetoluminescence effect may produce extra dileptons.

good enough to predict the relevant ϵ_n and their respective correlations. Suppose we do so using the Bhalerao-Ollitrault model [24] and the relation (10): the results depend on integrals like $\int d^2r r^P \bar{n}(r)$ with large powers $P = 6, 8$. What this tells us is that the correlation is strongly localized at the very surface of the system, and thus subject to significant uncertainties.

G. The map of the sounds

We will argue below that the number of harmonics needed to describe the initial state is rather large, counted in hundreds. In Fig.10 we show a map of those, in terms of momentum (rather than angular momentum). The curved line – corresponding to “acoustic systematics” discussed above – show their lifetime. This curve crosses the freezeout time: smaller k waves can be observed at freezeout. Larger k cannot: they are weakened due to viscous damping. (A suggestion to detect those via the MSL process will be discussed in section IX B.)

Fluctuation-dissipation theorem tells us that while the initial perturbations are damped, new ones should be produced instead. There should be some noise produced at the hydro stage. For a paper exploring hydro *with noise* see Young et al [46]. Unfortunately, the authors have not yet identified observables which sensitive only to the *late – time* perturbations. I suggest those should be azimuth+rapidity correlations, exploring the fact that early time perturbations must be rapidity-independent

This idea came from the paper [48] in which a very specific late-time fluctuations were considered, namely sounds from collapsing QGP clusters inside the hadronic phase. Those collapse must happen, since this phase is unstable in the bulk, once $T < T_c$: its physics is simi-

lar to the celebrated Rayleigh bubble collapse. Another discussed – and as yet unobserved – are sounds from jets depositing its energy into the ambient matter and then propagated via hydro perturbations, known as Mach cone. Extensive recent discussion of how one can observe those can be found in Ref. [49].

H. Sounds in the loops

The hydrodynamical longitudinal pressure waves – the sounds – are the best quasiparticles we have. They are Goldstone modes, related with spontaneous breaking of the translation invariance by matter, and thus their interaction fall into certain pattern familiar from physics of the pions. For large wavelengths they have long lifetime, exceeding the freezeout time. Therefore, in both the Little and the Big Bangs, one can observe “frozen” traces of the initial perturbations, provide one looks at large enough wavelengths.

So, the set of sounds have their own lifetime scales, and one may wander about an ensemble of sounds, their interactions etc. One way to introduce those is to add to hydro equations a Langevin-type noise term, with some Gaussian distribution, and then rewrite the theory with certain artificial fields into a QFT-like form. Progress into this direction has been recently summarized by Kovtun in a nice review [96]. Discussion of formal issues cannot be made in this review, however, and thus I illustrate the physics involved by one example, also due to Kovtun and collaborators [97]. Let me remind that matter viscosity can be defined via certain limit of the stress tensor correlator, known as the Kubo formula. Kovtun et al calculated a “loop corrections” to this correlator induced by the equilibrium sounds. Technically the calculation is done as follows: in the $\langle T^{\mu\nu} T^{\mu'\nu'} \rangle$ correlator one substitute hydrodynamical expression for stress tensor containing sound perturbation velocities and make it into a loop diagram with the “sound propagators”

$$\Delta^{mn} = \int d^4x e^{-ip_\alpha x^\alpha} \langle u^m(x) u^n(0) \rangle \quad (13)$$

for two pairs of the velocities. (We use latin indices indicating that they are only space-like here. For shear viscosity those used are $m = x, n = y$). Skipping the derivation I jump to the answer obtained from this calculation, which can be put into the form of loop correction to the viscosity

$$\delta\eta_{loop} = \frac{17}{120\pi^2} \frac{p_{max} T (\epsilon + p)}{\eta_0} \quad (14)$$

which is UV divergent and thus includes p_{max} , the largest momentum for sound which still makes sense. What is important here is that the zeroth-order viscosity enters into the denominator. This should not be surprising: a very good liquid with small η_0 support very long-lived sounds, which can transfer momentum far, which means

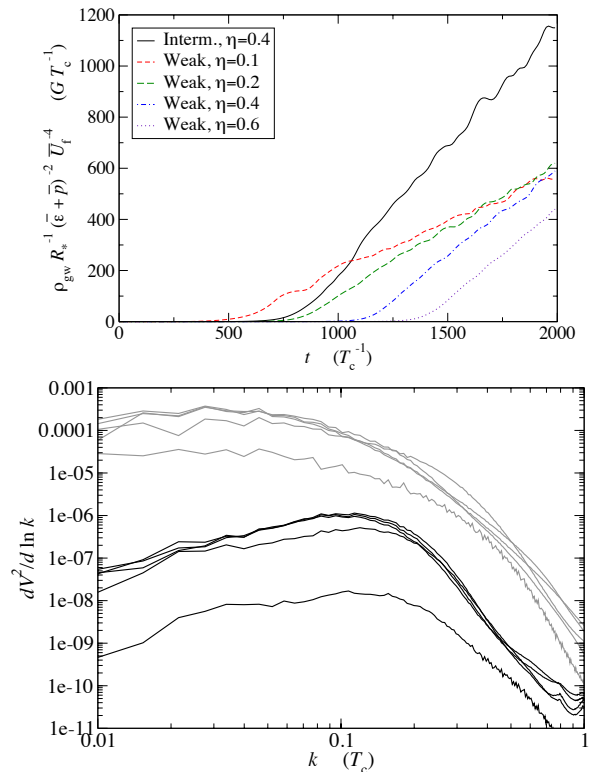


FIG. 11: (From [76]) (a) The density of generated gravity waves ρ_{GW} versus time t , in units of inverse T_c . The density continue to grow linearly even at the longest times, well after the phase transition itself is over. (b) The power spectrum of the velocity squared versus the wave momentum k . The grey upper curves are for sounds, from down up as time progresses. The black curves downwards are for rotational excitations.

they produce *large* contribution to the effective viscosity! (Like ballistically moving phonons in liquid helium or neutrinos in supernova, the most penetrating modes always dominate the transport.)

Completing this section we would like to remind the reader about existence of other hydro modes, the rotational ones. It is those ones which are e.g. responsible for the atmospheric turbulence. Unlike sounds, which are always damped, rotational modes can get excited under certain conditions. Very little theory work has been done in this direction so far. Floerchinger and Wiedemann [94] analyzed rotational modes on top of the Bjorken flow, and formulated conditions for one mode to get unstable. Csernai et al [95] had also found an unstable hydro mode, for non-central collisions with rotation. While this effect does not develop into a full-scale turbulence in heavy ion collisions, due to limited time it exists, it does contribute to an overall fireball rotation and thus it can perhaps be observed.

I. Cosmological gravitational waves from sounds of the QCD phase transition

We think that our Universe has been “boiling” at its early stages at least three times: (i) at the initial equilibration, when entropy was produced, at (ii) electroweak and (iii) QCD phase transitions. On general grounds, these should have produced certain out-of-equilibrium effects. It remains a great challenge to us, to observe their consequences experimentally, or at least evaluate their magnitude theoretically. The first question is then, what observable may have a chance to see through the subsequent evolution, back to the early moments of the Big Bang.

From the onset of the QGP physics in heavy ion collisions a specially important role has been attributed to the “penetrating probes”, production of photons/dileptons [84]. In this section (only) we will jump from our customary Little Bang to the discussion of the Big Bang. So it is quite logical to start with a question whether it also possesses some kind of a “penetrating probe”. The answer is quite clear: while the electromagnetic and weak interactions are in this case not weak enough, the gravitational one is. Thus the only “penetrating probe” of the Big Bang are the *gravity waves* (GW).

30 years ago Witten [75] had discussed the cosmological QCD phase transition, assuming it to be of the first order: he pointed out bubble production and coalescence, producing inhomogeneities in energy distribution and mentioned production of the gravity waves. Jumping many years to recent time, we mention that Hindmarsh *et al* [76] recently found the hydrodynamical sound waves to be the dominant source of the GW, while doing numerical simulations of (variant of) the electroweak (EW) phase transition in the first order transition setting. Since this work had triggered our interest to the subject, we start illustrating its main findings shown in Fig.11. The upper figure shows time evolution of the GW energy, in different simulations. In all cases the evolution is simply linear: it means that the GW generation rate remains constant *long after* the phase transition itself is over. Their further studies had shown that GW originates from the long-wavelength sound waves, not from the rotational modes, which are several orders of magnitude down, see lower Fig.11.

The sound velocity squared is proportional to the energy of the sound waves, which one can also view as $\sim \omega_k n_k k^3$, where $\omega_k = c_s k$ is the sound frequency and n_k is the density of the momentum distribution, to be discussed below. So, a flat spectrum seen in lower Fig.11 corresponds to $n_k \sim 1/k^4$. The spectra go 2 orders of magnitude from the UV scale T down, and evolution time about 3 orders of magnitude. The question is what happens near the IR end of the dynamical range, many orders of magnitude away of what was simulated in that work.

Kalaydzyan and myself [77] discussed sound-based GW production and argued that generation of the cosmolog-

ical GW can be divided into four distinct stages, each with its own physics and scales. We will list them starting from the UV end of the spectrum $k \sim T$ and ending at the IR end of the spectrum $k \sim 1/t_{life}$ cutoff by the Universe lifetime at the era :

- (i) the production of the sounds
- (ii) the inverse cascade” of the acoustic turbulence, moving the sound from UV to IR
- (iii) the final transition from sounds to GW.

The stage (i) remains highly nontrivial, associated with the dynamical details of the QCD (or electroweak EW) phase transitions. The stage (ii), on the other hand, is in fact amenable to perturbative studies of the acoustic cascade, which is governed by Boltzmann equation. It has been already rather well studied in literature on turbulence, in which power attractor solutions has been identified. Application of this theory allows to see how small-amplitude sounds can be amplified, as one goes to smaller k . The stage (iii) can be treated via standard loop diagram for sound+sound \rightarrow GW transition,

Before we come to it, let us briefly remind the numbers related to the QCD and electroweak transition. Step one is to evaluate redshifts of the transitions, which can be done by comparing the transition temperatures $T_{QCD} = 170$ MeV and $T_{EW} \sim 100$ GeV with the temperature of the cosmic microwave background $T_{CMB} = 2.73$ K. This leads to

$$z_{QCD} = 7.6 \times 10^{11}, \quad z_{EW} \sim 4 \times 10^{14}. \quad (15)$$

At the radiation-dominated era – to which both QCD and electroweak ones belong – the solution to Friedmann equation leads to well known relation between the time and the temperature [163]

$$t = \left(\frac{90}{32\pi^3 N_{DOF}(t)} \right)^{1/2} \frac{M_P}{T^2} \quad (16)$$

where M_P is the Planck mass and $N_{DOF}(t)$ is the effective number of bosonic degrees of freedom (see details in, e.g., PDG, Big Bang cosmology). Plugging in the corresponding T one finds the the time of the QCD phase transition to be $t_{QCD} = 4 \times 10^{-5}$ s, and electroweak $t_{EW} \sim 10^{-11}$ s. Multiplying those times by the respective redshift factors, one finds that the t_{QCD} scale today corresponds to about 3×10^7 s \sim year, and the electroweak to 5×10^4 s \sim day.

GW from the electroweak era are expected to be searched for by future GW observatories in space, such as eLISA. The observational tools for GW at the period scale of *years* are based on the long-term monitoring of the millisecond pulsar phases, with subsequent correlation between all of them. The basic idea is that when GW is falling on Earth and, say, stretches distances in a certain direction, then in the orthogonal direction one expects distances to be reduced. The binary correlation function for the pulsar time delay is an expected function of the angle θ between them on the sky. There are existing collaborations – North American Nanohertz Observatory for Gravitational Radiation, European Pulsar

Timing Array (EPTA), and Parkes Pulsar Timing Array – which actively pursue both the search for new millisecond pulsars and collecting the timing data for some known pulsars. It is believed that about 200 known millisecond pulsars constitute only about 1 percent of the total number of them in our Galaxy. The current bound on the GW fraction of the energy density of the Universe is approximately

$$\Omega_{GW}(f \sim 10^{-8}\text{Hz})h_{100}^2 < 10^{-9}. \quad (17)$$

Rapid progress in the field, including better pulsar timing and formation of a global collaborations of observers, is expected to improve the sensitivity of the method, perhaps making it possible in a few year time scale to detect GW radiation, either from the QCD Big Bang GW radiation we discuss, or that from colliding supermassive black holes.

The temperature T provides the micro (UV) scale of the problem: here the phase transition provides the sound source. The cosmological horizon is the IR cut-off on the gravitational radiation wavelength: here two sounds generate the GW. In between UV and IR scales there is the “dynamical range”, of about 18 orders of magnitude! The challenge is to understand if and how the *inverse acoustic cascade* can be developed there, and what n_k dependence is generated. It turns out that the answer crucially depend on the *sign* of the third derivative of the sound dispersion curve

$$\omega = c_s k + Ak^3 + \dots \quad (18)$$

which remains unknown, both for QGP and electroweak plasma.

If $A > 0$ sound decays 1 into 2 is kinematically possible. If so the turbulent cascade based on 3-wave interaction can only develop in the *direct* – that is toward large k or UV – cascade, not the one we are interested in.

However when the dispersive correction coefficient $A < 0$, is negative, and there are no binary decays of the sounds, the answer is different. Turbulent cascade switches to higher order process, of $2 \leftrightarrow 2$ scattering and $1 \leftrightarrow 3$ processes, (see e.g. [45]) generating an *inverse* cascade, with a particle flow directed to IR. In this case of the weak turbulence, the index of the density momentum distribution $n_k \sim k^{-s}$ is known to be

$$s_{weak} = 10/3 \quad (19)$$

Furthermore, as discussed in [77], large value of the density at small k leads to violation of weak turbulence applicability condition and the regime is known as “strong turbulence”. We follow the philosophy of Berges et al renormalization of similar cascades in the case of relativistic scalar with quartic interaction. Unfortunately sound waves have triple vertex are they are Goldstone particles, so the problem is much more involved. The scattering is dominated by t -channel diagrams with small denominators, producing small angle scattering with large cross sections, like it is the case for gluons. We do not yet have

a complete solution of this problem, only an estimate of the renormalized index which we think is increasing to $s_{strong} \sim 5$. Given huge – 18 decades for QCD – dynamical range of the problem at hand this will imply a significant increase of n_k at IR.

Another key result of our paper [77] is the calculation of the transition rate of the sound to gravity waves. We found it to be rather simple process, an *on shell* collision of the two sound waves. The calculation of the rate [77] is straightforward, following from the evaluation of the “sound loop” diagram (already discussed in the previous section, but in different kinematics). Since two sounds collide, it depends quadratically on n_k : so the GW production can be hugely amplified by the inverse acoustic cascade.

IV. THE PRE-EQUILIBRIUM STATE, GLOBAL OBSERVABLES AND FLUCTUATIONS

A. Perturbative versus non-perturbative paradigms

The requirements to any theory of the early stage can be formulated as follows: It should be able to

- (i) specify certain the wave function of the colliding particle, in a wide rapidity range;
- (ii) explain what happens at the collisions and just after it;
- (iii) explain how it evolves into the final observed hadronic state.

It is perhaps fair to say, that approaches based on the weak coupling (pQCD) has been able to explain (i) and (ii) but not (iii). Strong coupling ones (AdS/CFT) can do (iii) but not (i,ii).

More specifically, perturbative (pQCD) regime is natural for hard processes, for which the QCD running coupling is weak. Already in 1970’s the pQCD developed *factorization framework*, which divided production amplitudes into “past”, “during” and “after” parts. The “past” and “after” parts are treated empirically, by structure (or distribution) and fragmentation functions. The “during”, near-instantaneous, part is described by explicit partonic process under consideration. (These three stages is the simplest example of three goals formulated above.) The strength of this approach is based on the separation of hard and soft scales, by some normalization scale μ , on which the final answer should not depend. Dependence of PDFs and fragmentation functions on μ is described by renormalization group tool, the so called DGLAP evolution: it let us tune them to the particular kinematics at hand. It works very well for very hard processes: high energy physicists at LHC looking at the electroweak scale and beyond, $Q > 100 \text{ GeV}$, do not need to know anything else. People who want to study mini-jets have to worry to “higher twist” corrections to GLAP, not under control yet.

Yet pQCD approach has serious weaknesses as well.

The PDFs describe only the *average* nucleon (or nucleus). As soon as a particle is touched – e.g. the impact parameter (multiplicity bin) is selected – factorization theorems are no longer applicable. The absence of good practical models describing partonic state with fluctuations remains a problem: e.g. for understanding pp collisions with multiplicity several times the average one. As we will discuss below in detail, pQCD can hardly be used for assessing the transverse plane distributions/correlations of partons.

For “baseline” processes – minimally biased pp, pA collisions, with rather low multiplicity – pQCD processes can be supplemented by string fragmentation, leading to rather successful “event generators”, descendent of the so called Lund model. In the approximation of independent string fragmentation their relative positions/correlations/interactions are unimportant. However, experiments which trigger higher multiplicity bins and look for subtle correlations have found phenomena clearly beyond the reach of such simple models: we will discuss those in detail.

At the opposite case of high multiplicity collisions – central pA, AA – the theory of the initial state is in first approximation classical, and general initial conditions for hydrodynamics is in the zeroth approximation given just by nuclear shape and NN cross section. The main parameter hydro needs is the total entropy generated: this is taken from parton density times some empirical coefficient, entropy/parton, not yet explained. In the first approximation – including fluctuations in the positions of nucleons in versions of the Glauber or eikonal models – one also finds simple and reasonable predictions for ϵ_n and their correlations/fluctuations. The next approximations, involving fluctuating nucleons in terms of their parton substructure, have been proposed, but their relevance is disputed.

Partonic description of the initial state of the collision at asymptotically high parton density evolved into the so called Color-Glass-Condensate (CGC)- GLASMA paradigm originated from McLerran-Venugopalan model [78]. Let me briefly remind the main points. Since the number of colored objects is large, charge fluctuations will eventually also become large producing strong gauge fields known as CGC. If gluonic fields become so strong that the occupation numbers reach $O(1/\alpha_s)$, the derivative and the commutator terms are comparable and one can use *classical* Yang-Mills nonlinear equations for its description. GLASMA is a state made of such random classical fields, starting from CGC at the collision time and then evolving as the system expands, till the occupation numbers reduce to $O(1)$. Self-consistency of the model is provided by the fact that 2-d parton density define the characteristic patron *saturation momentum* $n \sim Q_s^2$, which is treated as a scale in the evolution equations. At early time the charges at each “glasma cell”, of area $\sim 1/Q_s^2$, start separate longitudinally, producing longitudinal electric and magnetic fields. Cells are statistically independent and fluctuate with their own

Poisson-like distributions. The explicit modelling of resulting field, from cells in the transverse plane, is now known as an *impact – parameter* (IP) glasma models.

High-multiplicity initial state then evolve into sQGP: we know that because it must be complemented by hydro evolution, to describe RHIC/LHC observations. We will go over observables below in more detail, let me illustrate it here by one particular observable, the *elliptic* flow v_2 . Suppose there is no sQGP stage: patrons – gluons and quarks – simply “get real” after collision, more or less like the Weitzsacker-Williams photons do in QED, fragment into mini-jets and fly to the detector. Hard partons at large momentum scale Q_s of GLASMA belonging to individual cells cannot possibly know about other cells and nuclear geometry: those would be mainly produced isotropically in the transverse plane. If they re-interact later, the probability of that is higher where there is more matter – contributing *negative* correction to v_2 . Much softer patrons, with momenta $Q \sim 1/R$, will know about the “overlap almond” shape of the initial state: their distribution will be anisotropic, perhaps even with v_2 of the order of several percents, as observed for momentum-integrated data. Thus the prediction would be of v_2 *decreasing* with p_t , to negative values. Needless to say, hydro-based theory and experiment had shown $v_2(p_t)$ to be instead growing up to $p_\perp \sim 3 GeV$, producing anisotropies as large as $O(1)$.

Strong-coupling models of the initial stage and equilibrated matter fall into two categories. One is based on classical strongly-coupled plasmas developed in [28] and based on the notion that the ratio

$$\Gamma = \frac{V_{interaction}}{T} > 1 \quad (20)$$

In other words, the potential energy of a particle exceeds its kinetic energy. Simulations and experiments with QED strongly coupled plasmas show that for relevant $\Gamma = 1 - 10$ one deals with *strongly correlated liquids*. Screening in this regime was studied in [29], and viscosity and diffusion constant in [8] in a version with electric and magnetic charges. Apart of jet quenching applications, it has not yet been used for heavy ion physics, and thus we will not discuss it here.

The second – much wider known – strong coupling framework is based on holography and AdS/CFT correspondence: we will also discuss recent progress in detail. It describes rapid equilibration by black hole formation in the dual theory space: we will discuss it in significant detail below.

B. Centrality, E_\perp and fluctuations

Before diving into theory developments, let me briefly remind some basic facts about the global observables and their fluctuations. One of the first practical question for AA collisions is determination of centrality classes, related to observables like the number of participant nu-

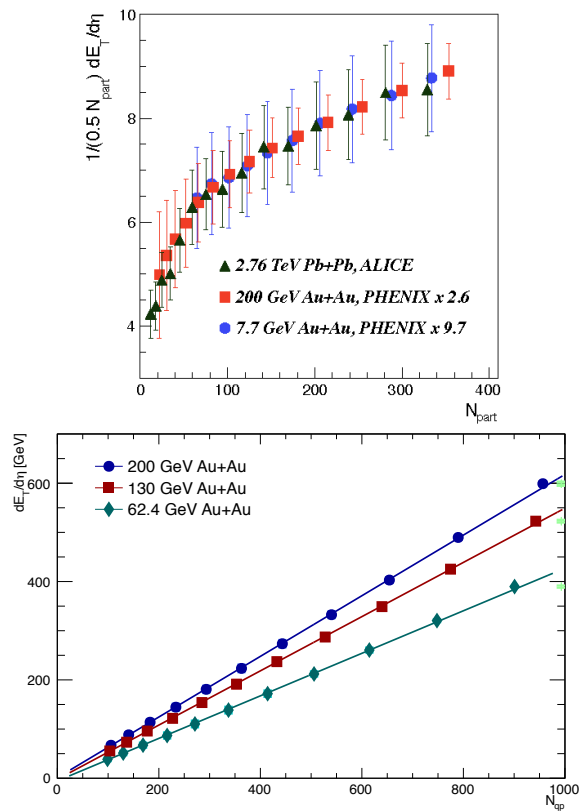


FIG. 12: Distributions over participant nucleons (a) and participant quarks (b), from [15].

cleons N_p , correlated to total multiplicity N or transverse energy E_\perp . The N_p is defined by forward-backward calorimeters, while the others by the central detectors. Correlation plots between those and precise cuts defining the centrality classes are the basic technical issues of the field.

Historically, the ratio of the E_\perp rapidity distributions for AA and pp collisions were fitted by a parameterization

$$\frac{dE_\perp^{AA}}{d\eta} / \frac{dE_\perp^{pp}}{d\eta} = (1-x) \frac{N_p}{2} + x N_{coll} \quad (21)$$

with a parameter x interpreted as an admixture of the “binary collisions” N_{coll} to the main “soft” term, proportional to the number of participants. It was a nice fit: yet we now know that a “hard” components in particle spectra - is 3-4 orders of magnitude down from the “soft” exponent (thermal-hydro contribution). So, the interpretation of x becomes questionable.

One possibility can be that “hard” interpretation just mentioned remains correct at early time, yet with subsequent equilibration and disappearance from spectra. Since hydro preserves entropy, one may argue that it will still show up in the total multiplicity. It is however more difficult to imagine preservation of E_\perp at the hydro stage.

But this is not the end of the story. The multiplicity and E_\perp distributions were measured and connected to

the geometric distribution over the r.h.s. of (21). These studies bring along a notion of some intermediate “clusters” (or ancestors as ALICE papers call it) which generate the secondaries in independent random processes of their decay.

Tannenbaum [15] provided another, and very simple, interpretation to these distributions. A nucleon is represented by 3 constituent quarks which interact separately – the additive quark model of 1960’s. Defining the number of “quark participants” N_{qp} he showed that – within a 1% accuracy (!) – it is proportional to the r.h.s. of (21). Thus, the E_\perp is perfectly linear in N_{qp} , see fig 29(b). If so, each participant quark is connected by the QCD string to the other one, and those strings are the “clusters” or ancestors for final secondaries. (We will return to “wounded quarks” concept in the discussion of the Pomeron in section VIII C.)

On the other hand, the additive quark model does not agree with pQCD paradigm, which views color dipoles – not charges – as having separate cross sections (or couplings to the Pomeron). The CGC/GLASMA theory adds another suggestion: it is its GLASMA cells that are expected to be statistically independent “clusters”, producing entropy/secondaries. (The McLerran-Venugopalan “flux tubes” differ from the QCD strings: unlike those they exist in dense deconfined phase, are not quantized and they do not have universal tension).

A view that the CGC-glasma picture is a high density regime, while simpler Lund-type models with QCD strings (and perhaps constituent quarks) are in low density regime must be correct. The problem is we do not see transition which will help us to tell at which density we need to switch between those two pictures.

Let us seek further guidance from phenomenology. Note that the number of “clusters” N which fluctuate independently define the width of observed distributions, being $O(N^{-1/2})$. So, we take these three models: (i) the usual Glauber in which N is the number of participant nucleons N_p ; (ii) its Tannenbaum’s modification with the number of participant constituent quarks N_{pq} ; (iii) and the CGC-glasma, and calculate the fluctuations.

In the last case

$$N_{GLASMA} \sim (\pi R^2) Q_s^2 \quad (22)$$

For central AA the area is geometrical Area=100 fm^2 and

$$N_p \sim 400, N_{pq} \sim 1000, N_{GLASMA} \sim 10^4 \quad (23)$$

For central pA the area is given by the NN cross section $\sigma \sim 100 mb = 10 fm^2$. So one gets very different number of “clusters”

$$N_p \sim 16, N_{pq} \sim 40, N_{GLASMA} \sim 10^3 \quad (24)$$

Therefore these models predict vastly different fluctuations.

There are two ways to measure fluctuations. The first is based on *multiplicity fluctuations*. Going to the tail of

it, beyond the most central collisions, in AA,pA and pp we find some tail usually fitted by the negative binomial or similar distribution with two parameters, or convolution of two random processes with different parameters. Its second moment should tell us how many “progenitors” (clusters, clans, ancestors) the system goes through.

The second one is to look at *angular deformations* ϵ_n . If created by statistically independent small-size objects, they are all very similar and again parametrically $O(N^{-1/2})$ [164]. We return to them in section VI C.

For E_t distributions, one finds that participant quark model describes AuAu and dAu data extremely well, while in pp it clearly underpredicts the tail of the distribution. Even 6 participant quarks – the maximal of the model – is not enough. Recalling our density estimates above, one may think that the highest multiplicity pp is the first case when “soft” models become insufficient. The models which have pQCD gluons in the wave function are doing better on the “tails”. Popular quantitative model with pQCD component is Pythia (pQCD+strings): the version used by CMS describes the multiplicity tail of pp reasonably well, while it underpredicts a bit the tail in pA . (see e.g. CMS pages with public info).

C. Anisotropy of the excited matter and the boundaries of hydrodynamics

Partonic initial state has small p_t and large longitudinal momenta: so initial out-of-equilibrium stage of the collision is highly anisotropic. However, after collisions, patrons are naturally separated in time according to different rapidities, and create “floating matter” in which cells have a spread of longitudinal momenta *smaller* than the transverse one, reversing the sign of momentum anisotropy. At later hydrodynamical stages the viscosity effects produce local anisotropy of the particle distributions, which is however small due to small viscosity of the fluid.

What happens in between is still a matter of debates. Weak coupling approaching –partonic cascades – predict anisotropy to be rising to quite large values, while the strong coupling (holographic) approaches lead to rapid convergence to small values, consistent with hydrodynamics. (For more detailed discussion see e.g. [51]).

The issue of anisotropy has two practical aspects. The experimental one – to which we return in section IV C – is a question how one can experimentally monitor the anisotropy of matter, at various stages of the evolution. The theoretical question is whether one can extend the hydrodynamical description for strongly anisotropic matter. Recently there were significant development along the line of the so called *anisotropic hydrodynamics*, or aHydro. The idea [51, 52] is to introduce the asymmetry parameter into the particle distribution, and then derive separate equation of motion for it from Boltzmann equation. More recently, solutions of various versions of hydro-

drodynamics were compared to the exact solution of the Boltzmann equation itself, derived for Gubser geometrical setting in [53]. This paper contains many instructive plots, from which I selected the normalized temperature shown in Fig.13 and the sheer stress Π_ξ^ξ shown in Fig.14. In both cases the pairs of points correspond to small and very high viscosity values, separated by two orders of magnitude and roughly representatives of the strongly and weakly coupled regimes.

Gubser’s variable ρ is the “time” coordinate. At all four plots one can see that all curves coincide in the interval $-2 < \rho < 2$, but deviate from each other both at large negative values, corresponding to the very early stage, and for large positive ones, corresponding to very late times. In fact all practical applications of hydrodynamics were indeed made inside this interval of ρ , with other regions being “before formation” and “after freeze-out”.

Solutions for two – hugely different - viscosities show a very similar trends. Israel-Stuart hydro seems to follow Boltzmann in the most accurate way. Even the free streaming regime is not very far from all hydros and exact Boltzmann: this would be surprising for the reader if we would not already know that the radial flow – unlike higher harmonics – can indeed be “faked”. If these authors would calculate the elliptic and higher flows, the results would be quite different. It is not done yet, but one expects that for $4\pi\eta/s = 100$ those would be completely obliterated.

The plots for the sheer stress show different behaviors for small and large viscosity, but again all curves coincide inside the “hydro window” of $-2 < \rho < 2$. Even going well outside that domain, we never see discrepancies between them by more than say 20%.

The overall conclusion one can draw from all of those impressive works is quite simple: all versions of hydro used in practice are very accurate for realistic viscosities $4\pi\eta/s \approx 2$ and the times hydro is actually applied in practice.

V. THE SMALLEST DROPS OF QGP

We have described above some successes of hydrodynamics for description of the flow angular harmonics, showing that those are basically sound waves generated by the initial state perturbations. We also emphasized a significant gap which still exists between approaches based on weak and strong couplings, in respect to equilibration time and matter viscosity. Needless to say, the key to all those issues should be found in experimentations with systems smaller than central AA collisions. They should eventually clarify *the limits of hydrodynamics* and reveal what exactly happen in this hotly disputed “the first 1 fm/c” of the collisions.

Let us start this with another look at the flow harmonics. What is the spatial scale corresponding to the highest n of the v_n observed? A successful description of the n -th

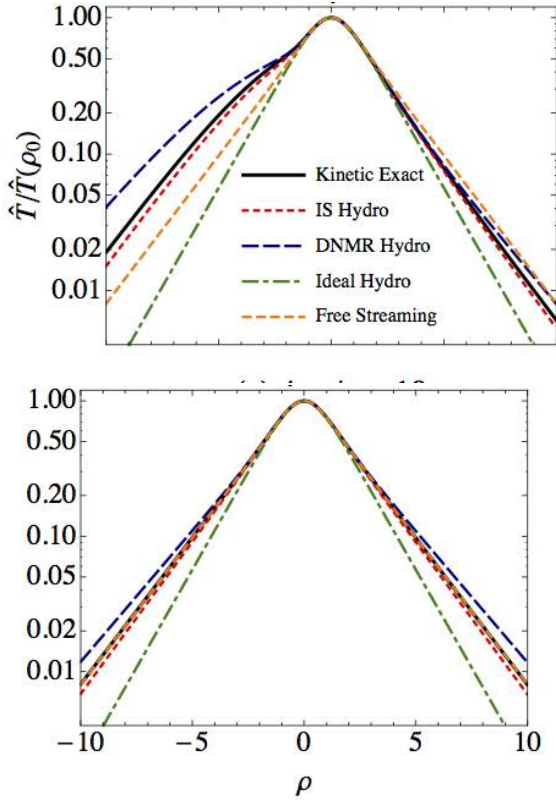


FIG. 13: From [53]: the normalized temperature for $4\pi\eta/s = 1,100$, upper and lower plots, respectively. The meaning of different curves is explained in the upper plot.

harmonics along the fireball *surface* implies that hydro still works at a wavelength scale $2\pi R/n$: taken the nuclear radius $R \sim 6 \text{ fm}$ and the largest harmonic studied in hydro $n = 6$ one concludes that this scale is still few fm. So, it is still large enough, and it is impossible to tell the difference between the initial states of the Glauber model (operating with nucleons) from those generated by parton or glasma-based models (operating on quark-gluon level). And indeed, we don't see harmonics with larger n simply because of current statistical limitations of the data sample. Higher harmonics suffer stronger viscous damping, during the long time to freezeout. In short, non-observation of $v_n, n > 6$ are *unrelated* to the limits of hydrodynamics.

(Except in the region of high $p_\perp \sim 4 \text{ GeV}$ in which indeed the relevant region becomes too thin to be treated macroscopically. Unfortunately, there is still little progress in understanding v_n at and above such momenta.)

In principle, one can study AA collisions for smaller and smaller systems, looking for the lighter nuclei which still see flow harmonics. Note that in such case the time to freeze out scales with the radius, so angular correlations stay about at the same angles and n . In our pocket formula for viscous damping, it changes TR downward,

allowing to understand the sound damping phenomena from another angle.

However, it is not the way of the actual development, as unexpected discoveries of flows in very small systems – pp and pA collisions, with high multiplicity trigger. It is those which we discuss in this chapter. As we will see, there are similarities but also important differences of the two cases.

Before we go into details, let us try to see how large those systems really are. At freezeout the size can be directly measured, using femtoscopy method. (Brief history: so called Hanbury-Brown-Twiss (HBT) radii. This interferometry method came from radio astronomy. The influence of Bose symmetrization of the wave function of the observed mesons in particle physics was first emphasized by Goldhaber et al [106] and applied to proton-antiproton annihilation. Its use for the determination of the size/duration of the particle production processes had been proposed by Kopylov and Podgoretsky [107] and myself [108]. With the advent of heavy ion collisions this “femtoscopy” technique had grew into a large industry. Early applications for RHIC heavy ion collisions were in certain tension with the hydrodynamical models, although this issue was later resolved [109].)

The corresponding data are shown in Fig.15, which combines the traditional 2-pion with more novel 3-pion correlation functions of identical pions. An overall growth of the freezeout size with multiplicity, roughly as $\langle N_{ch} \rangle^{1/3}$, is expected already from the simplest picture, in which the freezeout density is some univer-

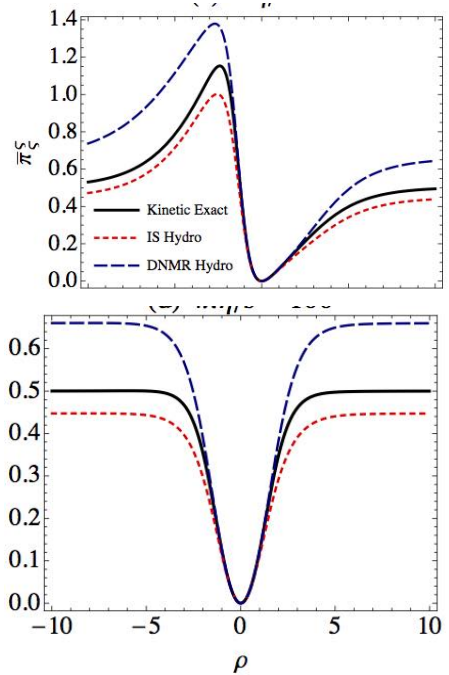


FIG. 14: From [53]: shear stress for $4\pi\eta/s = 1,100$, upper and lower plots, respectively

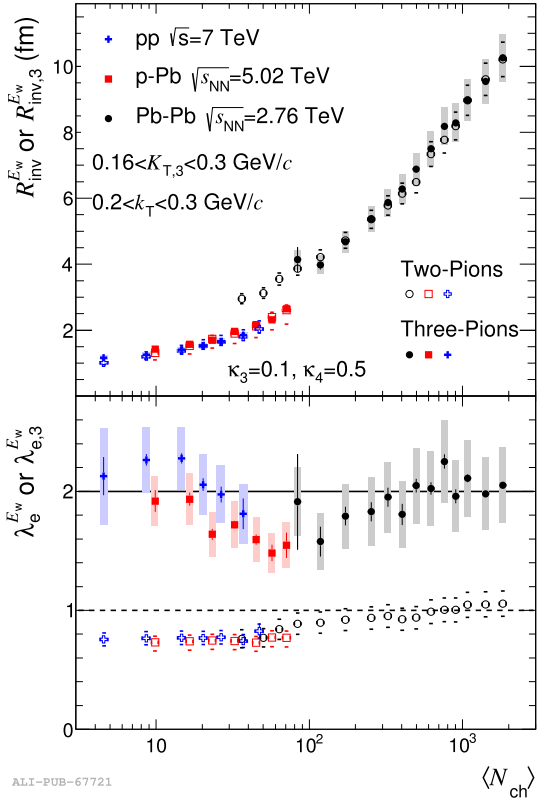


FIG. 15: Alice data on the femtoscopy radii (From [26]) (upper part) and “coherence parameter” (lower part) as a function of multiplicity, for pp , pPb , $PbPb$ collisions.

sal constant. For AA collisions this simple idea roughly works: 3 orders of magnitude of the growth in multiplicity correspond to one order of magnitude growth of the size.

Yet the pp , pA data apparently fall on a different line, with significantly smaller radii, even if compared to the peripheral AA collisions at the same multiplicity. Why do those systems get frozen at higher density, than those produced in AA? To understand that one should recall the *freezeout condition*: “the collision rate becomes comparable to the expansion rate”

$$\langle n\sigma v \rangle = \tau_{coll}^{-1}(n) \sim \tau_{expansion}^{-1} = \frac{dn(\tau)/d\tau}{n(\tau)} \quad (25)$$

Higher density means larger l.h.s., and thus we need a larger r.h.s.. So, more “explosive” systems, with larger expansion rate, freezeout earlier. We will indeed argue below that pp , pA high-multiplicity systems are in fact more “explosive”: it is seen from radial flow effects on spectra as well as HBT radii.

But *how* those systems become “more explosive” in the first place? Where is the room for that, people usually ask, given that even the final size of these objects is smaller than in peripheral AA, which has a rather

weak radial flow. Well, the only space left is at the beginning: those systems must *start accelerating earlier*, from *even smaller* size. Only then they would be able to get enough acceleration, and eventually strong collective flow, by their freezeout.

A. Collectivity in small systems

Let us briefly recall the time sequence of the main events. The first discovery – in the very first LHC run – was due to CMS collaboration [101] which found a “ridge” correlation in high multiplicity pp events, enhanced by a special trigger. That was required because, unfortunately, the effect was first seen only in events with a probability $P \sim 10^{-6}$ [165].

Switching to most central pA CMS [102] and other collaborators had observed a similar ridge there, now with much higher – few percent – probability. By subtracting high multiplicity and low multiplicity correlators CMS and ALICE groups soon had concluded, that “ridge” is accompanied by the “anti-ridge” in other hemisphere, and thus it is basically a familiar elliptic flow v_2 .

PHENIX collaboration at RHIC also found a ridge-like correction in central dAu collisions, Furthermore, their v_2 is *larger* than in pPb at LHC, by about factor 2. This was soon attributed to different initial conditions, for d and p beams, since the former have “double explosion” of two nucleons. Quantitative prediction came from pioneering hydrodynamical studies of such collisions by Bozek [42], and then many others. Hydro predicts the effect correctly: and that was the first indication for the collectivity of the phenomenon. Another contribution of PHENIX was the observation that dA HBT radii display the famous decreasing trend with p_t well known for AA collisions, which is another – and very direct – evidence for presence of the collective flow.

Truly amazing set of data came from CMS [27]. Their v_2 measurements from 4,6 and even 8 particles are shown in Fig.16. Previous data for AA collisions had shown perfect agreement between those, and new data for pA are in this respect the same. This establishes *collectivity* of the flow in pA , “beyond the reasonable doubt”.

Taken collectivity for granted, one can further ask if the v_2 observed is caused by the pre-collision correlations or by the after-collision collective flows. A very nice control experiment testing this is provided by dA and He^3A collisions. Two nucleons in d are in average far from each other and 2 MeV binding is so small that one surely can ignore their initial state correlations. So, whatever is the “initial shape” effect in pp , in dA it should be *reduced* by $1/\sqrt{2}$ because two shapes cannot be correlated. It should be reduced further in He^3A by $1/\sqrt{3}$, if the same logic holds.

Hydrodynamical predictions are opposite: double (or triple) initial explosions lead to a common fireball, with the anisotropies *larger* than in pA . Data from RHIC by PHENIX and STAR on dAu , He^3Au do indeed show

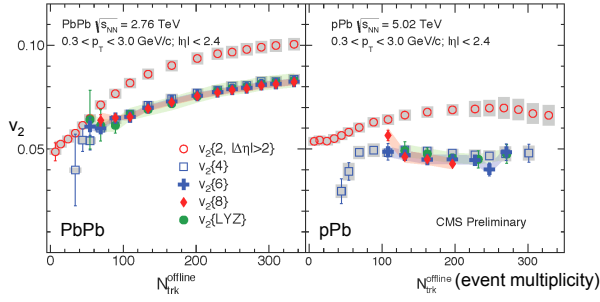


FIG. 16: CMS data [27] for v_2 calculated using 2,4,6, 8 particle correlations, as well as Lee-Yang zeroes (basically all particles). Good agreement between those manifest collectivity of the phenomenon.

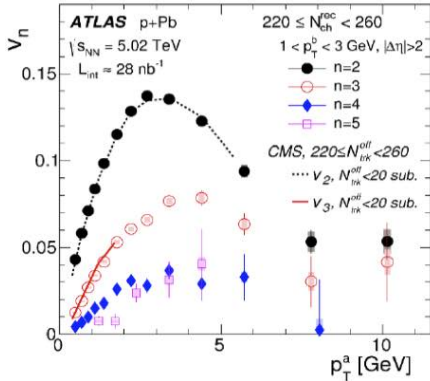


FIG. 17: v_n for $n = 2, 3, 4, 5$ versus p_t in GeV, for high multiplicity bin indicated on the figure. The points are from Atlas, lines from CMS (presentation at QM2015).

such an *increase* of the v_2, v_3 , relative to pAu , again in quantitative agreement with hydro [43, 44]. It looks like this issue is now settled.

Recently Atlas was able to perform the first measurements of higher harmonics $v_n, n = 4, 5$ in central pPb , see Fig. 17. Except at very high p_t , those two harmonics seem to be comparable in magnitude: it is the first contradiction to “viscous damping” systematics seen so far. (No idea so far why does it happen.)

B. Pedagogical digression: scale invariance of sQGP and small systems

Acceptance of hydrodynamical treatment of “small system explosions” need to pass a psychological barrier: people repeatedly ask if it is indeed possible to treat a system of less than 1 fm in size as macroscopic. (And indeed, just 15 years ago the same question was asked about systems of 6 fm size.) So, let us take a step back from the data and consider the issue of scales.

If one takes smaller and smaller cells of ordinary fluid –

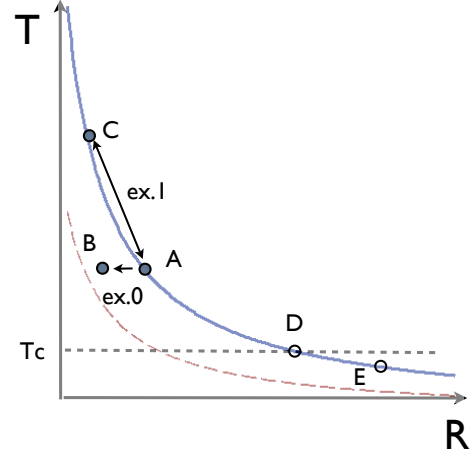


FIG. 18: (color online) Temperature T versus the fireball size R plane. Solid blue line is the adiabatic $S = const$, approximately $TR = const$ for sQGP. Example 0 in the text corresponds to reducing R , moving left $A \rightarrow B$. Example 1 is moving up the adiabatic $A \rightarrow C$. Example 2 corresponds to adiabatic expansion, such as $A \rightarrow E, C \rightarrow E$. If in reality C corresponds to pA , the freezeout occurs at the earlier point D .

such as water or air – eventually one reaches the atomic scale, beyond which water or air, as such, do not exist: just individual molecules. QGP is *not* like that: it is made of essentially massless quarks and gluons which have no scale of their own. The relevant scale is given by only one parameter T – thus QGP is approximately scale invariant. (The second scale Λ_{QCD} only enters via logarithmic running of the coupling, which is relatively slow and can in some approximation be ignored.)

As lattice simulation show, above the phase transition $T > T_c$ QGP thermodynamics soon becomes scale invariant $\epsilon/T^4, p/T^4 \approx const(T)$. The comparison of LHC to RHIC data further suggests that it is similarly true for viscosity as well $\eta/s \approx const(T)$ (although with less accuracy so far). Thus, QGP does not have a scale of its own, and thus would show *exactly the same behavior* if conditions related by the scale transformation

$$R_A/R_C = \xi, T_A/T_C = \xi^{-1} \quad (26)$$

are compared.

Consider a *thought experiment 1*, in which we compare two systems on the same adiabatic A and C . For scale invariant sQGP the points A, C are related by this scale transformation mentioned above, and have the same entropy. Since the scale transformation is approximate symmetry, we expect the same output. A smaller-but-hotter plasma ball C will explode in exactly the same way as its larger-but-cooler version A .

Let us now proceed to the *thought experiment 2*, which is the same as above but in QCD, with a running coupling. In the sQGP regime it leads to (very small, as

lattice tells us) running of s/T^3 , some (unknown) running of η/T^3 , etc. The most dramatic effect is however not the running coupling *per se*, but the lack of supersymmetry, which allows for the chiral/deconfinement phase transition, out of the sQGP phase at $T = T_c$ to hadronic phase. The end of the sQGP explosion D thus has an *absolute scale*, not subject to scale transformation!

So let us consider two systems A, C of the same total entropy/multiplicity, initiated in sQGP with conditions related by scale transformation and left them explode. The sQGP evolution would be related by nearly the same set of intermediate states (modulo running coupling) till $T \approx T_c$, after which they go into the “mixed” and hadronic stages, which are *not* even close to be scale invariant! Thus the result of the explosions are not the same. In fact the smaller/hotter system will have an advantage over the larger/cooler one, since it has *larger* ratio between the initial and final scales T_i/T_f .

(In the language of holographic models the scale is interpreted as the 5-th coordinate x^5 , and evolution is depicted as gravitational falling of particles, strings, fireballs etc toward the AdS center. The ratio of the scales is the distance along the 5-th coordinate: thus in this language two systems fall similarly in the same gravity, but smaller system starts “higher” and thus got larger velocity at the same “ground level” given by T_c .)

The hydro expansion does not need to stop at the phase boundary D . In fact large systems, as obtained in central AA collisions are known to freezeout at $T_f < T_c$, down to 100 MeV range (and indicated in the sketch by the point E . However small systems, obtained in peripheral AA or central pA seem to freezeout at D , as we will show at the end of the paper.

Short summary of these thought experiments: not only one expects hydro in the smaller/hotter system to be there, it should be very similar to that in larger/cooler system, due to approximate scale invariance of sQGP.

C. Preliminary comparison of the peripheral AA, central pA and high multiplicity pp

Now is the time to go from thought experiment with some ideal systems to the real ones. We will do it in two steps, first starting in this section with “naive” estimates for three cases at hand, based on standard assumptions about the collision dynamics, and then returning to more realistic studies of the last two cases in the next subsections.

We aim at *initial* transverse radii and density, thus we use the initial size of the nuclei rather than that of the fireball at freezeout, after hydro expansion. The multiplicity is the final one, but due to (approximate) entropy conservation during the hydro stage we think of it as a proxy for the entropy at early time as well. (Entropy generated by viscosity *during* expansion is relatively small and can be corrected for, if needed.)

(i) Our most studied case, the central AuAu or PbPb,

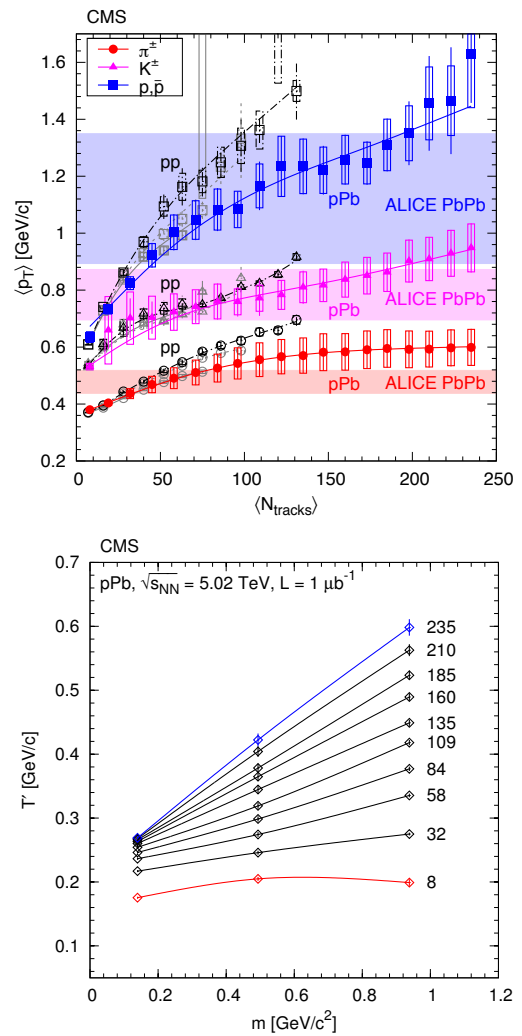


FIG. 19: (color online) (From [41].) (a) Average transverse momentum of identified charged hadrons (pions, kaons, protons; left panel) and ratios of particle yields (right panel) in the range $|y| < 1$ as a function of the corrected track multiplicity for $|\eta| < 2.4$, for pp collisions (open symbols) at several energies, and for pPb collisions (filled symbols) at $\sqrt{s_{NN}} = 5.02$ TeV. (b) The slopes of the m_{\perp} distribution T' (in GeV) as a function of the particle mass. The numbers on the right of the lines give the track multiplicity.

is the obvious benchmark. With the total multiplicity about $N_{AA} \approx 10^4$ and transverse area of nuclei $\pi R_A^2 \approx 100$ fm² one gets the density per area

$$n_{AA} = \frac{N}{\pi R_A^2} \sim 100 \text{ fm}^{-2} \quad (27)$$

which can be transformed into entropy if needed, in a standard way.

(ii) Central pA (up to few percent of the total cross section) has CMS track multiplicity of about 100. Accounting for unobserved range of p_t, y and neutrals in-

creases it by about factor 3, so $N_{pA}^{central} \sim 300$. The area now corresponds to the typical impact parameter b in pp collisions, or $\pi < b^2 > = \sigma_{pp} \approx 10 \text{ fm}^2$. The density per area is then

$$n_{pA}^{central} = \frac{N_{pA}^{central}}{\sigma_{pp}} \sim 30 \text{ fm}^{-2} \quad (28)$$

or 1/3 of that in central AA. Using the power of LHC luminosity CMS can reach – as a fluctuation with the probability 10^{-6} – another increase of the multiplicity, by about factor 2.5 or so, reaching the density N_{pA}^{max}/σ_{pp} in AA. Another approach used is a comparison of central pA with peripheral AA of the same multiplicity, or more or less same number of participants. Similar matter density is obtained.

(iii) Now we move to the last (and most controversial) case, of the high multiplicity pp collisions. (Needless to say the density is very low for min.bias events.) “High multiplicity” at which CMS famously discovered the “ridge” starts from about $N_{pp}^{max} > 100 * 3$ (again, 100 is the number of CMS recorded tracks and 3 is extrapolation outside the detector covered).

The big question now is: *what is the area?* Unlike in the case of central pA , we don’t utilize standard Glauber and full cross section (maximal impact parameters): we address now a fluctuation which has small probability. In fact, nobody knows the answer to that. Based on the profile of pp elastic scattering (to be discussed in section VIII C) I think it should correspond to impact parameter b in the black disc regime. If so $\pi b_{b.d.}^2 \sim 1/2 \text{ fm}^2$, which leads to density per area

$$n_{pp}^{max} \approx \frac{N_{pp}^{max}}{\pi b_{b.d.}^2} \sim 600 \text{ fm}^{-2} \quad (29)$$

Other evidences about glue distribution in a proton comes from HERA diffractive production, especially of $\gamma \rightarrow J/\psi$: they also suggest a r.m.s. radius of only 0.3 fm , less than a half of electromagnetic radius.

Let us summarize those (naive) estimates: in terms of the initial entropy density one expects the following order of the densities per area involved

$$\frac{dN_{maximal}^{pA}}{dA_{\perp}} \sim \frac{dN_{peripheral}^{AA}}{dA_{\perp}} \ll \frac{dN_{central}^{AA}}{dA_{\perp}} \ll \frac{dN_{maximal}^{pp}}{dA_{\perp}} \quad (30)$$

One may expect that the radial flow follows the same pattern: yet the data show it is *not* the case.

D. The “radial flow puzzle” for central pA

The simplest consequence of the radial flow is increasing mean transverse momentum. CMS data on those, as a function of multiplicity, are shown in Fig.19(a). While pp and pA data are shown by points, the AA ones (from ALICE) are shown by shaded areas: the central ones correspond to its upper edge. While one invent many mechanisms of the mean p_t growth – e.g. rescattering, larger

saturation momentum Q_s at higher multiplicity, etc – those explanations generally do to explain why heavier particles – protons – get this effect stronger than the pions.

True experimental signatures of the radial flow are based on the observation that collective flow affect spectra of secondaries of different mass differently. While (near) massless pions retain exponential spectra, with blue-shifted slope, massive particles have spectra of a modified shape. Eventually, for very heavy particles (e.g. d or other nuclei) their thermal motion gets negligible and their momenta become just mv where v is the velocity of the flow. Its distribution has a characteristic peak at the fireball’s edge.

More specifically, a measure proposed in [99] is to look at the so called “violation of the m_{\perp} scaling”. The m_{\perp} slopes T' are defined by the exponential form (above certain p_t)

$$\frac{dN}{dydp_{\perp}^2} = \frac{dN}{dydm_{\perp}^2} \sim \exp\left(-\frac{m_{\perp}}{T'}\right) \quad (31)$$

and they are the best indicators of the radial flow. A sample of such slopes for pA collisions, from CMS, is shown in Fig.19 (similar data from ALICE but for smaller multiplicities are also available, see Fig.58). The multiplicity bins (marked by 8 and 32 at the bottom-right) show the same T' for all secondaries: this is the m_{\perp} scaling indicating that the flow is absent. This behavior is natural for independent string fragmentation, rescattering or glasma models.

Flow manifests itself differently. For pions T' is simply the freezeout temperature, blue-shifted by the exponent of the transverse flow rapidity

$$T' = T_f e^{\kappa} \quad (32)$$

For more massive particles – kaons, protons, lambdas, deuterons etc – the slopes are mass-dependent. As seen from Fig.19(b), they are growing approximately linearly with the mass, and the effect gets more pronounced with multiplicity. This is the signature of the collective flow. Furthermore, the central pA bin has slopes *exceeding* those in central PbPb collisions at LHC, the previous record-holding! (Predicted to happen before experiment: see version v1 of [90].)

This gives rise to what we call *the radial flow puzzle*. Indeed, naive estimates of densities in the previous subsection may suggest that explosion in highest multiplicity pA case should still be *weaker* than in AA. Indeed, both the system is smaller and the initial entropy density seem to be smaller as well. Yet the data show the opposite: the observed radial flow strength follows a different pattern

$$y_{\perp}^{AA,central} < y_{\perp}^{pA,central} < y_{\perp}^{pp,highest} \quad (33)$$

Hydrodynamics is basically a bridge, between the initial and the final properties of the system. For the radial flow dependence on the size of the system it is convenient

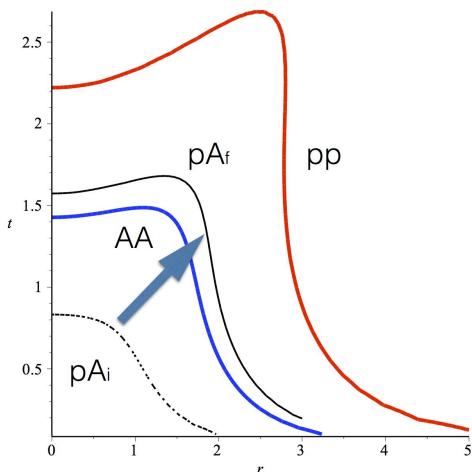


FIG. 20: (color online) The freezeout surface in universal dimensionless time t and radial distance r coordinates. (Blue) thick solid line in the middle corresponds to central AA (PbPb) collisions, (red) thick solid line on the top to the highest multiplicity pp . Two (black) thin ones correspond to central p Pb case, before and after collapse compression, marked pA_i, pA_f respectively. The arrow connecting them indicates the effect of multi string collapse.

to follow Ref. [90] based on Gubser’s flow, see section B. One single analytic solution describes all cases considered: we will proceed from the dimensional variables \bar{t}, \bar{r} with the barto dimensionless variables

$$t = q\bar{t}, \quad r = q\bar{r} \quad (34)$$

using rescaling by a single parameter q with dimension of the inverse length. In such variables there is a single solution of ideal relativistic hydrodynamics, which for the transverse velocity (B3) and the energy density (B4) dependence on time and space is known. The second equation fixes the shape of the freezeout surface, usually an isotherm $T = T_f$.

Before turning to actual plot of such surfaces, let us recall our thought experiment 1 in the subsection VB: two collisions which are conformal copies of each other would look the same in dimensionless variables. And indeed, the blue line marked AA in Fig.20 corresponds not only to central PbPb collisions at LHC, but actually to any AA collisions. (Its parameters, for the record, are $q = 1/4.3 \text{ fm}$, $\hat{\epsilon}_0 = 2531$, $T_f = 120 \text{ MeV}$, a benchmark with “realistic” radial flow.) Two black lines are for the pPb case: they both have $T_f = 170 \text{ MeV}$ and the same multiplicity but different scale parameters: $q = 1/1.6 \text{ fm}$ for the lower dotted line but twice smaller spacial scale $q = 1/0.8 \text{ fm}$ for the upper thin solid line. As an arrow indicates, in order to explain the data one has to start hydro not from the “naive” initial size, the former line, but from the “compressed” size, according to “spaghetti collapse” scenario we will discuss in section VB. If this is

done, the freezeout surface “jumps over” our AA benchmark blue line, and its radial flow gets stronger. The maximal transverse velocities on these curves (located near the turn of the freezeout surface downward) are

$$v_{\perp}^{pAu} = 0.56 < v_{\perp}^{AA} = 0.81 < v_{\perp}^{pAu,f} = 0.84 \quad (35)$$

The upper red line is our guess for the maximal multiplicity pp collisions, assuming its $q = 1/0.5 \text{ fm}$: it has even stronger radial flow, with maximal $v_{\perp}^{pp} \approx 0.93$. So, paradoxically, small systems are in fact larger than AA in appropriate dimensionless variables, and that is why their radial flow is better developed.

In summary: the observed pattern of radial flow magnitude can only be explained if the initial size of the pA system is significantly reduced, compared to the naive estimates in the preceding section.

E. Radial flow in high multiplicity pp

According to our preliminary discussion of the densities per area, in this case it is much higher than in AA collisions. The initial state must be in a GLASMA state, if there is one. Yet we do not have theoretical guidance about the size. (It is not at all surprising: those are fluctuations with small probability $\sim 10^{-6}$, and understand their precise dynamics is difficult.) Lacking good theory guidance, one may invert our logical path, and proceed as follows: (i) extract the magnitude of the flows – radial, v_2, v_3 – from the data, at freezeout. Then (ii) “solved hydro backwards”, deriving the initial conditions needed to generate such a flow.

One phenomenological input can be the mean p_t and spectra of the identified particles in high multiplicity pp : some of those we have already shown in Fig.19.

Another approach is to use is the femtoscopy method. It allows to detect the magnitude and even deformations of the flow. Makhlin and Sinyukov [110] made the important observation that HBT radii decrease with the increase of the (total) transverse momentum $k_1 + k_2 = \vec{k}_t$ of the pair. Modification of their argument for our purposes is explained in a sketch shown in Fig.21. At small k_t the detector sees hadrons emitted from the whole fireball, but the larger is k_t , the brighter becomes its small (shaded) part in which the radial flow is (i) maximal and (ii) has the same direction as \vec{k}_t . This follows from maximization of the Doppler-shifted thermal spectrum $\sim \exp(p^\mu u_\mu / T_{freezeout})$. One way to put it is to note that effective T in it is increased by the gamma factor of the flow.

Hirono and myself [113] had calculated such effect and compare the results with the ALICE HBT data [112] shown in Fig.22. We deduced the magnitude of the flow in high multiplicity pp collisions, directly visible in those data. The effect is best seen in the so called “out”-directed radius R_{out} (the top plot). While low multiplicity (connected by the blue dashed line) are basically

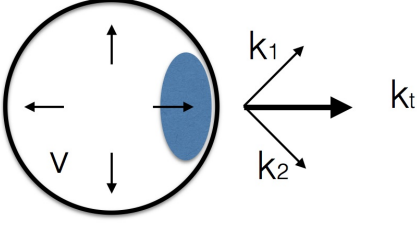


FIG. 21: Sketch of the radial flow (arrows directed radially from the fireball center) explaining how it influences the HBT radii. At small k_t the whole fireball (the large circle) contributes, but at larger k_t one sees only the part of the fireball which is co-moving in the same direction as the observed pair. This region – shown by shaded ellipse – has a smaller radii and anisotropic shape, even for central collisions.

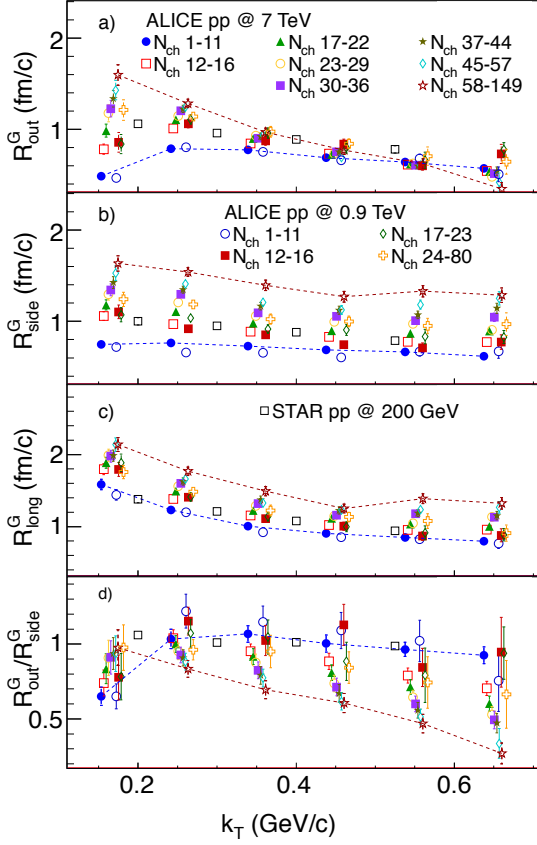


FIG. 22: HBT radii versus the pair transverse momentum k_T , for various multiplicities of the pp collisions, from ALICE [112].

independent on the pair momentum, at high multiplicity (stars and red dashed line) they are decreasing, by a rather large factor. Another consequence of the flow is anisotropy of radii. In the bottom plot the ratio of

two radii are shown: at small multiplicity it is always 1 – that is the source is isotropic – but at high multiplicity the source becomes anisotropic, the radii in two directions are quite different, with their ratio dropping to about 1/3, at the largest k_t . It means, only 1/3 of the fireball emits pairs of such momenta, a direct consequence of the flow.

In Fig.23 we show a series of calculations in which the initial QGP stage of the collision is modelled by numerical hydro solution close to Gubser analytic solution with variable parameter q . (The late stages need to deviate from Gubser since near T_c the EOS is very different from conformal $\epsilon = 3p$ assumed in Gubser’s derivation).

Let us summarize what we learned in this subsection so far. Unlike central pA , the highest multiplicity pp events are significantly denser/hotter than central AA. Very strong radial flow, seen in spectra of identified particles and HBT radii, require very small, sub femtometer, initial size of the system. In spite of high cost associated with those events, their studies are of utmost importance because here we produce the most extreme state of matter ever created in the lab.

F. Can flows in small systems be “fake”?

The question and subsequent development is due to Romatschke [121], who proposed a particular model of what I call “the fake flow”. In this scenario quarks and gluons at the QGP phase have no interactions and free stream from the point of the initial scattering. Only at some hadronization surface the system switches to hadronic cascade.

In Fig.25 one see a comparison of the radial flow profiles of the two cases, with and without interaction at the QGP phase. One can see that crudely the profiles are in fact very similar, becoming linear Hubble-like as

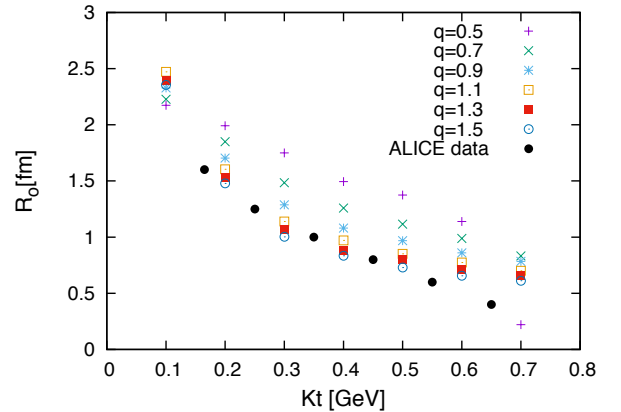


FIG. 23: From [113]: HBT radii compared to ALICE data (closed circles), for solutions starting with different initial size of the fireball, indicated by Gubser scale parameter q (which is inversely proportional to the size).

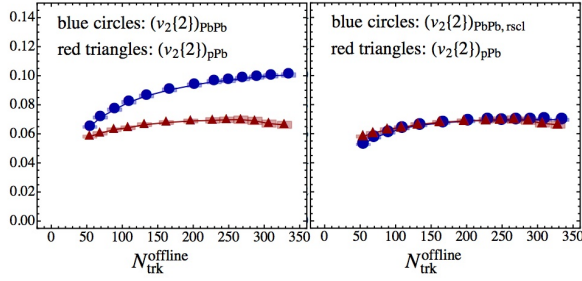


FIG. 24: The integrated $v_2\{2\}$ for PbPb and pPb vs. multiplicity from [23]. Left: Original values. Right: The fluctuation dependent elliptic flow, with the geometrical part subtracted. This geometrical part was calculated using the Phobos Glauber Model and is not a fit.

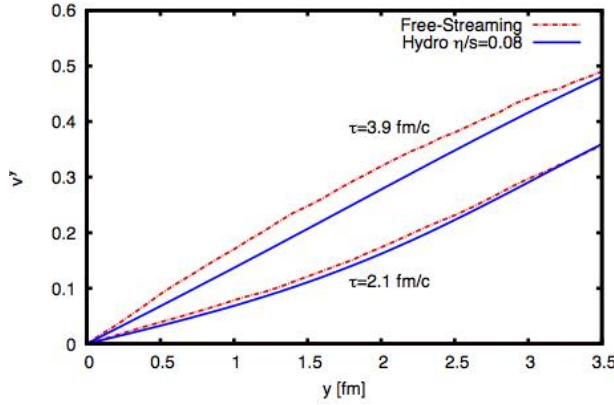


FIG. 25: Comparison of the flow profile, for hydrodynamics and free streaming, from [121].

time goes on. (In fact free streaming generates even a bit stronger flow, because free streaming uncouples from longitudinal direction, and equilibrated hydro medium does not.) Comparing particle spectra and HBT radii Romatschke shows that this “fake” radial flow is indeed *indistinguishable* from the hydro one.

What about flow harmonics? The results for PbPb collisions are shown in Fig.26. As one can see, without hydro those (crudely speaking) disappear. It is not surprising since if there is no hydrodynamics then there should be no sound waves, and initial bumps are simply dissolved without trace.

(In fact it is an interesting question how *any* v_n can be generated in the free streaming. The initial momentum distribution of partons is isotropic, and so it must be related to the interaction after hadronization. Romatschke found that indeed before hadronization they are absent. However this happens because two component of $T_{\mu\nu}$, the flow $\sim u_\mu u_\nu$ part and the dissipative $\Pi_{\mu\nu}$ part, have nonzero values but cancel each other in sum. After hadronization the hadronic interaction kills the second component $\Pi_{\mu\nu} \rightarrow 0$ and reveals the effect of

the first one.)

Not only the “fake” flow harmonics are small, they do not show two important features of the “true” hydro ones: (i) they do not show strong increase with p_\perp ; and (ii) they do not show strong decrease with the number $\sim \exp(-n^2)$ induced by the viscosity during the time before hadronization

So, we now see that, unlike the radial flow, higher harmonics in large (PbPb) systems cannot be faked. What about smaller systems? Romatschke gives the results for pPb at LHC and dAu and He^3Au for RHIC energies. We show the first case in Fig.27, the rest can be looked at the original paper. Again the free streaming model seems to be failing for v_2 , is somewhat marginally possible for

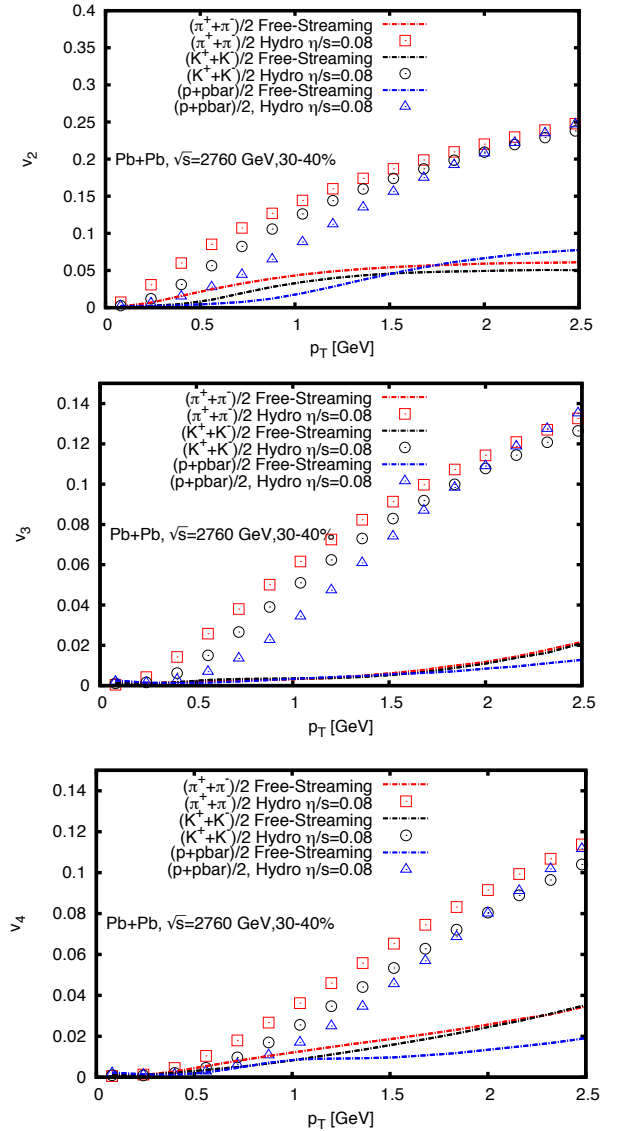


FIG. 26: Comparison of the flow harmonic, for hydrodynamics and free streaming for PbPb collisions, from [121].

v_3 , except for protons. The v_4 are comparable but both too weak to be observed.

So, flow harmonics seem not to be “faked” even for smaller systems. Yet, taking into account remaining uncertainties of the initial stage models and thus ϵ_n values, this conclusion is not as robust as for the AA. Perhaps some scenarios intermediate between equilibrated hydro and free streaming, with larger viscosity, may still be possible in these cases.

G. Shape fluctuations: central pA vs peripheral AA

Scaling relation between central pA and peripheral AA has been proposed and tested by Basar and Teaney [30].

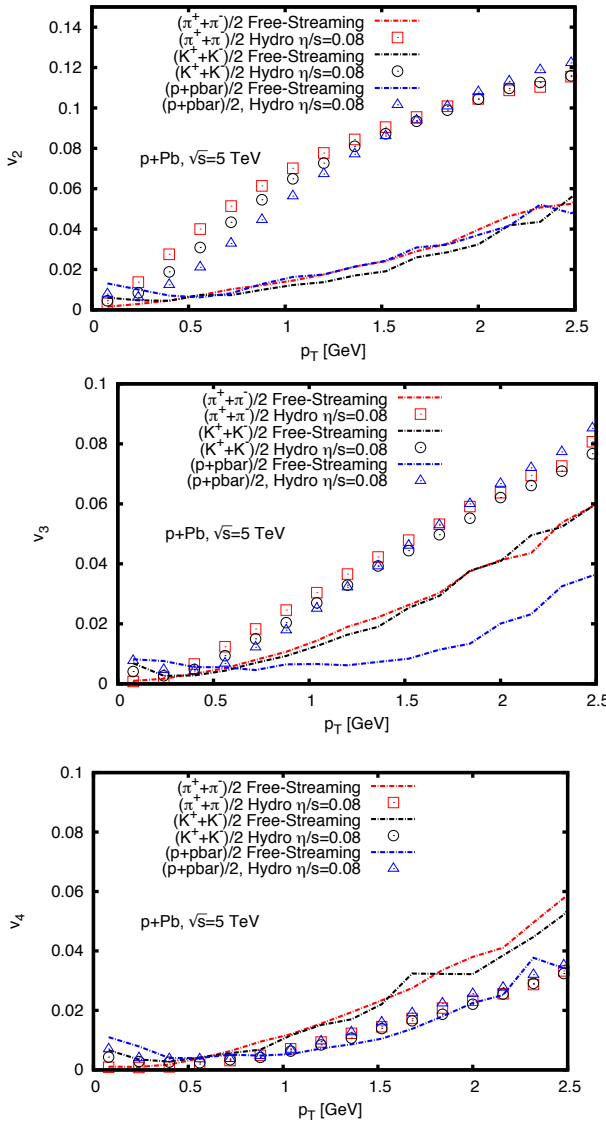


FIG. 27: Comparison of the flow harmonic, for hydrodynamics and free streaming in the pPb central bin, from [121].

Step one of their paper has been prompted by the fact (noticed in the CMS paper already): at the same multiplicity, v_3 in central pA and peripheral AA are basically the same. Some people called for new paradigms based on this fact: but in fact it is hardly surprising: equal multiplicity means equal number of participant nucleons, and thus equal fluctuations of the shape. After Basar and Teaney removed the geometrical contribution to v_2 in peripheral AA, they found that the remaining – fluctuation-driven – part of elliptic flow is also the same in both cases, see Fig.24.

Their second proposal is that the p_t dependence of (the fluctuating part) of the v_n has an universal shape, and AA and pA data are only different by a scale of mean p_t

$$v_n^{pA}(p_t) = v_n^{pA}\left(\frac{p_t}{\kappa}\right) \quad (36)$$

where the scaling factor is defined as

$$\kappa = \frac{\langle p_T \rangle_{pPb}}{\langle p_T \rangle_{PbPb}} \approx 1.25 \quad (37)$$

and is due to difference in the radial flow. This relation also works well.

two possible effects, as the multiplicity grows:

- (i) it increases the initial temperature T_i . Since the final one is fixed by hadronization near the phase transition $T_f \approx T_c$, the contrast between them gets larger and hydro flow increases;
- (ii) the initial size of the fireball *decreases*, increasing the initial temperature T_i even further.

VI. EQUILIBRATION IN QCD-BASED MODELS

A. CGC and turbulent GLASMA

The idea of continuity, from a state before collision to early time after it, is most directly realized in the so called CGC-GLASMA approach. Technically it is based on McLerran-Venugopalan argument [78] that high density of partons leads to large color charge fluctuations, which should create strong color fields. If fields are strong enough, then classical Yang-Mills equations are sufficient, and those can be solved numerically. It is important that at this stage the fields get strong, the occupancy of gluons $n_g \sim 1/\alpha_s \gg 1$ and rescaling them one can get the coupling out of YM equations. It means that GLASMA is non-perturbative, in spite of weak coupling. It remains so till gluon occupation numbers drop to their thermal magnitude $n_g \sim 1$.

When density of gluons gets large enough and non-linear effects become important, glasma is in its “dense regime”. Its boundary in a “glasma phase diagram” is shown in Fig.28. It is defined by the saturation momentum $Q_s(x)$, separating it from the dilute or partonic phase. It is expected to grow with collision energy (smaller x) and higher atomic number A .

A good news from the plot is that at the highest LHC energies and $A Q_s^2 \sim 10 \text{ GeV}^2$, perhaps in the perturbative domain. I however would not accept that the “confining regime” at the bottom of the figure is delegated to very small $Q^2 < 0.03 \text{ GeV}^2$. In fact the boundary of pQCD is a factor 30 or more higher: there are no gluons with virtuality below 1 GeV! Nambu-Jona-Lasinio noted (already in 1961!) that some strong non-perturbative forces turns on at $Q < 1 \text{ GeV}$, creating chiral symmetry breaking. By now we have plenty of evidences from the lattice simulations that all correlation functions of the gauge fields do not behave perturbatively at distances larger than 0.2 fm or so. Heavy quark potential is also nor Coulombic but string-like, and the string width is only .2 fm or so.

Theoretical study of parton equilibration in weak coupling domain has a long history. The so called “bottom up” approach by Baier, Mueller, Schiff and Son [79] was based on soft gluons radiated by scattered hard partons. The name means that thermal occupation starts from the IR end. (Note that it is opposite to the “top-down” equilibration in holographic models we will discuss below.) The main prediction of that model was the equilibration time and the initial temperature scaling with the coupling

$$\tau_{eq} \sim 1/(\alpha_s^{13/5} Q_s), \quad T_i \sim \alpha_s^{2/5} Q_s \quad (38)$$

Some details were changed as later one tried to incorporate Weibel, Nielsen-Olesen and any other instabilities which may occur into the model. The validity domain of this theory is restricted by its core assumption of small angle scattering of the gluons, justified by large impact parameters of the order of inverse (perturbative) Debye mass. Perturbative means $M_D \approx gT \ll T$ or small $g \ll 1$. If so, $g = 1, \alpha_s = 1/4\pi$ and one finds very long equilibration time $\tau_{eq} Q_s \sim 700$ exceeding du-

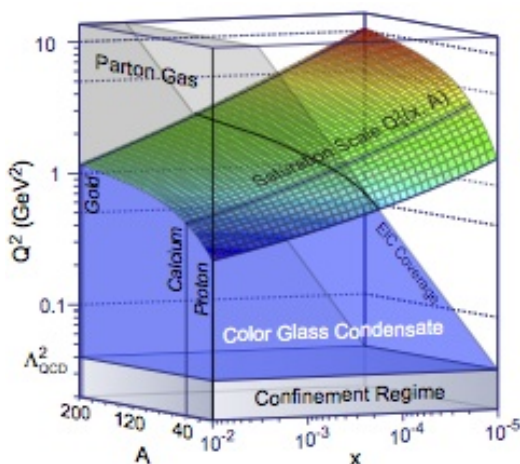


FIG. 28: The CGC phase diagram: the saturation momentum Q_s as a function of fraction of momentum x and the atomic number A , from [82].

ration of the collisions. (Not surprisingly, the pre-RHIC perturbative predictions have been that no QGP will be produced, just some “fireworks of mini-jets”, with small rescattering corrections.) One may take “more realistic” $\alpha_s = 1/3, 1/2$ and get shorter time, but then the question is whether pQCD series are at such coupling meaningful, and not divergent starting already from the first term.

In the last few years several groups made significant efforts to do numerical studies of parton equilibration using both Boltzmann equation or the field equations, for many field harmonics. Typically, in such studies the coupling constant is taken to be extremely small. In fact, so small that one can treat not only powers of α_s but even its log as a large parameter $\log(1/\alpha_s) \gg 1$, allowing the total GLASMA evolution scale

$$\tau_{GLASMA} \sim \frac{\log^2(1/\alpha_s)}{Q_s} \quad (39)$$

to be considered large.

Significant progress in this directions has been incorporation of certain ideas from general theory of turbulent cascades. Not going into its long history, let me just mention Kolmogorov-Zakharov stationary power-like solutions for a vast number of systems with nonlinear interaction of waves for Boltzmann equation, and time-dependent self-similar solutions. (For sound cascades in early universe some of that we already discussed in section III.) J.Berges and collaborators developed it for scalar and gauge fields, pointing out different regimes for UV and IR-directed cascades, and identifying such regimes in impressive numerical simulations.

New paradigm, resulting from this body of work, is that the pre-equilibrated plasma may be captured by a *nontrivial turbulent attractor* – certain self-similar power solution, before progressing toward thermal equilibrium. let me comment on one aspect of the result, on the momentum anisotropy p_l/p_\perp . Epelbaum and Gelis [80] performed a next-order GLASMA simulation, with $g = 0.5$, in which p_l/p_\perp keep approximately constant value during the whole time of the simulation $\tau Q_s = 10 - 40$. Berges, Schenke, Schlichting, Venugopalan [81] found that, at $g = 0.3$, the longitudinal pressure p_l/ϵ remains close to zero at similar times. These results are shown in Fig.29.

Recently Kurkela and Zhu [83] performed cascade simulations at larger couplings. In Fig.30 from this paper one can see two sets of trajectories, shown by solid and dashed lines, starting from two different initial distributions. At zero coupling (upper left curve) the longitudinal momenta of particles gets very small compared to transverse one, and anisotropy steadily increases. This is a scaling-like classical regime with a nontrivial fixed point. However all other paths stay more or less at the same initial anisotropy, and then rapidly turn downward, to locally isotropic distributions (marked by diagonal crosses at the bottom).

It is a pity there are no simulations done with λ between 0 and 0.5: perhaps at some critical coupling a bifurcation of the trajectories happens, separating those

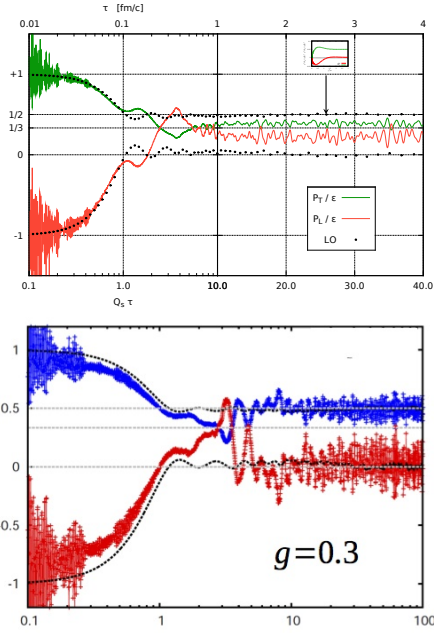


FIG. 29: (a) Upper green curve is p_t/ϵ , lower red is p_l/ϵ , as a function of time in units of saturation scale, τQ_s , at $g = 0.5$, from [80]. (b) Upper blue curve is p_t/ϵ , lower red is p_l/ϵ , at $g = 0.3$, from [81].

who proceed toward the new and the equilibrium fixed points. Yet the issue is rather academic, since the realistic relevant coupling value $\alpha_s = g^2/4\pi \approx 0.3$ corresponds to 't Hooft coupling constant $\lambda = \alpha_s N_c 4\pi \approx 10$, which is the *largest* value shown in this figure (bottom right). The corresponding curve rapidly approaches the equilibrium point, with coordinates (1,1) at this figure.

B. From Glasma to hydro

Summarizing the previous subsection in few words, one may say that weak coupling cascades predict highly anisotropic pressure $p_l \ll p_t$. The question is whether it persists for the time of few fm/c, or is rapidly reduced to the values prescribed by viscous hydrodynamics. The latter scenario is predicted by strong coupling approaches, to be discussed later. We do not know when exactly a transition between these regimes happen. This question is central for our field, and one should not jump to conclusions without serious evidences, one way or the other.

(Example of a premature statement: “No need for strong coupling to get hydrodynamization” is conclusion of Epelbaum’s QM14 talk. Hydrodynamics is not just some instantaneous value of the stress tensor, but the equations to follow. The value of viscosity (mean free path) is central to their validity: and simulations done at $g = 0.5$, $\alpha_s = 0.02$ correspond to viscosity hundreds times larger than the actual values of sQGP extracted

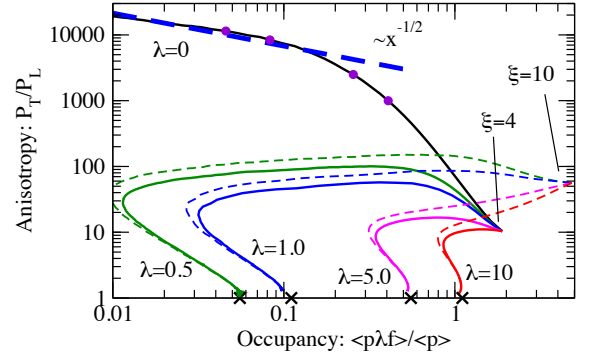


FIG. 30: From [83]: Trajectories of the systems on the occupancy-anisotropy plane for various settings. The parameter λ near curves show the corresponding 't Hooft coupling constant $\lambda = g^2 N_c$. All solid line originate from one initial distribution characterized by the anisotropy parameter $\xi = 4$, the dashed lines originate from a different point with $\xi = 10$.

from data. Anyone who doubt that should just try to derive harmonic flows from such cascades, without hydro.)

Surprisingly, there are little discussion of how to test for persistence of such anisotropy in experiment, so let me start with some comments on that. First, one can indeed measure an early-time anisotropy, via dilepton polarization, see section IX C. Second, one can study the effect of the longitudinal pressure on the rapidity distribution. Historically, the original papers of Landau focused on the longitudinal expansion, driven by gradient of p_l . However Landau’s initial condition – the instantaneous stopping – looks rather unrealistic today. Since all hydro modeling starts after certain time – when partons already passed each other – it needs certain initial distribution. Its width in rapidity, appended by the calculated longitudinal hydro effect, was compared with the data. Uncertainties, in particular related with removal of the fragmentation regions near beam rarities, makes an accuracy of p_l extraction poor.

Since 1990’s hydro effects focused on the transverse motion, the radial and elliptic flows. Since sQGP is believed to be near-conformal, the trace of stress tensor remains zero even out of equilibrium: so even for vanishing $p_l = 0$ one finds $p_t = \epsilon/2$ instead of $\epsilon/3$ in equilibrium. If strong anisotropy be there for $\tau \sim 2$ fm or so, this difference would already be seen in the magnitude of the elliptic flow. This issue deserves however dedicated studies.

Let us look what practitioners actually do while combining glasma and hydrodynamics. Fig.31 illustrate what is done in the so called impact parameter (IP) glasma approach. An important feature of glasma is independent fluctuations of color in different cells, which seeds the harmonic flows. At certain proper time – 0.2 fm/c in

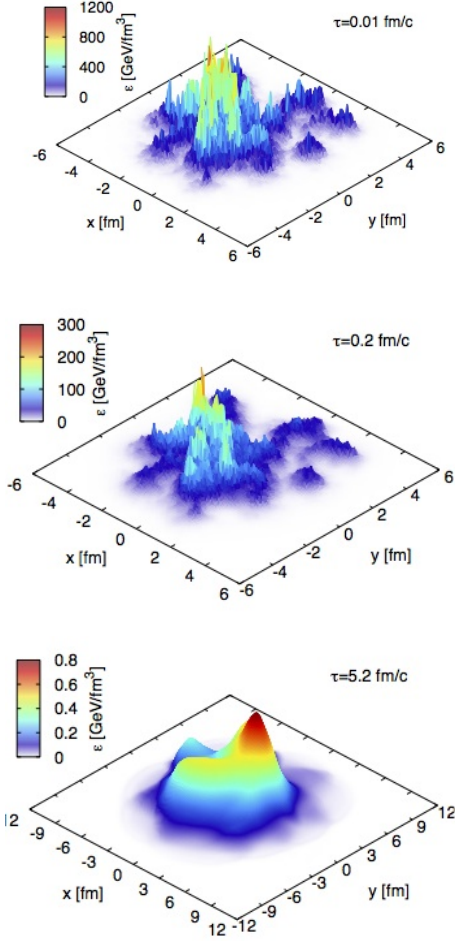


FIG. 31: From [23]: Transverse energy profile from the IP glasma model for a semiperipheral ($b = 8$ fm) Au+Au collision at $s = 200$ A GeV, at times $\tau = 0.01, 0.2,$ and 5.2 fm/c. From $\tau = 0.01$ fm/c to 0.2 fm/c the fireball evolves out of equilibrium according to the Glasma model.

this example – glasma evolution is stopped and then the energy momentum tensor is matched to ideal fluid. For technical reasons the value of the viscous tensor is put to zero.

How important is the time 0.2 fm/c selected? Note first that the second picture is hardly different from the first, except the overall scale of the energy density is reduced. Indeed, even moving with a speed of light one can only shift by 0.2 fm, a very small distance relative to the nuclear size. Glasma is diluted by purely longitudinal stretching: thus transition time can be shifted up. Many other practitioner start hydro at 0.6 fm/c or so.

By starting hydro right from the second picture Schenke and collaborators implicitly assume that hydro cells can indeed be as small as 0.2 fm, and that their code can cope with huge gradients between the cells.

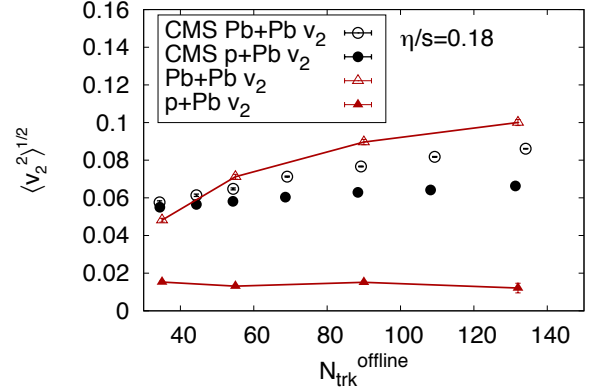


FIG. 32: (Color online) Multiplicity dependence of the root-mean-square elliptic flow coefficient v_2 in Pb+Pb (open symbols) and p+Pb collisions (filled symbols) from the IP-Glasma+music model (connected triangles) [23] compared to experimental data by the CMS collaboration.

(Note that the bottom figure, at time 5.2 fm/c, looks very different. The original bumps disappeared and instead a new one is formed. The reason is sound refuses to stand still and is moving with a speed of sound. At intersections of “sound circles” from the primary bumps random enhancements of the density are observed. Yet since the bumps are statistically uncorrelated, those should get averaged out, at least in 2-particle correlations, and only correlations from the same circle will stay.)

How many harmonics are needed to describe pictures like that shown in Fig.31? Taking 0.2 fm as a resolution and 4 fm as a size, one finds that the upper picture requires about $20 \times 20 = 400$ pixels to be represented by certain stress tensor components. At the freezeout there are only several angular harmonics observed, so 99% of the information included in those pictures does not survive till the freezeout. In the hydro simulation just described those disappear predictably, via viscous damping. It is possible that this systematic will fail at shorter wavelength: so it is worth trying to measure higher harmonics which perhaps deviate from it. Other ways to observe density waves can perhaps be invented: one of such is potential observation of those in the dilepton via the so called MSL process.

C. The initial state and angular correlations

Importance of the initial state information can be demonstrated further using “small systems”, such as central pA collisions. When a nucleon is going along the diameter of heavy nucleus the mean number of participant nucleons is

$$\langle N_p \rangle = n_0 \sigma_{NN} 2R_A \quad (40)$$

so for pPb at LHC one gets $\langle N_p \rangle \approx 16$. The question however remains, where exactly the deposited energy is?

In Fig.34 we sketched two opposite models of the initial state. In (a) we show each of the N_p participants represented by N_g gluons (ignoring sea quarks and antiquarks) from their PDFs each, so the total number of partons $N_p N_g$. We assume all gluons uncorrelated in the spot of the size of pp cross section. In (b) we had shown an alternative picture, the stringy Pomeron, in which there are no gluons but $2N_p$ QCD strings instead. Since those are “cold” (unexcited) we show those by straight lines. Note that the picture a bit exaggerates the ratio of two parameters involved. Those are (i) the mean impact parameter between the nucleons $b \sim \sqrt{\sigma_{NN}}/\pi \approx 1.6 fm$ and (ii) the size of the quark-diquark dipole $d \sim .4 fm$, so $b \gg d$.

Let us estimate the deformation of the initial state in each case. Since it is central collision, there is no mean geometrical effects and all deformations comes from fluctuations. As discussed above, for all n one expects the same magnitude

$$\epsilon_n \sim \frac{1}{\sqrt{N}} \quad (41)$$

where $N = N_p N_g$ for (a) and only $N = N_p$ for (b). Evaluating N_g from PDF's at LHC energy includes integration from $x_{min} \sim 10^{-3}$ to 1: one gets roughly the ratio

$$\frac{\epsilon_n^{(b)}}{\epsilon_n^{(a)}} \sim \frac{1}{\sqrt{N_g}} \sim 4 \quad (42)$$

Let us now switch to practical calculations and comparison to data. Schenke and Venugopalan [23] had recently studied v_2, v_3 flows in (very peripheral) AA and central pA. They found that the IP-glasma model they developed does a very good job for the former and underpredicts them in the latter case, see Fig. 32.

As we already discussed above, in the peripheral AA ϵ_2 is large, $O(1)$, in any model, and in order to get the right

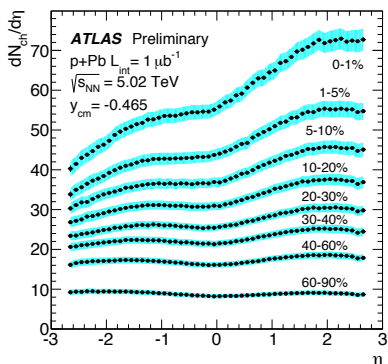


FIG. 33: Rapidity distribution in pPb collisions for different centrality classes, from [62] .

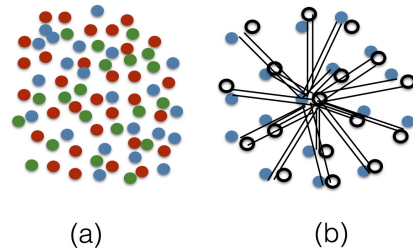


FIG. 34: Sketch of the initial state in central pA collisions. The plot (a) corresponds to IP-glasma model, with colored circles representing multiple gluons. Fig.(b) is for $N_p = 16$ Pomerons, each represented by a pair of cold strings. The open circles are quarks and filled blue circles are diquarks.

v_2 one has to have correct viscosity – which apparently these authors have. The central pA is indeed the test case: we argued above that the density is not yet large enough to apply the IP-glasma model, and that stringy Pomerons should be more applicable one. If so, using (42) we should increase the v_2 by a factor of 4, which brings it to an agreement with the CMS measurements. We thus conclude that the stringy model Fig.34(b) is preferable over the picture (a), the uncorrelated gluons.

(The actual IP glasma model is not the uncorrelated gluons: it should be uncorrelated glasma cells of $1/Q_s$ size: so our model (a) is just a straw man holding place before more consistent calculation is done.)

Above we simplistically assumed a Glauber picture in which each wounded nucleon (or a participant) interact with the projectile proton by the usual single Pomeron. This means one color exchange with each participant, who therefore is connected to the projectile by (at least) two strings.

If this picture be correct and the strings were simply independently fragmenting, the rapidity distributions of secondaries would be flat (rapidity independent) for all centrality classes. This is not the case in reality, as is seen in ATLAS data shown in Fig.33. As one can see, the peripheral bins have flat rapidity distribution: this corresponds to few strings extending from one fragmentation region to the other one without a change. Yet central bins have rather asymmetric distributions, with larger multiplicity at the Pb side.

In the Pomeron language it is explained by the so called “fan diagrams” in which one Pomeron can split into two. The “triple Pomeron vertex” is however small and we do not have developed “Pomeron cascades”. The multiplicity difference between the r.h.s. and the l.h.s. of the plot is not too dramatic, certainly not factor $N_p \sim 20$ as the old wounded nucleon model would suggest. For example, for the most commonly used centrality bin 1-5% the rapidity density $dn_{ch}/d\eta$ changes from about 35 to 55, across the rapidity interval shown in this figure. If on the Pb end there are say $N_s > 2N_p \approx 40$ strings, then on the p end there are not one or few, but still 20 strings or so. Since

the area on the l.h.s. is reduced by an order of magnitude or so, and the number only by factor 2, it is by far more dense system than the r.h.s.!

If one thinks of that, one may conclude that flows and development of collectivity should strongly depend on rapidity. Yet, at least in some crude sense, this is not the case: for example, the famous v_2 “ridge” is rather flat in rapidity. So, the issue needs more attention.

Finally, let me mention high multiplicity pp . We do not yet know ϵ_n in this case. Experiment should do 4,6 particle correlators and separate non-collective 2-particle correlations from collective ones. Hydro practitioners still have to do v_n/ϵ_n and establish its viscosity dependence and accuracy. Theoretical predictions for pp cover the whole range: from elongated transverse string [63] predicting large $\epsilon_2 \sim 1$ to a IP-glasma or “string ball” picture [73] which predicts very small ϵ_2 instead.

D. Multi-string state: spaghetti

A version of the initial state theory, alternative to glasma picture, is old Lund model, used in event generators like PYTHIA. It is suppose to be applicable for lower matter density, remaining in the confined phase. Multiple color charges, moving relativistically from each other after collision, are in such case connected by multiple QCD strings. As those are rapidly stretched longitudinally, strings become nearly parallel to each other, and we will call this state “spaghetti” for short.

Transition from such a spaghetti state to GLASMA can be relatively smooth, since in both pictures the color fields have similar longitudinal structure. Florkowski at a talk at QM14 [55] discussed dynamics of spaghetti-like GLASMA state. Interesting oscillations of such system is predicted, see Fig.35.

Transition between two picture is naturally expected when the diluteness of the QCD strings become of the

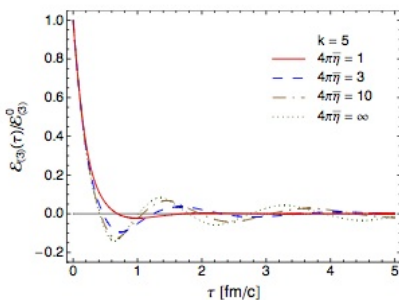


FIG. 35: Oscillation of the energy density in simulations starting from “glasma”-like initial conditions. $k = 5$ is the number of fluxes through the flux tubes, from [55].

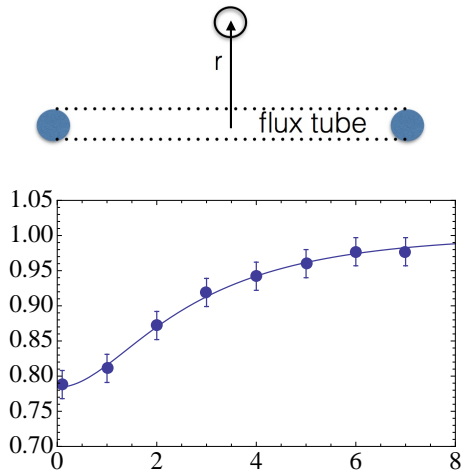


FIG. 36: (Color online). (a) Static quark-antiquark pair are indicated by shaded circles: those are connected by the flux tube (QCD string). At distance r from the tube one place the operator $\bar{q}q$, whose average is measured, with and without the static quark-antiquark pair. (b) Normalized chiral condensate as a function of the coordinate r transverse to the QCD string (in lattice units). Points are from the lattice calculation [39]. The curve is the expression (44) with $C = 0.26$, $s_{string} = 0.176$ fm.

order 1, so they can no longer be separated

$$\frac{N_{string}}{Area} \sim \frac{1}{\pi r_{string}^2} \sim 10 \text{ fm}^{-2} \quad (43)$$

where in the numerical value we use the field radius in the string $r_s \approx 0.17 \text{ fm} \sim 1/\text{GeV}$.

The interaction between the QCD strings in a

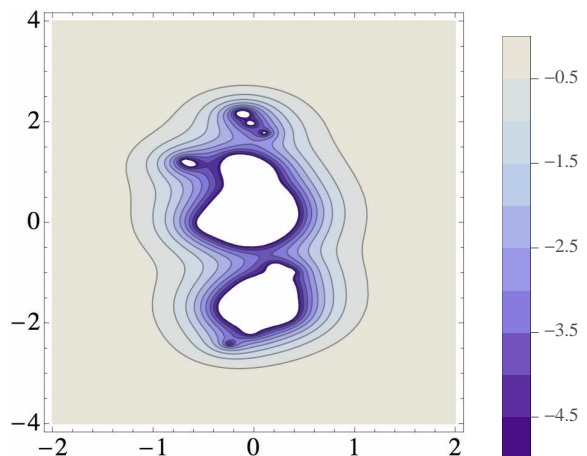


FIG. 37: (Color online) Instantaneous collective potential in units $2g_N\sigma_T$ for an AA configuration with $b = 11$ fm, $g_N\sigma_T = 0.2$, $N_s = 50$ at the moment of time $\tau = 1$ fm/c. White regions correspond to the chirally restored phase.

spaghetti state has been studied in recent paper by Kalaydzhyan and myself [73]. First of all, we observed that the string interaction is, as expected, mediated by the lightest scalar σ . Indeed, the theoretical expression

$$\frac{\langle \bar{q}q(r_\perp)W \rangle}{\langle W \rangle \langle \bar{q}q \rangle} = 1 - CK_0(m_\sigma \tilde{r}_\perp), \quad (44)$$

(where K_0 is the modified Bessel function and the “regularized” transverse distance \tilde{r}_\perp is

$$\tilde{r}_\perp = \sqrt{r_\perp^2 + s_{string}^2}, \quad (45)$$

which smoothens the 2D Coulomb singularity $\sim \ln(r_\perp)$ at small r_\perp) described lattice data well, see Fig. 36. The sigma mass here was taken to be $m_\sigma = 600$ MeV as an input, and not fitted/modified). According to our fit, the “intrinsic” width is $s_{string} \simeq 0.176$ fm, confirmed by other lattice results.

Since the strings in a spaghetti are almost parallel to each other, the problem is reduced to the set of point particles on a plane with the 2D Yukawa interaction. From the fit (44) one can see [73], that the main parameter of the string-string interaction (in string tension units) is numerically small,

$$g_N \sigma_T = \frac{\langle \sigma \rangle^2 C^2}{4\sigma_T} \ll 1, \quad (46)$$

typically in the range $10^{-1} - 10^{-2}$. So, it is correctly neglected in the situations, for which the Lund model has been originally invented – when only $\mathcal{O}(1)$ strings are created.

The interaction starts playing a role when this smallness can be compensated by a large number of strings. As seen from Fig. 36, a magnitude of the quark condensate $\sigma = |\langle \bar{q}q \rangle|$ at the string position is suppressed by about 20% of its vacuum value. So, in a “spaghetti” state one should think of the quark condensate suppression of about 0.2 times the diluteness, which is still less than 1.

On the other hand, about 5 overlapping strings would be enough to eliminate the condensate and restore the chiral symmetry. If $N_s > 30$ strings implode into an area several times smaller than σ_{in} (which is the case as we will argue below), then the chiral condensate will be eliminated inside a larger region of 1 fm in radius, or about 3 fm² in area. This is nothing but a hot QGP fireball.

As discussed above, the strings can be viewed as a 2D gas of particles (in transverse plane) with unit masses at positions \vec{r}_i . The forces between them are given by the derivative of the energy (44), and so

$$\ddot{\vec{r}}_i = \vec{f}_{ij} = \frac{\vec{r}_{ij}}{\tilde{r}_{ij}} (g_N \sigma_T) m_\sigma 2K_1(m_\sigma \tilde{r}_{ij}) \quad (47)$$

with $\vec{r}_{ij} = \vec{r}_j - \vec{r}_i$ and “regularized” \tilde{r} (45).

In our simulations we used a classical molecular dynamics code. The evolution consists of two qualitatively

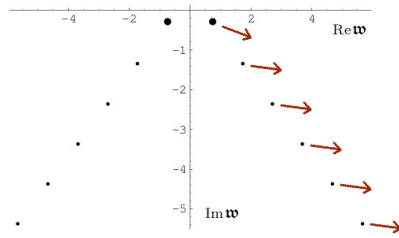


FIG. 38: A set of frequency modes, on ω complex plane, from [66]. Dots are for a particular wave vector k , arrows indicate the direction of motion as k increases.

distinct parts: (i) early implosion, which converts potential energy into the kinetic one, which has its peak when fraction of the particles “gravitationally collapse” into a tight cluster; and (ii) subsequent approach to a “mini-galaxy” in virtual quasi-equilibrium. Only the first one is physical, as the imploded spaghetti has density sufficient for production of QGP fireball, and after that explodes hydrodynamically. The whole scenario thus resembles the supernovae: implosion leads to more violent explosion later.

In Fig. 37 we show an example of the instantaneous collective potential produced by the strings in the transverse plane. The white regions correspond to the values of potential smaller than $-5 \cdot 2g_N \sigma_T (\text{fm}^{-1}) \approx -400$ MeV, i.e. the chiral symmetry can be completely restored in those regions. Large gradient of this potential at its edge can cause quark pair production, similar to Schwinger process in electric field: one particle may flow outward and one falls into the well. Such phenomenon is a QCD analog to Hawking radiation at the black hole horizon.

VII. HOLOGRAPHIC EQUILIBRATION

A. Near equilibrium

Since this development is with heavy ion community for over a decade, no general introduction is perhaps needed. And relating it to string theory background from which AdS/CFT correspondence came will take us too far from the topics. I will only comment on a couple of issues to be relevant to discussion later in this chapter.

The equilibrium setting includes the so called “AdS-black hole” metric, with its horizon located at the 5-th coordinate $z_h = 1/\pi T$, so the gauge theory – located at the $z = 0$ boundary feels the Hawking radiation temperature T . (Hawking radiation in asymptotically flat background leads to evaporation of BH. Indeed, one BH cannot heat up an infinite Universe. But AdS asymptotics means basically a finite box, and in this case BH can get into an equilibrium state with the Universe.)

Various gravity waves propagating in this background have dispersion relations $\omega(\vec{k})$ with calculable real and

imaginary parts, see an example in Fig.38. (Such quasinormal[166] modes are known for various examples of BHs for a long time, these particular ones were calculated by Kovtun and Starinets [66]). In this channel the lowest eigenvalue, shown by larger dots, is close to the origin and describes the sound mode. For reference let me mention several known terms at small k (from [54])

$$\frac{\omega}{2\pi T} = \pm \frac{\tilde{k}}{\sqrt{3}} \left[1 + \left(\frac{1}{2} - \frac{\ln 2}{3} \right) \tilde{k}^2 - 0.088 \tilde{k}^4 \right] - \frac{i\tilde{k}^2}{3} \left[1 - \frac{4 - 8 \ln 2 + \ln^2 2}{12} \tilde{k}^2 - 0.15 \tilde{k}^4 \right], \quad (48)$$

where $\tilde{k} \equiv (k/2\pi T)$. First, note that at small k the imaginary viscous term is $Im\omega \sim k^2$: we already used that fact in discussion of the “acoustic damping” phenomenology. Second, the dispersive correction to the speed of sound has positive coefficient: thus sound wave can decay into two: we already discussed that in discussion of the cosmological acoustic turbulence. Third: note that higher order corrections to viscosity are both negative. This is in contrast to some popular second order ad hoc schemes such as Israel-Stuart.

All “non-hydrodynamical modes” have $Im(\omega)/(2\pi T) = O(1)$, indicating that during the time of the order of $z_h \sim 1/(2\pi T)$ they all “fall into the black hole”. (It is amusing to note that a mystifying process of QGP equilibration is, in AdS/CFT setting, reduced to the problem number one in physics history, the Galilean falling stone in gravity field.) The essence of the AdS explanation of the rapid equilibration is thus simple: any initial objects gets irrelevant, all of those are absorbed by a black hole. The only memory which remains is their total mass, which the BH transforms into corresponding amount of Bekenstein entropy. (Plus conserved charges, if they are there.)

B. Out of equilibrium 1: the shocks

Shocks are the classic objects used in studies of out-of-equilibrium phenomena. They traditionally are divided into weak and strong shocks. In the former case there is small difference between matter before and after the shock: so those can be treated hydrodynamically, e.g. using the Navier-Stokes (NS) approximation. Strong shocks have finite jumps in matter properties. Their profiles have large gradients: so one needs some more powerful means to solve the problem, not relying on hydrodynamics, which is just an expansion in gradients.

The reason we put this example as number one is because it is the only one which can be considered in *stationary approximation*. Indeed, in the frame which moves with the velocity of the shock, its profile is *time-independent*.

Strong shocks in AdS/CFT setting were discussed in my paper [128]. A particular example worked out in detail starts with NS profile shown in Fig.39. From left to

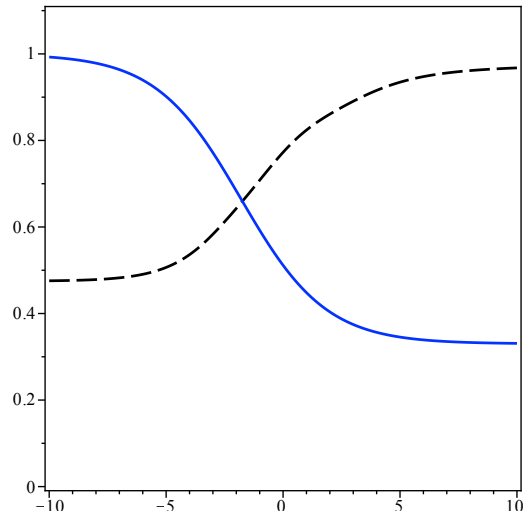


FIG. 39: An example of a strong shock in QGP, according to the Navier-Stokes hydro. Pressure shown by (blue) solid line is in units of its initial value: thus the curve starts near 1 on the left side. The (black) dashed line is the rapidity. From [128].

right the pressure decreases, and rapidity increases: the energy and momentum fluxes are tuned to be the same. One may think of it as a process in which higher-density QGP on the left, moving more slowly, “burns” into a lower density QGP floating out with higher rapidity.

In the AdS/CFT setting one however can solve the problem from first principles, by solving the Einstein equations. Of course the setting has an extra holographic dimension, and so all the functions depend not on one but on two variables: the longitudinal coordinate x and z . So I plugged in the NS solution, and worked out corrections to it (by a somewhat novel variational approach). Not going to the details of that, let me jump directly to the surprising conclusion: those corrections happen to be small, at a scale of few percent, even without any apparent small parameter in the problem.

Another tool used to correct the NS solution was the so called “re-summed hydrodynamics” by Lublinsky and myself: it also lead to corrections at the percent level. (Unfortunately, the accuracy I had on AdS/CFT solution was insufficient to tell whether both agree or not).

The lesson: all higher order gradient corrections to the NS solution have strong tendency to cancel each other.

C. Out of equilibrium 2: the falling shell

This setting has been proposed by Lin and myself [129] and it is in a way orthogonal to the previous one: there is time dependence but no dependence on space point. The motion occurs only along the holographic 5-th direction.

The physical meaning of this motion is as follows. First of all, recall that the 5-th coordinate $z = 1/r$ corresponds to a “scale”, with small values near the boundary (large r) corresponding to the UV end of the scales, and large z , small r corresponding to the IR or small momenta end. Since everything happens much quicker in UV as compared to IR, the equilibration process should naturally proceed from UV to IR, also known as “top-down” equilibration.

One can imagine that this process can in some sense be reduced to a thin “equilibration shock wave”, propagating in the z direction. The key idea of the paper [129] was that this shock can be thought of as a certain material objects – a shell or an elastic membrane – falling *under its own weight*. (See the sketch in Fig.40(a)). If this is the case, the total energy of the membrane is *conserved* (potential energy goes into kinetic). The consequences of that are very important: while the shell is falling toward the AdS center, the metric – both above and below the membrane – is actually time independent, as it can only depend on its total energy. So there is no need to solve the Einstein equations. (Recall the Newton’s proof that a massive sphere has the outside field the same as a point mass, and that there is no gravity inside the sphere. This is also true if the sphere is falling. It also remains true in GR.) In the case of an extreme black hole at the AdS center (the blue dot in Fig.40(a)) the solution consists of (i) thermal Schwarzschild-AdS metric above the shell and (ii) “empty vacuum” or the AdS_5 solution below it.

The only equation of motion which needs to be derived and solved are those of the shell itself, $r(t) = 1/z(t)$. It is not so trivial to derive it, since the coordinates below and above the shell are discontinuous. Fortunately, a thin shell collapse has already been solved in GR literature: the key to it is the so called “Israel junction condition”. The shell velocity (in time of the distant observer t) is given by the following expression

$$\frac{dz}{dt} = \frac{\dot{z}}{\dot{t}} = \frac{f \sqrt{(\frac{\kappa_5^2 p}{6})^2 + (\frac{3}{2\kappa_5^2 p})^2 (1-f)^2} - \frac{1+f}{2}}{\frac{\kappa_5^2 p}{6} + \frac{3}{2\kappa_5^2 p} (1-f)} \quad (49)$$

where $\kappa_5^2 p$ is the 5-dim gravity constant and shell elastic constant and $f = 1 - z^4/z_h^4$ is the “horizon function” in thermal AdS. The qualitative behavior of the solution is as follows: The shell starts falling with zero velocity from certain height, gets accelerated, to near the speed of light, and then is “braking” toward the horizon position z_h , which the shell asymptotically approaches with velocity zero.

After solution is found, one can calculate what different observers at the boundary – that is, in the gauge theory – will see. In particular, one may ask if/how such an observer can tell a static black hole (the thermal state with stationary horizon) from that with a falling shell?

A “one-point observer” O_1 Fig.40(b) would simply see stress tensor perturbation induced by a gravitational propagator indicated by the red dashed line. Since the metric above the shell is thermal-AdS, he will find *time-*

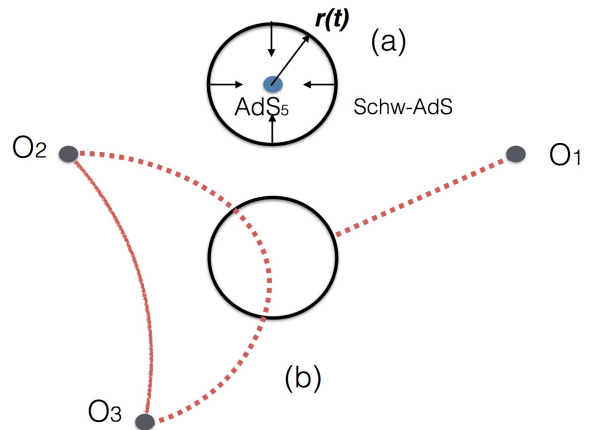


FIG. 40: (a) A sketch of a falling shell geometry. Its radius $r(t) = 1/z(t)$ which is used in the text. (b) Single-point observer O_1 and the two-point observers O_2, O_3

independent temperature, pressure and energy density corresponding to static final equilibrium. Yet more sophisticated “two-point observers” O_2, O_3 can measure certain correlation functions of the stress tensors. They will see effects from gravitons flying along the line shown by the solid line above the shell, that is in the thermal metrics, as well as from gravitons flying over the path shown by the dashed line which penetrate *below* the shell: those would notice deviations from equilibrium. Solving for various two-point functions in the background with falling shell/membrane we found such deviations. They happen to be oscillating in frequency around thermal ones. This observation is explained [129] by certain “echo” times due to a signal reflected from the shell. So, here is the lesson: one can in principle experimentally observe an echo, from the 5-th dimension!

For further discussion of the scenarios of top-down equilibration, with infalling scalar fields etc – the reader is referred to [130] and subsequent literature.

D. Out of equilibrium 3: anisotropic plasma

Our next example, due to Chesler and Yaffe, is a setting in which one starts with some *anisotropic* but homogeneous metric, and then follow its relaxation to equilibrium. It is nicely summarized by Chesler [67], so I will be brief. The metric is of the form of diagonal, time dependent but space-independent components, and Einstein equation is solved numerically. Rapid relaxation to AdS-Schwarzschild-like solution is observed. The typical behavior found is displayed in Fig.41. The characteristic relaxation time is shorter than $1/T$, even when the system is initially quite far from equilibrium.

A number of initial states can be compared, with the condition that all of the evolve to the same equilibrium energy density (or horizon, or T). While at early time the

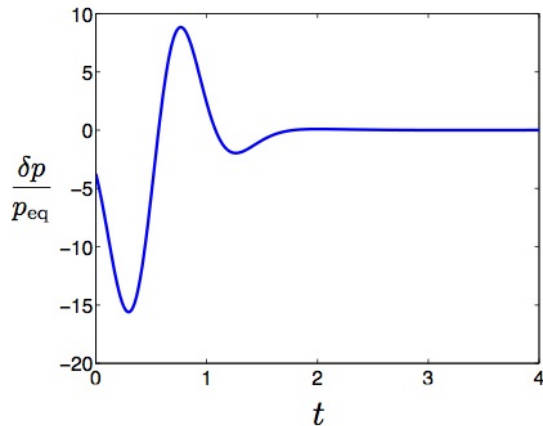


FIG. 41: Pressures anisotropy as a function of time, from [67].

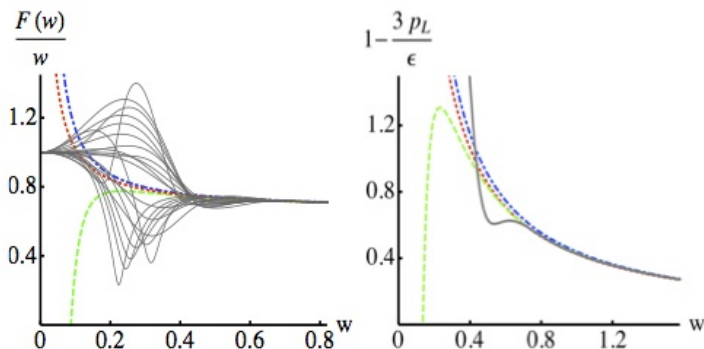


FIG. 42: (left) From Heller et al [57]: The temperature evolution combination $d \log(w)/d \log \tau$ for different initial conditions (black thin curves) converging into a universal function of $w = T\tau$, compared to hydro. (right) The pressure anisotropy for one of the evolutions compared to 1-st (NS), 2-nd and 3-ed order hydrodynamics.

momentum asymmetry can be very large – say, an order of magnitude – it becomes very small exponentially in time. Any deviations from equilibrium get strongly red-shifted as they approach the horizon.

If a more detailed analysis is made, one can locate few specific quasi normal modes. There are no hydro modes since the setting is homogeneous, and the lowest is $\lambda = (2.74 + i3.12)\pi T$. So, the basic lesson is that in the strong coupling regime the isotropization time is as short as

$$\tau_{\text{isotropization}} \sim \frac{0.1}{T} \quad (50)$$

E. Out of equilibrium 4: rapidity independent collisions

Various “bulk” objects may fall into the AdS center. In an early paper Sin, Zahed and myself [114] argued that all “debris” created in high energy collisions form bulk black hole which then falls toward the AdS center. Its hologram is the exploding/cooling fireball seen by observer on the boundary. The specific solution discussed in that paper was spherically symmetric (and thus more appropriate for cosmology than for heavy ion applications).

Subsequent series of papers by Janik and collaborators (see e.g. [56] and references therein) had developed rapidity independent “falling” horizons, corresponding to Bjorken hydro solution. In this case one has homogeneous x-independent horizon falling as a function of time $z_h(\tau)$. At late time it converges into hydro and

$$z_h(\tau) = 1/\pi T(\tau) \sim \tau^{1/3} \quad (51)$$

The variable $w = T\tau$ has the meaning of the macro-to-micro scale ratio: at late time it grows indicating that the system becomes more macroscopic and hydro more accurate. The question is *when* hydro description becomes valid and *with what accuracy*.

Fig.42 from Heller et al [57] displays time evolutions of many initial states, all approaching the same hydrodynamical solution. Fig.42(left) shows that this happens via convergence to certain *universal function* of the variable $w = \tau T$ defined by

$$\frac{dw}{d \ln \tau} = F(w), \quad (52)$$

Existence of such universality is the essence of the “re-summed hydro” proposed by Lublinsky and myself [54]. Depending on accuracy required, one may assign specific value of w at which “hydrodynamics starts”. Its value is in the range $w_i = 0.4.. - 0.6$. The plot on the right demonstrates that at such time the anisotropy is still large and viscosity is important.

The lesson from this work can be better explained by comparing its result to “naive expectations”, that hydro starts when macro and micro times are the same, $w = \tau T > 1$, and that the accuracy of hydro should be bad $O(1)$, say 100%. Calculations show instead that at *twice smaller* time $w \sim 1/2$ the accuracy of (the lowest-order Navier-Stokes) hydro suddenly becomes good, at few percent level!

Why is it so? Note, that while gradients are not yet small at that time, but the combined effect of all of them is. Lublinsky-Shuryak re-summation provides an answer: higher gradient series have alternating signs and can be Pade re-summed a la geometric series to a decreasing function.

The issue has its practical aspect, related to one of the first observations made at the first LHC PbPb run. It was found that the (charged hadron) multiplicity in PbPb collisions grow with energy a bit more rapidly than

in pp :

$$\frac{dN^{PbPb}}{dy}(y=0, s) \sim s^{0.15} \quad \frac{dN^{pp}}{dy}(y=0, s) \sim s^{0.11} \quad (53)$$

From the RHIC energy ($E = 0.2 TeV$) to the LHC, the double ratio

$$\frac{\frac{dN}{d\eta}|_{PbPb,LHC} / \frac{dN}{d\eta}|_{pp,LHC}}{\frac{dN}{d\eta}|_{AuAu,RHIC} / \frac{dN}{d\eta}|_{pp,RHIC}} = 1.23. \quad (54)$$

shows a noticeable change with the energy, which calls for an explanation.

Lublinsky and myself [72] proposed a simple form for the function $F(w)$ and calculate the entropy produced, from the time w_i on. It turns out to be about 30%. Furthermore, we get the following expression for the contribution to this double ratio $\approx 1 + \frac{3[\bar{\eta}(LHC) - \bar{\eta}(RHIC)]}{2w_i + 3\bar{\eta}(RHIC)}$ and show, that the observed growth can be naturally explained by the viscosity growth, from RHIC to LHC, predicted by a number of phenomenological models.

VIII. COLLISIONS IN STRONG COUPLING

A. Trapped surfaces and the entropy production

The simplest geometry to consider is the wall-on-wall collisions, in which there is no dependence on two transverse coordinates, and only the remaining three – time, longitudinal (rapidity), and the holographic direction – remain at play. Needless to say, it is a very formidable problem, solved by Chasler and Yaffe via clever “nesting” of Einstein equations. The reader can find explanations in a summary [67].

Collisions of finite size objects are even more difficult to solve, but those historically brought into discussion very important issues of *trapped surface* formation and the *entropy production*. It was pioneered by Gubser, Pufu and Yarom [133] who considered head-on (zero impact parameter) collisions of point black holes. The setting is shown in Fig.43(a).

Trapped surface is a technical substitute to the horizon – for this review it is not too technical to discuss the difference – and its appearance in the collision basically means that there exists a black hole inside it. Classically, all information trapped inside it cannot be observed from outside, and lost information is *entropy*. (Needless to say, for known static black hole solutions this area does give the black hole Bekenstein entropy.) So, locating this surface allows one to limit the produced entropy *from below*, by simply calculating *its area*. The reason why this entropy estimate is from below is because the trapped surface area is calculated at the *early* time $t = 0$ of the collision, not at its end. No particle can get out from trapped surface, but some can get into it *during* the system’s evolution, increasing the black hole mass and thus its entropy.

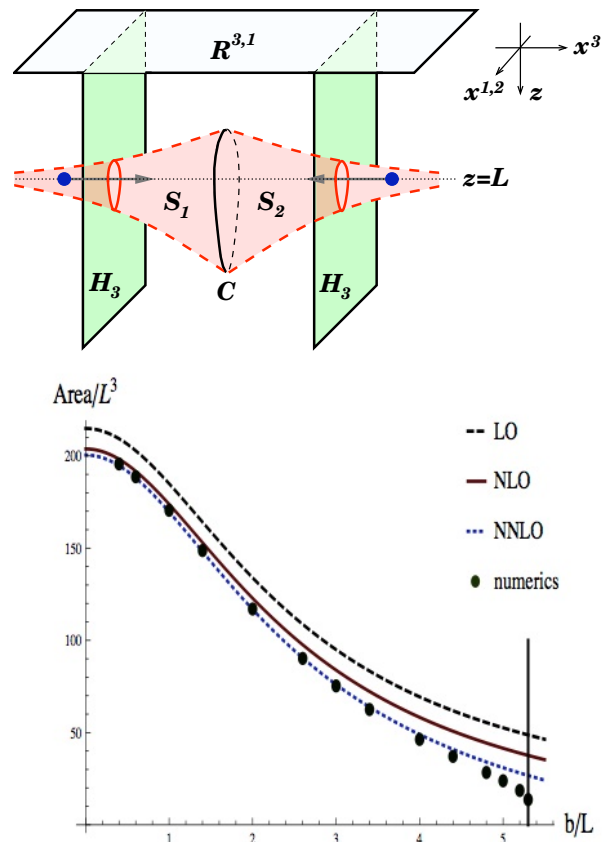


FIG. 43: (a) From [133]: A projection of the marginally trapped surface onto a fixed time slice of the AdS geometry. (b) The area of the trapped surface versus impact parameter, with the comparison of the numerical studies [134] shown by points and analytic curves from [135]. The vertical line shows location of the critical impact parameter b_c beyond which there is no trapped surface.

The setting of Gubser et al have the parameter L , the distance separating colliding b.h. from the boundary: we will discuss its physical meaning below. Naively, central collisions have only axial $O(2)$ symmetry in the transverse plane x_{\perp} , but using global AdS coordinates these authors found higher $O(3)$ symmetry of the problem, which becomes black hole at the collision moment at its center, thus in certain new coordinate

$$q = \frac{\vec{x}_{\perp}^2 + (z - L)^2}{4zL} \quad (55)$$

the 3-d trapped surface C at the collision moment becomes a 3-sphere, with some radius q_c . One can find q_c and determine its relation to CM collision energy and Bekenstein entropy. For large q_c these expressions are just

$$E \approx \frac{4L^2 q_c^3}{G_5}, \quad S \approx \frac{4\pi L^3 q_c^2}{G_5}, \quad (56)$$

from which, eliminating q_c , the main conclusion follows: the entropy grows with the collision energy as

$$S \sim E^{2/3} L^{5/3} \quad (57)$$

Note that this power is in general $(d-3)/(d-2)$ directly relates to the $d=5$ -dimensional gravity, and is different from the 1950's prediction of Fermi/Landau who predicted $E^{1/2}$ as well as from the data, which indicate the power of about 0.30 (53).

Let me now return to the meaning of the parameter L . Gubser et al relate the “depth” of the colliding objects with the nuclear size, $L \sim 1/R_A$ which cannot depend on the energy. Lin and myself [134] argued that L should rather be identified with the inverse “saturation scale”, the typical parton’s momenta in the wave function of the colliding objects

$$L \approx \frac{1}{Q_s(E)} \sim E^{-\alpha} \quad (58)$$

It becomes especially clear if one would like to turn back to wall-on-wall collisions, in which the nuclear size R_A goes to infinity while Q_s remains fixed. If so, L has a completely different scale, it is not of the $O(10 \text{ fm})$ scale but rather $O(0.1 \text{ fm})$. Furthermore, it is expected to *decrease* with the energy $L \sim 1/Q_s(E)$ with certain empirical index $\alpha \approx 1/4$. Including this dependence into (57) one gets

$$S \sim E^{(2/3)-(5/3)\alpha} \sim s^{0.125} \quad (59)$$

now in reasonable agreement with the observed multiplicity.

The generalization of this theory to non-central collisions, by Lin and myself [134], have technical details I would omit here and proceed directly to the results shown in Fig.43(b). The figure shows dependence of the trapped surface area on the impact parameter is actually from the paper by Gubser, Pufu and Yarom [135], comparing our results (points) with analytic series of curves obtained by these authors.

From gravity point of view the qualitative trend shown is clear: two colliding objects may merge into a common black hole only provided that the impact parameter is less than some critical value $b_c(E)$, depending on the collision energy. Indeed, with b rising, the trapped energy decreases while the total angular momentum increases: so at some point Kerr parameter exceeds 1 and thus no black hole can be formed. Interestingly, the calculation had shown that it happens as a jump – the first order transition in impact parameter. Just a bit below this impact parameter reasonable trapped surface and black hole exist and nothing obvious indicates that at large b none is formed.

(Note that conclusion about the first order transition is consequence of the large N_c approximation and classical gravity: those perhaps may be smoothed at finite N_c . Furthermore, the problem of trapped surface in quantum gravity is way too complicated, not studied so far.)

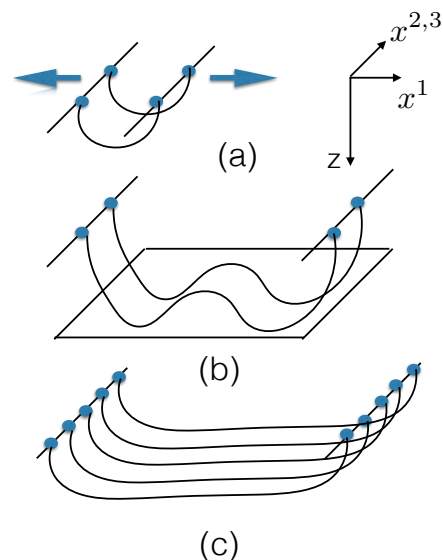


FIG. 44: (a) An early time snapshot of a pair of strings created after one color exchange. The coordinates are explained on the right: the colliding objects move with a speed of light away from each other and strings are stretched. (b) Later time snapshot, in QdS/QCD background. Strings reached the “levitation surface” shown by a rectangular shape and start oscillate around it; (c) In case of high density of many strings they can be approximated by a continuous membrane.

This transition should be interpreted as follows: at $b < b_c$ a creation of QGP fireball takes place, while the system is in hadronic phase for peripheral $b > b_c$ collisions. Still, from a physics point of view a jump in entropy as a function of impact parameter is surprising. Interesting, that the experimental multiplicity-per-participant plots do show change between non-QGP small systems and QGP-based not-too-peripheral AA collisions. It would be interesting to compare it with recent information on small systems, undergoing transition to explosive regime.

In the same paper [134] we have pointed out that the simplest geometry of the trapped surface would be that for a wall-wall collision, in which there is no dependence on transverse coordinates x^2, x^3 . Thus a sphere becomes just two points in z , above and below the colliding bulk objects. We elaborated on this in [136], considering collision of two infinite walls made of material with different “saturation scales” (e.g. made of lead and cotton) and studied conditions for trapped surface formation.

B. From holographic to QCD strings

AdS/CFT is a duality with a string theory, so fundamental strings are naturally present in the bulk. In fact already the first calculation, made in Maldacena’s original paper, the “modified Coulomb law”, was based on

the evaluation of the shape and total energy of a “pending string”, sourced by “quarks” on the boundary. (This example is so classic, that must be known to most readers.)

Lin and myself in two papers [131, 132] extended it to non-static strings. We first solved for a falling string with ends moving away from each other with velocities $\pm v$, and the second calculating its hologram (stress tensor distribution) at the boundary. This study can be thought of as a “strongly coupled version of the $e+e-$ annihilation into two quarks”. The hologram showed a near-spherical explosion: the early indication that at strong coupling setting *there are no jets*.

These works used the setting associated with conformal gauge theory: in AdS_5 string falling continues forever. This is of course *not* what we observe in the real world, in which there is confinement and there are jets. Modern strong coupling models moved into what is collectively known as AdS/QCD, for review see e.g. [137, 138]. In contrast with the original AdS/CFT, the background metric is not conformally invariant and incorporates both *confinement* in the IR and the *asymptotic freedom* in UV. These models use additional scalar (“dilaton”) field, with certain potential, complementing a gravity background.

In such settings bulk strings (and other objects) can “levitate”, at some position z_* , at which the downward gravity force is compensated by the uplifting dilation gradient. The hologram of such levitating string at the boundary is *the QCD string*: its tension, width and stress tensor distribution inside are calculable. The potential between point charges is given by a pending string: in the AdS/QCD background it changes from Coulombic at small r to linear at large r . Furthermore, allowing fundamental fermions in the bulk – via certain brane construction – and including their back reaction in a consistent manner one can get quite nice description of the so called Veneziano-QCD ($N_c, N_f \rightarrow \infty, x = N_f/N_c = fixed$) [139].

Since in the UV these models also possess a weak coupling regime, one can also model perturbative glasma, by putting certain density of color “sources” at the two planes, departing from each other. In such setting there would be smooth transition between two alternatives description of the initial state we discussed above – from the perturbative glasma made of longitudinal field cells to a “spaghetti” made of the QCD strings. When time τ is small, Fig.44(a), strings are in the UV domain (at small distance $z \sim 1/Q_s$ from the boundary) their hologram is Coulombic or glasma-like. When strings fall further and reach the “levitation point” z^* they start oscillating around it [140], Fig.44(b). This is very similar to oscillations discussed by Florkowski (see sect.VI D) without AdS/QCD.

At this point one may wander about AdS/QCD predictions for string-string interaction. This subject is now under investigation in [140]. We already discussed this issue in the QCD context above, and concluded that its

long-range attraction is dominated by the σ meson exchanges (just like between nucleons, in nuclear forces): so we need to see if it is indeed the case in the AdS/QCD, and whether one can learn something new using it. This is indeed the case, and in order to explain why we need to briefly remind the reader some basics on how hadronic spectroscopy comes out in this setting.

AdS/QCD has very few fields in the bulk – gravity, dilation and (quark-related) “tachion”. Each of them (or their mixtures) produce towers of 4-dimensional hadronic states via the quantization of their dynamics in the 5-th coordinate. One may say that hadrons are standing waves in it, and their masses are just quantized 5-th momentum. So, a new perspective on hadrons one gets from this approach is that one can calculate not only the masses but also the *wave functions* in a scale space.

So the issue studied in detail in [140] is the mechanism of hadronic flavorless scalars, which includes the σ and others. Without any changes in the setting of AdS/QCD we found very good description of (quite involved) mixing pattern of the scalars, which puzzled spectroscopists for decades. Since strings are gluonic objects and σ interact strongly with quarks, understanding of such mixing is crucial for obtaining realistic string-string forces.

Note that there is so far no temperature or entropy in the problem: the dynamics is given by classical mechanics of strings moving in certain backgrounds.

That is because we so far considered a single (or few) strings. If there are very many charge exchanges and the number (or density) of strings is high enough, Fig.44(c), one should perhaps include the back reaction of their gravity and dilaton field, or even include mutual attraction of strings. Such AdS/QCD version of multi-string dynamics from [92] of what we discussed in section VI D following [91].

Not going into detail, let me comment on just one issue. Unlike GR, in which there is only gravity and thus universal horizon definition, in holographic models physics is more complex and interesting. In particular, gluons are strings vibrations. String have their 2D worldvolumes which can be curved and have black hole of their own. What it means is the wave on the string can have modes propagating left and right, but also can have regions where both waves move right. So gluons can fall into those, but cannot escape. Such feature can be induced, in particular, by collective gravity/dilaton of the strings themselves. Its meaning is a QGP fireball, and its experimental signature is hydro explosion.

C. Holographic Pomeron

Pomeron description of hadronic cross sections and elastic amplitudes originates from phenomenology, starting from 1960’s. Veneziano amplitudes derived in a “resonance bootstrap” ideology were the original motivation for existence of QCD strings.

The Pomeron is an effective object corresponding to

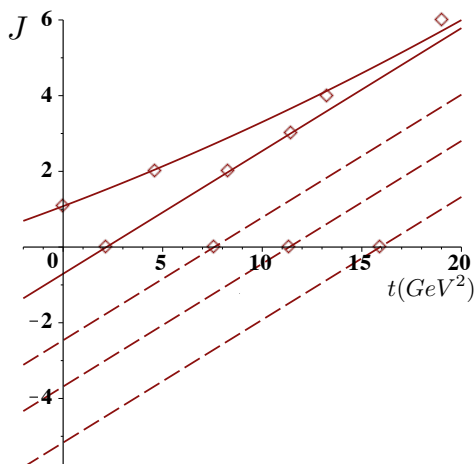


FIG. 45: Glueball masses calculated on the lattice (diamonds) organized in Regge trajectories (lines). (From [144]).

the “leading” Regge trajectory $\alpha(t)$ which dominates the high energy asymptotics of the hadron-hadron cross sections. Fig.45 is a recent version of the Regge plot (angular momentum J versus the mass squared m^2 for glueballs). The Pomeron corresponds to scattering and thus has small non-physical mass $t < 0$ and a non-integer J slightly above 1: the trajectory $\alpha(t)$ has of course physical states as well. It enters the elastic cross section in a form

$$\frac{d\sigma}{dt} \approx \left(\frac{s}{s_0}\right)^{\alpha(t)-1} \approx e^{\ln(s)[(\alpha(0)-1)+\alpha'(0)t]} \quad (60)$$

Dualism of the Pomeron is seen from the very different roles which two main parameter play, the intercept $\alpha(0)$ and the slope $\alpha'(t=0)$. The former is a dimensionless index, describing the power with which the total cross section rises. Perturbative description of the Pomeron is well developed: the so called BFKL [141] re-summation of the gluon ladders provides perturbative $O(\alpha_s)$ value for it. The Pomeron slope $\alpha'(t=0)$ has dimension [$mass^{-2}$] and is nonperturbative for sure, related to the string tension. (By the way, the “string scale” in the fundamental string theory still is traditionally called α' , the only piece of QCD phenomenology left in it, for historic reasons.) The meson/baryon Reggion slope is related to a single open string and their $\alpha' = 1/(2\pi\sigma)$, glueballs such as Pomeron are closed strings should naively have the double tension or half the slope: phenomenologically it is closer to $1/3$. It perhaps indicates changes due to *two string interaction*.

Another way to see dual nature of the Pomeron phenomenology is when one considers the so called collision profile as a function of the impact parameter b . At small b people think of color dipoles and gluon exchanges. At large impact parameter $b = 1 - 2$ fm is naturally given in terms of a (double) string exchange (see below).

Holographic models of the Pomeron aim at describing both regimes inside the same model, in the spirit

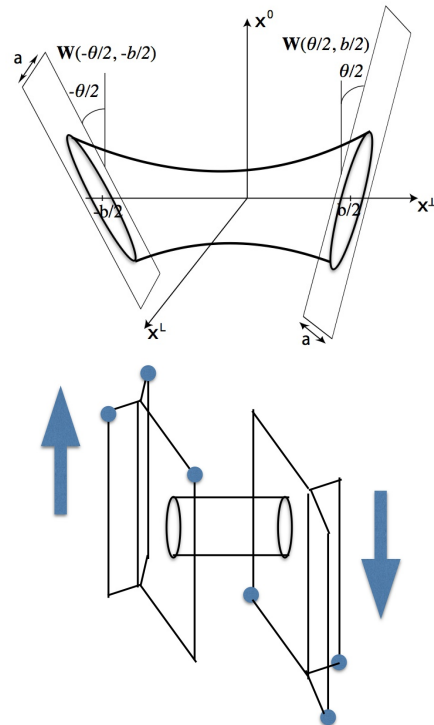


FIG. 46: (Color online) (a) Dipole-dipole scattering configuration in Euclidean space. The dipoles have size a and are b apart. The dipoles are tilted by $\pm\theta/2$ (Euclidean rapidity) in the longitudinal $x_0 x_L$ plane. (b) A sketch illustrating Pomeron exchange for baryon-baryon scattering: only one pair of quarks become “wounded quarks”.

of AdS/QCD. As the main representative of the related work let me mention two works of Zahed and collaborators [142] and [143]. Strings live in the 5-dimensional space, which is weakly coupled in UV and strongly coupled in IR. Furthermore, a semiclassical (instanton-like) derivation of the Pomeron amplitude is given in terms of closed string production – similar to Schwinger pair production in an electric field. The string worldvolume has the shape depicted in Fig.46(a): it is a “tube” connecting two flat strips, the world volume of propagating color dipoles. In Fig.46(b) we sketch a Pomeron in a collision of two nucleons, now consisting to 3 quarks and 3 string, joined by a string junction: in this case a Pomeron tube “punctures” one of the three surfaces. This produces one “wounded quark”, as we discussed in connection to Tannenbaum’s description of fluctuations.

Direct semiclassical derivation of the scattering amplitude was obtained in [143] using minimization of the Nambu-Goto action (the tube’s area). Fig.(a) indicate Euclidean setting in which difference in rapidity is represented by twisted angle θ between the direction of two dipoles. Fig.(b) illustrates a baryon-baryon scattering, in which the Pomeron tube can be connected to any of the

available dipoles, explaining the concept of the “wounded quarks” we mentioned in section IV B. More than one Pomeron means more tubes, connecting perhaps other quarks.

The classical action of this configuration provides the α' term, while the intercept deviation from 1 is due to the next order (one-loop) corrections due to string vibrations. It gives the amplitude squared: if cut in half by the unitarity cut the “tube” provides two strings of certain shape, which should be taken as the shape which “jumps from under the barrier” and should be used as the initial conditions to real-time evolution.

Not going into details, we just note that the amplitude has alternative derivation from string diffusion equation, and that 5-d space is actually important numerically. Scattering pp data as well as deep-inelastic ep (DESY data) are well reproduced by this model, see [143].

It was further argued by Zahed and myself [144] that because the “tube” has a periodic variable, resembling the Matsubara time, its fluctuations take the thermal form. Appearance of an effective temperature and entropy was new to the Pomeron problem: but once recognized the analogy to thermal strings can be exploited. We in particular argued that between two known regimes of the Pomeron – (cold) string exchange at large impact parameter b and perturbative gluon exchange at small b – there should be a third distinct regime in which a string is highly excited due to the Hagedorn phenomenon. This is what we know to happen at finite temperature gluodynamics, which possesses a “mixed” phase between the confined (hadronic) and the deconfined (partonic) phases. As it is known from decades of theoretical and numerical (lattice) research, this is described most naturally by the *near-critical strings*, namely the strings in the Hagedorn regime.

In Fig.47(a) one finds the so called profile of the elastic scattering, the Bessel transform of the imaginary part of the elastic amplitude. Basic prediction of the model is shown by the dashed line, which has the “first order transition”. By circles we show more realistic prediction of the model coming from averaging of that expression over the dipole sizes: it should be compared to empirical fit (solid line) to the LHC elastic scattering data. The difference is relatively small, although it becomes noticeable in scattering with momentum transfer Q beyond the minimum, see Fig.47(b). Apparently the predicted “transition edge” in b is a bit sharper than in the experimental data.

Concluding this section: decades-old Pomeron amplitude can be derived in a “stringy” manner, in the AdS/QCD setting. Surprisingly, this approach relates the Pomeron to the thermal theory of excited strings, with an effective temperature proportional to the inverse impact parameter. Rapid “phase transition” in b , from black to gray, corresponds to the deconfinement transition, with an intermediate regime dominated by highly excited strings (“string-balls”). So far only for the tunneling (Euclidean) stage of the system is considered, pre-

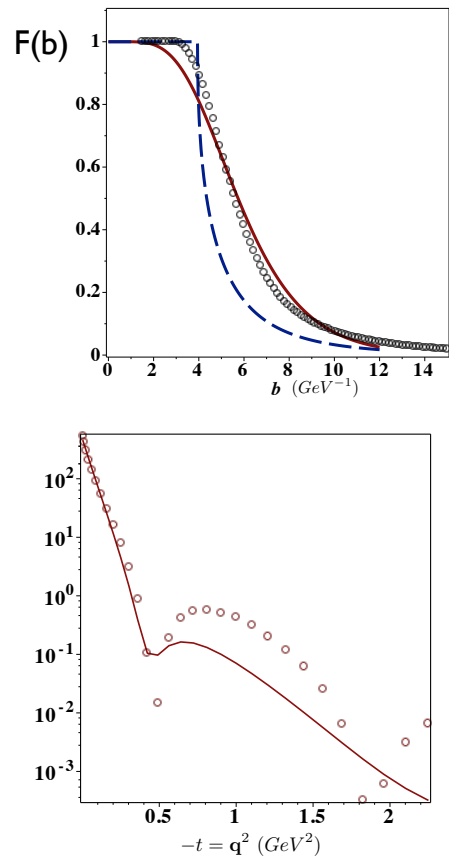


FIG. 47: (a) The solid line is the empirical LHC data parametrization. The dashed line is the shape corresponding to the “excited string” approximation for fixed sizes of the dipoles, while the circles correspond to the profile averaged over the fluctuating dipoles. (b) The corresponding elastic amplitude (the absolute value squared of the profile Bessel transform) as a function of the momentum transfer. Model prediction agrees with parameterization well at small t , up to the dip.

dicting elastic amplitude. The remaining challenge is to describe the subsequent evolution of the system and to extend this theory to *inelastic* collisions.

D. Collisions at ultrahigh energies

Discussions about Pomeron regimes ultimately drive us to the old question: what happens at the ultrahigh energies, well above the LHC reach?

The highest observed energies, by Pierre Auger Observatory and similar cosmic ray detectors, reach

$$E_{\text{lab}} \lesssim E_{\text{max}} \sim 10^{20} \text{eV}. \quad (61)$$

limited by the so-called Greisen-Zatsepin-Kuzmin (GZK) bound at which interaction with cosmic microwave photons become important.

For future comparison with the LHC observation it is convenient to convert the laboratory energy into the energy in the center of mass frame and use a standard Mandelstam invariant, assuming it is a pp collision,

$$\sqrt{s_{\max}} = (2E_{\max}m_p)^{1/2} \approx 450 \text{ TeV}. \quad (62)$$

While significantly higher than current LHC pp energy $\sqrt{s_{LHC}} = 8 \text{ TeV}$, the jump to it from LHC is comparable to that from Tevatron $\sqrt{s} = 1 \text{ TeV}$ or RHIC $\sqrt{s_{RHIC}} = 0.5 \text{ TeV}$. In view of smooth small-power s -dependence of many observables, the extrapolation to LHC worked relatively well, and further extrapolation may seem to be a rather straightforward task. And yet, smooth extrapolations using standard event generators plus, of course, the cascade codes do not reproduce correctly the experimental data of the Pierre Auger collaboration (e.g., the so called muon size of the showers).

This makes the issue subject to speculations. As an example of an exotic model let me mention the paper [64] which suggest that somehow freezeout is entirely different and the pion production becomes suppressed. According to their simulations, a model in which mostly nucleons are produced explains the Pierre Auger data better.

More modest (but still significant) change between LHC and ultrahigh energies, has been proposed by Kalaydzhyan and myself [65]. Our main statement is that at the ultra-high energies $\sqrt{s_{\max}}$ observed in cosmic rays, the “explosive regime” even in pA collision is expected to change from a very improbable $P \sim 10^{-6}$ fluctuation to the mean behavior, with $P = \mathcal{O}(1)$. The reason for it is simply an increase in mean particle (entropy) density with energy \sqrt{s} . Extrapolations suggest an increase of dN/dy by about factor 3. In Fig.48 we show the freeze out surfaces and hydro velocities at them, corresponding to our calculations. By “compression” we mean the phenomenon of “spaghetti collapse” discussed above. The mean transverse momenta of secondaries is shown in the Table.

Another generic reason for a change is that both primary collisions and subsequent cascade of ultra high energy cosmic rays all happen in the Earth atmosphere, so the targets are not protons but light (N or O) nuclei. Furthermore, the projectiles themselves are also most likely to be not protons but some nuclei. It is either also some light nuclei or some mixture including heavier ones, believed to be up to Fe .

Taking into account large pp cross section at ultra high energies, $\sim 150 \text{ mb}$, one finds that its typical impact parameters $b \approx 2 \text{ fm}$. Thus the range of the interaction in the transverse plane is comparable to the radius of the light nuclei (oxygen $R_O \approx 3 \text{ fm}$) and therefore even in the pO collisions most of its 16 nucleons would become collision “participants”. For light-light AA collisions like OO the number of participants changes from 32 (central) to zero. Accidentally, the average number of participants is comparable to the average number of participant nucleons $\langle N_p \rangle \approx 16$ in central pPb collisions at the LHC.

The question of principle still remains: and what

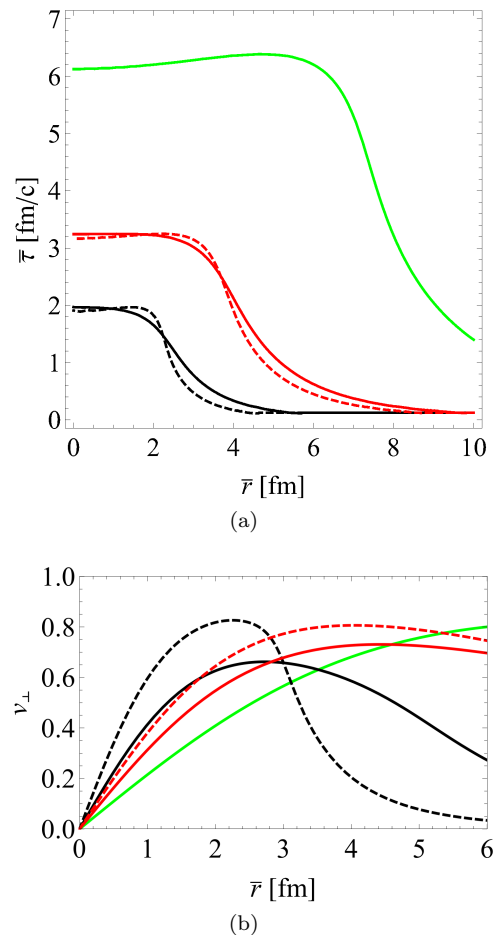


FIG. 48: (color online) (a) The freezeout surfaces in the $(\bar{\tau}, \bar{r})$ plane (no rescaling) and (b) the distribution of the transverse flow velocity on those surfaces. In both plots the green solid curve at the top is our “benchmark”, the central $PbPb$ collisions at LHC. Black solid line is for light-light nuclei collisions, black dashed (coincident with green by chance) are light-light collisions with the size compression. Similarly, red solid and red dashed are heavy-light collisions without and with the size compression, respectively.

particles	FeO	FeO comp.	pO	pO comp.	PbPb
π^\pm	0.56	0.69	0.53	0.76	0.73
K^\pm	0.71	0.88	0.66	0.96	0.92
p, \bar{p}	0.90	1.09	0.83	1.17	1.13

TABLE I: Mean p_T [GeV/c] for pions, kaons and protons obtained from the particle spectra. By “comp” we mean compressed initial state, as explained in the text.

should happen when the collision energy goes to infinity? Qian and Zahed [154] had proposed an argument which would stop multiplicity growth. The argument is that when the produced string becomes so long and heavy that it basically collapses due to its self-interaction into a black hole, the entropy produced would be limited by

the Bekenstein bound. In their opinion, not only the parton density growth, but also growth of the cross section, should stop at certain collision energy.

IX. ELECTROMAGNETIC PROBES

A. Brief summary

Let us on the onset remind standard terminology to be used below. The sources of the dileptons are split into the following categories:

- (i) instantaneous $\bar{q}q$ annihilation, known as the Drell-Yan partonic process;
- (ii) the pre-equilibrium stage, after the nuclei pass each other;
- (iii) the sQGP stage, in which matter is usually assumed to be equilibrated.
- (iv) hadronic stage in which rates are calculated via certain hadronic models;
- (v) “cocktail” contribution of leptonic decays of secondaries occurring *after* freezeout.

The corresponding windows in the dilepton mass are: $M > 4\text{GeV}$ for (i), $1 < M < 3\text{GeV}$ for (iii) and $M < 1\text{GeV}$ for (iv). So the early stage dileptons mostly fall into the 3-4 GeV window. While it contains also $J/\psi, \psi', \psi$ states, one should rely on their subtraction, which depends on mass resolution of the detector. This coincidence adds difficulty to the measurements.

Status of the dilepton/photon measurements, in brief, is as follows.

At SPS: NA60 has been very successful, in particularly:

- (a) Large enhancement at small masses $M < m_\rho$ and deformation of the spectral density of the electromagnetic current is documented;
- (b) using p_t slope as a function of M one sees that $M < 1\text{GeV}$ are produced when flow is developed,
- (c) while intermediate mass dileptons (IMD) $1\text{GeV} < M < 3\text{GeV}$ are produced early when it is still absent;
- (d) the IMD come from QGP thermal radiation rather than charm decays.

At RHIC: (a) Low mass dileptons are enhanced, the magnitude still somewhat disputed between STAR and PHENIX in the most central bin.

(b) IMD are well measured but the contribution from charm/bottom decays remains unsubtracted. PHENIX is solving it with new vertex detector, STAR with $e - \mu$ correlations due to new muon system now in place;

(c) direct photons have spectra consistent with standard rates and hydrodynamics in shape, but not in absolute magnitude.

(d) unexpectedly large elliptic flow v_2 of direct photons persists.

LHC only starts to address these issues. Let me only mention one thing: ALICE confirmed large value of the direct photon v_2 found originally by PHENIX, and puzzling theorists since.

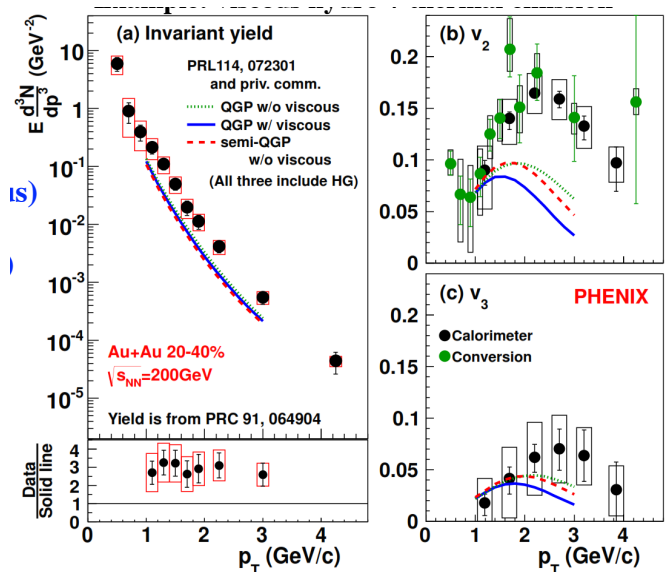


FIG. 49: Illustrations to “direct photon puzzle” (from A.Drees, PHENIX presentation at QM2015).

The yield (a), v_2 (b) and v_3 of the direct photons. Points are data and curves are from theory based on hydrodynamical model, the reference indicated on the figure.

Both (c,d) together are known as a “direct photon puzzle”, illustrated by the latest data in Fig. 49. My comment is that this field still uses a paradigm set up from its very beginning [2], using basically perturbative rates or those evaluated from hadronic models. Now we know that such approach fails elsewhere, in viscosity and jet quenching, and it is perhaps time to approach the issue in more flexible phenomenological way. If the photon production rates at the late (near T_c) stage of the collisions is increased, both (c) and (d) problems will disappear. Like for jet quenching parameter \hat{q} I would argue that may be due to additional scattering on monopoles, not present yet in any models.

B. New sources of photons/dileptons: multi-gluon or phonon+magnetic field

Theoretically, the production of photons and dileptons is tied to the presence of quarks, and is thus sensitive to the issue of *quark chemical equilibration* and its timing. The initial stages of the high energy collisions are believed to be dominated by gluons. Old perturbative arguments [86] show that chemical equilibration via quark-antiquark pair production is relatively slow and should be delayed relative to thermal equilibration of the glue. This idea led to a “hot glue” scenario in which the quark/antiquark density at early stage is suppressed by powers of quark fugacity $\xi_q < 1$. The basic process of the dilepton production

$$q + \bar{q} \rightarrow \gamma^* \rightarrow l_+ + l_- \quad (63)$$

is expected to be suppressed quadratically, $\sim \xi_q^2$.

This scenario has been challenged: higher order processes with *virtual quark loops* can produce electromagnetic effects as well, even without on-shell quarks. First, contrary to general expectations, the quark loop effect in GLASMA has been suggested to be significant [85], enhanced due to multigluon -to virtual quark loop -to dilepton processes like

$$ggg \rightarrow (\text{quark loop}) \rightarrow \gamma^* \rightarrow l_+ + l_- \quad (64)$$

To see how much correction to production rates these processes contribute one needs more explicit calculation of the absolute rates of such processes, which are still lacking.

An explicit calculation [87] of the rate of such type has been made, the two gluon to two photon rate $gg \rightarrow \gamma\gamma$, in which one of the photons is the ambient magnetic field and the gluons are combined into a colorless matter stress tensor, and one of the photons is rotated into the initial state

$$T_\mu^\mu + \vec{B} \rightarrow (\text{quark loop}) \rightarrow \gamma^*(= \text{dileptons}) \quad (65)$$

The terminology introduced in this paper is as follows: The process in which glue appears as “average” matter stress tensor $\langle T_{\mu\nu} \rangle$, producing photons (real or virtual) due to time-dependent magnetic field, is called *Magneto-Thermo-Luminescence*, MTL for short. By “average” we mean that the value of the stress tensor is averaged over the fireball and is nearly constant, with negligible momentum harmonics $p \sim 1/R$.

Individual events, however, are known to also possess fluctuations of the matter stress tensor $\delta T_{\mu\nu}$, with complicated spatial distribution and thus non-negligible momenta. Although these fluctuations include both longitudinal and transverse modes, in a somewhat a loose way we will refer to all of them as “sounds”. We will thus call the interaction of the ambient electromagnetic field and the fluctuations of the matter stress tensor that produces photons and dileptons *Magneto-Sono-Luminescence*, MSL.

The paper is rather technical, and it is probably not very useful to present here specific lengthy formulae, so let us only make some general comments on its potential importance. If observed, the MSL process tests both the amplitudes of the short-wavelength sounds and also harmonics of the magnetic field. We already discuss many uses of sounds above: let us here only comment on the magnetic field. It is easy to evaluate its early values, resulting from Maxwell equations and the currents due to the spectators in peripheral collisions. Since sQGP is believed to be a good conductor, these fields are expected to create currents capturing a fraction of the field inside the plasma [88], perhaps lasting for many fm/c. Magnetic field evolution is important to know for other applications as well, e.g. chiral magnetic effects and the like.

So far, luminosity and acceptance limitations had lead experiments to focus on most luminous central collisions. Now it is perhaps time to look at dileptons in semi-peripheral collisions as well.

C. Dilepton polarization and the (early time) pressure anisotropy

It is well known that when spin-1/2 particles (such as quarks) annihilate and produce lepton pairs, the cross section is not isotropic but has the following form

$$\frac{d\sigma}{d\Omega_k} \sim (1 + a \cdot \cos^2\theta_k) \quad (66)$$

where the subscript correspond to a momentum k of, say, the positively charged lepton and θ_k is its direction relative to the beam. The anisotropy parameter a in the Drell-Yan region – stage (i) in the terminology introduced at the beginning of this section – is produced by annihilation of the quark and antiquark partons, are collinear to the beams, and therefore $a = 1$.

In my note [89] it is suggested that parameter a can be used to control anisotropy of the early stage of the collision. In particular, if it is anisotropic so that longitudinal pressure is small relative to transverse, $p_l < p_t$, the annihilating quarks should mostly move *transversely* to the beam, which leads to *negative* $a < 0$. (Such regime is expected because such anisotropic parton distribution with small differences in longitudinal momenta is produced by a “self-sorting” process, in which partons with different rapidities get spatially separated after the collision.)

For illustration I used a simple one-parameter angular distribution of quarks over their momenta p in a form

$$W \sim \exp[-\alpha \cos^2\theta_p] \quad (67)$$

and calculate $a(\alpha)$ resulting from it. It does show that a may reach negative values as low as -0.2 at stage (ii), before it vanishes, when equilibration is over, at stages (ii-iv).

X. CHARM AND CHARMONIA

A. Charmonium theory: an overview

Quarkonia have always been among the first classic QGP signature, although rather confusing one. The views on what QGP actually does for charmonia yield had changed in a complicated path, which proceeded via a couple of turns of the famous logical spiral. Thus reviews which follow the historical development usually are rather confusing.

Instead, ignoring the historical order, we will proceed pedagogically, from simpler to more complicated settings. We will proceed though three fundamentally different settings:

- (i) time independent equilibrium state of charmonia;
- (ii) equilibration processes and rates;
- (iii) heavy ion collisions.

But before we discuss those, let us start with even simpler forth setting, (0) the case of static heavy quark. The so called *static potentials* which has been measured on the lattice, at zero and nonzero temperatures. A sample of 2-flavor QCD results from Bielefeld group [118] are shown in Fig.50. The linear potential at zero T is indicated at all plots, for comparison. Static potential gives the free energy, related to entropy and internal energy $V(T, r)$ by

$$V(T, r) = F(T, r) - T \frac{\partial F}{\partial T} = F(T, r) + TS(T, r) \quad (68)$$

So, determining the entropy term one can subtract $TS(T, r)$ term and get the *internal energy*. As one can see from Fig.50. they are rather different. The force – potential gradient – has a maximum just below T_c , and U itself reaches 4 GeV in magnitude. What are their physical meaning and which one, if any, should one use as the potential in the charmonium problem?

Liao and myself [122] had proposed a model describing these lattice findings, based on monopole-generated flux tubes. Its detailed discussion is out of context here: let me just mention how an entropy associated with static quarks can be understood. The key idea is the level crossing phenomena, occurring while the separation between charges is changed. Suppose a pair of static charges (held by external hands) are slowly moved apart in thermal medium at certain speed $v = \dot{L}$. For each fixed L , there are multiple configurations of the medium populated thermally. When L is changed, the energies of these configurations are crossing each other, and at each level crossing there is certain probability to change population of the states, depending on the speed of separation $v = dL/dt$. If the motion is adiabatically slow, then all the level crossing processes happen with probability 1: in thermodynamical context this leads to maintained equilibrium and maximal entropy/heat generation. If however the pair is separated fast, then the level crossing happens probabilistically, and certain entropy is developed. The medium is no longer in equilibrium with the pair. The amount of entropy generated is less than in the adiabatic case. In the extreme case one may expect that the pair, if moving on a time scale much shorter than the medium relaxation time scale, decouples from the media and produce negligible entropy. It is plausible, therefore, to identify the adiabatic limit as probing the free energy $F(T, L)$ measured on the lattice with the presence of static $Q\bar{Q}$ pair. The internal energy $V(T, L)$, on the other hand, is different from $F(T, L)$ by subtracting the entropy term and thus can be probed in the extremely fast limit in which possible transitions among multiple states via level crossing do not occur and no entropy is generated. We emphasize that such phenomenon in thermal medium is a direct analogue of what exists in pure quantum mechanical context. Perhaps the oldest example is the so called Landau-Zener phenomenon of

electron dynamics during the vibrational motion of two nuclei in a diatomic molecule. Specific electron quantum states are defined at fixed L (the separation between the two nuclei) with energies $E_n(L)$, and certain levels cross each other as the value of L changes. The issue is the probability of the transition during such crossing of two levels. Consider two levels with their energies given approximately by $E_1(L) = \sigma_1 L + C_1$ and $E_2(L) = \sigma_2 L + C_2$ near the crossing point. When the two nuclei approach the crossing point adiabatically slowly $v = dL/dt \rightarrow 0$, the electrons always change from the lowest state to the lowest other. But if dL/dt is finite, then the transition to *both* levels at crossing point may happen, with certain probability. This is how a pure state becomes a mixture, described by the density matrix, and entropy is produced.

(More quantitatively, Landau and Zener solved the problem and showed that the probability to remain in the original state (i.e. no transition) is exponentially small at small velocity v

$$P = \exp\left[-\frac{2\pi H_{12}}{v|\sigma_1 - \sigma_2|}\right] \quad (69)$$

where H_{12} is the off-diagonal matrix element of a two-level model Hamiltonian describing the transition between the two levels. In the opposite limit of rapid crossing, the system remains in the original state, and no entropy is produced again. So it has maximum at some speed.)

For more discussion of the role of the “entropic force” in charm motion, see paper by Kharzeev [119].

Now we return from static quarks to physical charmonium, and discuss cases (i-iii) subsequently.

(i) Suppose one put a J/ψ in matter at some temperature T . However small is its value, transitions from J/ψ to its excited states will happen. Eventually those will come to $\bar{D}D$ threshold and propagate further. Since any subsystem tends to equilibrium, at given T , and $\bar{D}D$ can eventually occupy an infinite volume, they will win over the bound states. So, given enough time, a given initial J/ψ will dissolve always, at *any* T .

On the other hand, random thermal transitions should also proceed in the opposite direction as well: $\bar{D}D$ can produce charmonia and those can get de-excited back to J/ψ . Thus *recombination* of charmonia states should also happen. Given infinite time, and equilibrium density of J/ψ will be reached.

Pure thermal occupation rate for $J/\psi \sim \exp(-M_{J/\psi}/T)$ is tiny at all temperatures of interest. But heavy quarks c, b are produced in hard processes, not in thermal reactions. Since heavy ion collision time is small compared to weak decays of those, their number is conserved. This leads to the concept of charm chemical potential μ_c . It is not coupled to charm quantum number, is the same for c and \bar{c} , and thus the overall charm neutrality is still intact. Now one may ask what is the density of certain quarkonia states i $n_i(T, \mu_c)$ in equilibrium with a particular μ_c .

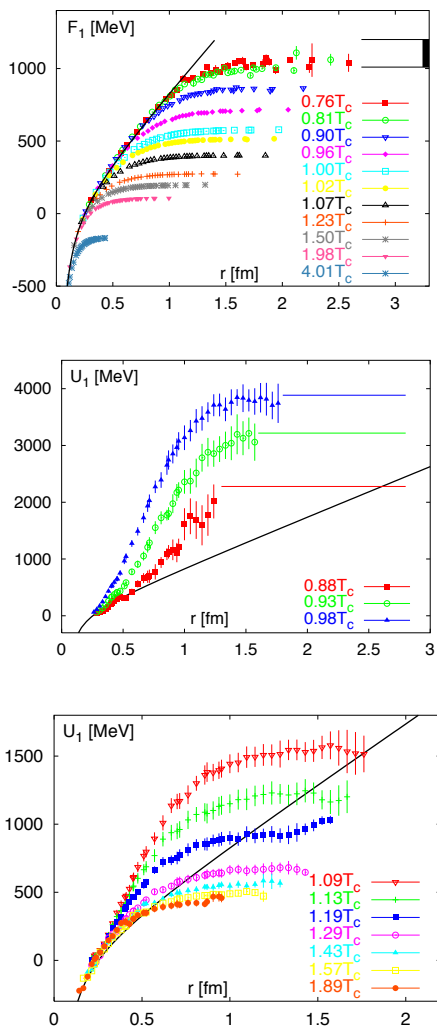


FIG. 50: from [118]. Free energy singlet potentials $F_1(T, r)$ (top plot) and the potential energy $U_1(T, r)$ below and above T_c .

While at low T this is perfectly good question, but it becomes difficult as T increases: the notion of a state gets ambiguous. Proper field theory object to study is a correlation function of local gauge invariant operators, such as charmed scalar/vector currents

$$K(x, y) = \langle \bar{c}\Gamma c(x)\bar{c}\Gamma c(y) \rangle \quad (70)$$

where the average is over the heat bath and x or time $x^0 = t$ can be Minkowskian or Euclidean. In both cases it is related with the same *spectral density* $\tilde{K}(\omega, k)$ characterizing all physical excited states with given energy and momentum. At low T one can see individual states as certain peaks at the lines $\omega = \omega_i(k)$ in the spectral density, but with increasing T they merge into a smooth continuum.

Euclidean correlation functions had been numerically calculated on the lattice: for a recent review see [117].

Unfortunately the problem of *spectral density reconstruction* from those is mathematically badly defined. In practice, highly accurate (and very expensive) Euclidean correlation functions are converted into a relatively poorly defined spectral density. Even when the individual states are seen, as some peaks in spectral density, there is hardly any accuracy to define their widths. Above certain T all peaks corresponding to charmonium states merge into one “near-threshold bump”, the imprint of the Sommerfeld-Gamow enhancement due to an attractive potential $\sim e^{-V/T} > 1$.

(ii) A more detailed – time dependent – set of questions can be asked about *transition rates* in equilibrium matter. Those has been addressed (at least) at three levels, (a) real time QFT; (b) quantum mechanical; (c) classical diffusion.

Real time QFT, also known as Schwinger-Keldysh formalism, can follow a system from some initial to some final state using the full Hamiltonian

$$\langle i|P \exp(-\int_i^f dt H)|f\rangle \quad (71)$$

which is viewed as a sum of that for the subsystem in question H_0 and matter perturbation V . Diagrammatic expansion, including two-time contours as well as Matsubara portion of an Euclidean time for thermal media are widely used in conduced matter problems, but they are not much used so far in the problem we discuss.

If H_0 corresponds to non relativistic quantum mechanical description of quarkonium, we will call it quantum mechanical approach. One can evaluate matrix elements of V over various quarkonia states. Already my first 1978 paper on QGP signals [84] had charmonia (called psions in its title). The first considered in it was J/ψ excitation to unbound states of $\bar{c}c$ due to photoeffect-like reactions of one gluon absorption $J/\psi + g \rightarrow \bar{c}c$. For heavy quarkonia the *diagonal part* of the real and imaginary part of the perturbation V can be considered as a modified potential: for recent review see [116]. More generally, one can define transition rates between states and write a *rate equation*. The fundamental question here is of course whether the “matter perturbation” V is small or not. (We will argue below that at very low and very high T perturbative approach may work, but at least for charmonium in the near- T_c matter the answer to this question is negative).

Suppose the “perturbation” V is not small comparable with the interparticle interaction: then quantum quarkonium states are no longer special and one can as well use for H_0 just free particles. Using mass as large parameter, one can argue [145, 146] that even in strong coupling setting the heavy quark motion should be described by classical stochastic equations, the Langevin or Fokker-Plank type. Let me only mention two crucial consequences of the argument. First, motion is diffusive, with $x \sim \sqrt{t}$ as it happens in random uncorrelated directions. Second, each step in space is very small. Suppose a perturbation delivers a kick of the order T to a heavy quark of mass $M \gg T$. Its velocity is changed little, by $\Delta v \sim T/M$

and by the time next kick comes $\Delta t \sim 1/T$ the shift in coordinate is small $\Delta x \sim 1/M$.

Suppose a quark needs to diffuse a distance large enough so that the gradient of the potential no longer pulls it toward the antiquark. From internal potentials displayed above one can see that the distance it needs to go is about 1.5 fm, or $\sim 10\Delta x$ jumps it can make. However, since it is moving diffusively, to get that far the quark would need $\sim 10^2$ jumps, which can well be larger than time available. Quantitative study of classical diffusion to charmonium made by Young and myself [120] confirmed that to climb out of the attractive potential in multiple small steps is hard. Contrary to common prejudice, using the realistic charm diffusion constant we found that the survival probability of J/ψ is not small but is of the order of 1/2 or so.

(iii) Finally, in order to model the fate of heavy quarks/quarkonia in heavy ion collisions, one need to follow them all the way, from initial hard collisions to the freezeout. In classical diffusion approach one starts with pair distribution in the phase space, as defined by the parton model, and at the end project the resulting distribution to the charmonia states using their Wigner functions.

If the reader is insufficiently puzzled by all that, let me finish this section presenting two opposite answers to the question: What is the effect of the QGP production on the charmonium survival? In 1986 Matsui and Satz [115] famously argued that QGP, via the Debye screening of the color potential, kills charmonium states *sequentially*, from excited states down to the ground one. In 2008 Young and myself [120] argued that strongly coupled QGP helps to preserve charmonium states, since small diffusion constant prevents $Q\bar{Q}$ to move away from each other. There are perhaps no identifiable charmonium states during the process: but so what? Close pairs at the end get projected back to the bound states.

B. Charmonium composition

Let me start with the most radial model of all, that of statistical hadronization of charmonium at chemical freeze out [37]. It assumes that charmonium states, like all light hadrons, are produced in thermal equilibrium state at this time. If true, all questions discussed in the previous subsection are completely irrelevant, since all charmonium history during the intermediate stages is simply forgotten.

The data at RHIC and LHC show that this is only partially true, and so we witness two component of the charmonium population, the “survived” one and the “recombination” contribution. Observations of the recombination component is one of the most important recent results from heavy ion experiments. Instead of showing the actual data, let me ask the reader to look at the original sources, such as Andronic’s summary talk at QM2014, which does it very well.

Let me proceed to next order questions, related in par-

ticular with relative population of charmonium states. If all of them come the statistical hadronization at chemical freezeout, the consequence should be

$$\frac{N_{\psi'}}{N_{J/\psi}} = \exp\left(-\frac{M_{\psi'2s} - M_{J/\psi}}{T_{ch}}\right) \quad (72)$$

and similar formulae for other states. However if we have two out-of-equilibrium components, with different history, the answer should be different. The “survival” component, with its flow of probability from small to large r , should be richer in lower states. The “recombination” component flows the opposite way, and it should have more higher states instead. In general, two components have different centrality and p_t dependences, and in principle can be separated.

Experimental data are rather incomplete: there is however puzzling double ratios found by CMS [38] which hint that the situation can be rather interesting.

C. New types of “quarkonia states” in a strongly coupled medium

Like in other parts of heavy ion theory, there is a weakly coupled and strongly coupled points of view on this question. Which one to chose is now parametric: if the quark mass is very large $M \gg T$, quarkonia are non-relativistic and perturbative. In zeroth approximation one thus starts from the unmodified vacuum states, with effects such as excitations and Debye screening included subsequently. Those can be described by corrections to real part of the potential δReV and appearance of its imaginary part ImV , see e.g. [116] for nice summary of this theory.

The opposite picture of very strong coupling has been discussed in [120]. If ImV is large, using the initial vacuum states make no sense. Indeed, there are no 2-particle bound states in a liquid, just certain correlations between the charges. Classical theory has two input parameters. The first is the diffusion constant D of the charm quark, and the second is the “interaction strength”, usually characterized by the “plasma parameter”

$$\Gamma = \frac{\text{mean potential energy}}{T} \quad (73)$$

in which the ambient temperature T stands for typical kinetic energy. Classical strongly coupled systems have $\Gamma > 1$.

Let us start with a simplified limit at infinite coupling and zero diffusion. Thus $c\bar{c}$ pair, locally produced, remains stuck at the same place during the sQGP period of time. At the end matter returns to hadronic phase and the ground state J/ψ is recreated, simply because it has the largest wave function at zero. If so, there should be *no* J/ψ suppression at all! sQGP helps preserve the charmonia.

More realistic simulations with finite diffusion constant can be set using Langevin or Fokker-Planck (FP) equations. One setting starts with close $\bar{c}c$ pair, which makes *positive* flow toward large relative distance $r \rightarrow \infty$. The other – recombination – setting starts with originally unrelated $\bar{c}c$ at large r , with negative diffusion current toward small r . Both are followed for some time of sQGP era, and at the hadronization the obtained distributions in the phase space are projected back to the vacuum quarkonia states, using their Wigner functions.

Which picture is closer to the truth, weak or strong coupling, depends on parameters such as the quark mass: perhaps bottomium is closer to the former regime while charm perhaps closer to the second one.

Not going into details here, let me just say that both the diffusion coefficient for a charm quark in QGP and the potential are reasonably well defined[167] and the simulations were done in [120] and in subsequent paper for the recombination: the difference is the direction of the diffusion, equations are the same.

The point I try to make does not depend on the details of those papers but concerns their qualitative observations: both the inward/outward diffusions are very slow, and the reason for that is quite interesting. The spatial distribution rapidly reaches certain shape which persists with only slow growth of its tail. The example is shown in Fig. 51. In this case the attractive Coulomb-like potential has been complemented by a repulsive quantum effective potential $\sim \hbar^2/mr^2$ which generates the hole in the distribution at small r and prevents classical falling of the charge on the center.

We called solutions with a nearly-permanent shape and small flux “quasi-equilibrium” solutions. This concept is – to my knowledge – not yet been noticed in this particular field, but it deserved to be. Let me show how quasi-equilibrium solutions works for the quark diffusion problem, using the FP equation

$$\frac{\partial P}{\partial t} = \frac{\partial}{\partial \vec{r}} D \left(\frac{\partial P}{\partial \vec{r}} + \beta P \frac{\partial V}{\partial \vec{r}} \right) \quad (74)$$

where $P(t, \vec{r})$ is the distribution over the $\bar{c}c$ separation \vec{r} at time t , D is the diffusion constant, $\beta = 1/T$ and $V(r)$ is the interquark potential. First of all, when

$$P \sim \exp(-\beta V) \quad (75)$$

two terms in the r.h.s. bracket cancels: this is stationarity of the true equilibrium. The bracket in the r.h.s. of (74) – the particle flux – is then zero.

Note however what happens when this bracket is nonzero but *constant*(r): the divergence of the flux still makes the r.h.s. to vanish. Then the l.h.s. is also zero: these solutions are stationary. Such solutions, while stationary, still possess a constant flow of particles. The direction depends on the sign of the constant, it can be from small to large r as in charmonium suppression problem, or from large to small r for recombination.

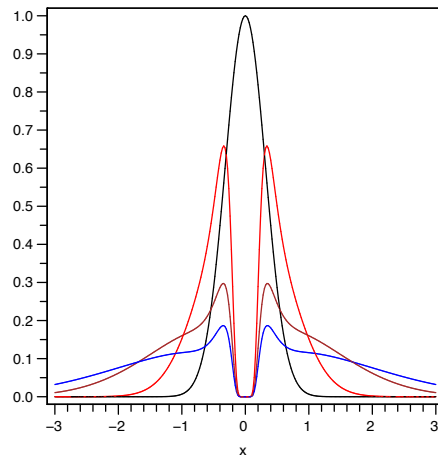


FIG. 51: from [120]: one-dimensional Fokker-Planck equation for an interacting $c\bar{c}$ pair. The relaxation of the initial narrow Gaussian distribution is shown by curves (black, red, brown, green, blue, or top to bottom at $r=0$) corresponding to times $t = 0, 1, 5, 10$ fm, respectively.

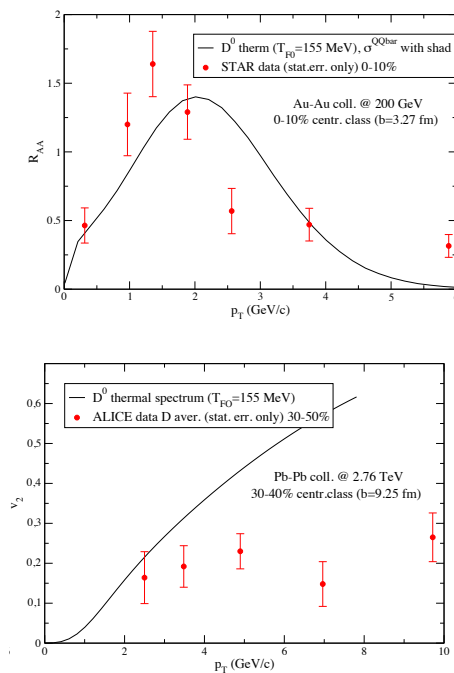


FIG. 52: STAR data on RAA of D mesons, and ALICE v2 of D, both from [150]

D. Do charmed mesons and charmonia flow?

Let me start with an observation that D mesons have a maximum in R_{AA} shown in Fig. 52(a) resembling that for protons: and we know the latter is of hydrodynamical origin. However the peak is at $p_t = 1.5$ GeV, lower than

for the nucleon, while the mass of D is higher. Direct comparison to hydro at Cooper Fry (the line) does not do such a good job as it does for light flavor hadrons. The observed elliptic flow shown in Fig.52(b) is nonzero but smaller than hydro predicts (curve). So, (i) either charm is heavy enough to be out of equilibrium with matter, or (ii) it is in kinetic equilibrium with it but spectra were not correctly calculated. (The meaning of the second option will be soon clarified.)

LHC data on charmonium dependence on p_{\perp} is transitionally done in the form of $R_{AA}^{J/\psi}(p_{\perp})$, normalizing it a la parton model. A comparison of PHENIX, RHIC and ALICE, LHC data, shown in Fig.53(a) (from [149]) display drastic change. There are much more charmonia at LHC than at RHIC at small p_{\perp} : those presumed to be due to the “recombined” ones. The observed v_2 of J/ψ Fig.53(b) is non-zero but smaller than hydro predicted.

The recombined component is produced from matter and thus it is maximal at small p_{\perp} , while the primordial are mostly fast (relativistic) $P/M > 1$. It is presumed that recombined component flows with matter. The question is whether the primordial component also do so, or “slip” relative to the medium: the data seem to favor the latter option.

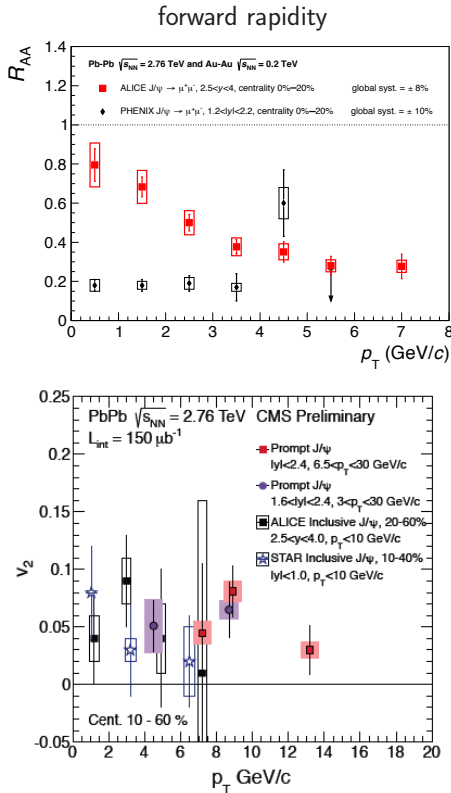


FIG. 53: Comparison between ALICE and Phenix charmonium R_{AA} (a) and charmonium elliptic flow (b), both from [150].

E. Inhomogeneous distributed charm

He, Fries and Rapp [74] had demonstrated that if one artificially increases the drag coefficient, one reproduces the p_t distribution obtained from hydrodynamical flow of charm. In other words, they nicely checked that at high enough scattering cross section charm is kinetically equilibrated with matter. In this calculation the original particles were homogeneously distributed over the fireball at some early time, which is indeed needed to get consistency between the two calculations.

Yet what would happen if the drag/cross section be still large, but the initial charm be distributed over the fireball in a *non-uniform* way. Introducing charm fugacity $f = \exp(\mu_c/T)$ in a standard manner, one should think of it as some function of time and space point, depending on the production mechanism. Charm recombination into charmonium states is calculated at the chemical freezeout surface, and it should be proportional to an average of over it $\langle f^2(t, \vec{r}) \rangle$, not square of the average $\langle f \rangle^2$ as it is done now. In short, I wonder what one should do for thermal recombination when the charm fugacity is not homogeneously distributed over the system, as is usually assumed.

This lead to nice hydro exercise I will briefly tell about. Let me start with the longitudinal hydro equation written as entropy conservation

$$[s(t, x)u^\mu]_{;\mu} = 0 \quad (76)$$

with the semicolon meaning the covariant derivative. The homogeneous distribution means that $n/s = \text{const}(t, x)$, and thus any solution for the entropy generates solution for $n(\tau, r)$ as well. If one would like to put an arbitrary distribution of charm (or any other conserved quantity) density at some initial time, in order to find its distribution later one has to solve its conservation equation $[n(\tau, r)u^\mu]_{;\mu} = 0$ at all times. I started with Gubser flow, in coordinates proper time transverse distance τ, r , for which $s(\tau, r)$ is known and put $n(\tau, r) = f(\tau, r) * s(\tau, r)$. The resulting “fugacity equation” reads

$$2r\tau\partial_r f + (1 + r^2 + \tau^2)\partial_\tau f = 0 \quad (77)$$

It has a solution with an arbitrary function ϕ of the following argument

$$f = \phi\left(\frac{2r}{1 - r^2 + \tau^2}\right) \quad (78)$$

The function ϕ can be fixed from the initial conditions at $\tau = 0$. Using it, one finds the corresponding distribution of our quantum number (charm) at the freezeout surface as well.

The problem was solved, but the meaning of this answer looked mysterious. It was further clarified when I used the co-moving coordinates (see appendix) ρ, θ . All one needs to know is that ρ has meaning of time and θ of space, and the particle conservation in a comoving frame

reads simply as

$$\frac{\partial n}{\partial \rho} = 0 \quad (79)$$

meaning that any function of θ independent on coordinate ρ solves the problem. And constant theta implies constancy of the combination I obtained in the original coordinates. The lesson I got from this is that even in numerical solutions of the hydro equations one perhaps should try to find the co-moving coordinates. Those would lead to very natural distributions of external objects like charm.

I did checked that for recombinant J/ψ the effect of $\langle f^2 \rangle \neq \langle f \rangle^2$ is actually small and can perhaps be ignored. I however further found that the inhomogeneity effect suppresses v_2 of charm, especially at higher p_t , because the fireball edge is a bit less populated by charm than its middle. My calculation gives

$$\frac{v_2^{inhomogeneous}}{v_2^{homogeneous}}|_{p_\perp=3 GeV} = 0.65 \quad (80)$$

which brings hydro prediction closer to experimental ones on $v_2^{J/\psi}$. Perhaps recombined charmonia do flow with the matter, after all.

XI. JET QUENCHING

Let me mention on the onset that hard QCD is expected to be perturbative, and this is not my field. I thus would not go into gluon radiation, in vacuum and in matter, in any detail. This small section contains only some remarks on recent theory developments.

A. “Quasi-equilibrium” in jets

I think it has been an important development relating jet-in-matter physics with a more general turbulence theory. In it I will follow ref.[123] by Blaizot et al. For a large enough medium, successive gluon emissions can be considered as independent: multiple emissions can be treated as probabilistic branching processes, with the BDMPSZ spectrum playing the role of the elementary branching rate. The inclusive gluon distribution function

$$\frac{dN}{d\log(x)d^2\vec{k}} = \frac{D(x, \vec{k}, t)}{(2\pi)^2} \quad (81)$$

satisfy certain diffusion-brunching equation. Integrating over transverse momentum one gets the so called zeroth moment $D(x, t) = \int_{\vec{k}} D(x, k, t)$ on which we focus for simplicity. This satisfies the equation

$$t_* \frac{\partial D(x, t)}{\partial t} = \int dz K(z) \left[\sqrt{\frac{z}{x}} D\left(\frac{x}{z}, t\right) - \frac{z}{\sqrt{x}} D(x, t) \right] \quad (82)$$

with the gain and the loss terms. The details such as the shape of the kernel K and time parameter t_* can be found in ref.[123]. The central feature I want to focus on is the analytic solution

$$D(x, t) = \frac{(t/t_*)}{\sqrt{x(1-x)^{3/2}}} \exp\left(-\frac{\pi t^2}{t_*^2(1-x)}\right) \quad (83)$$

Essential singularity at $x = 1$ is expected: it is known as the Sudakov suppression factor. The remarkable news is that apart of the exponent, the shape of the x -dependence remains the same at all times, only the normalization changes.

Let us see how it works in the most important small $x \ll 1$ region. If one simply plugs in the leading $x^{-1/2}$ dependence, the gain and loss terms simply cancel. This is the quasi-equilibrium solution under consideration. As a result, jets in matter are expected to approach some universal shape, not determined by the particular initial conditions, but by the quasiequilibrium solution to which it gets attracted as the process proceeds.

It is essentially the same phenomenon as we have seen in Fig.51 for diffusing charmonium: the shape itself is dictated by the balance of the gain and loss. Both are “quasi-equilibrium” attractor solutions: their main feature is *constant flux* of certain quantity, from one end of the spectrum to the other. (The flux in decaying charmonium comes from small to large distance between quarks, in the jet case it comes from large to small x .) Once again, the constancy of the flux in such solutions is the key idea going back to Kolmogorov’s theory of hydrodynamical turbulence, which I find quite remarkable. As Einstein once observed (approximate quote from memory): “... the number of good ideas in physics is so small, that they keep being repeated again and again in various context”.

B. Is jet quenching dominated by the near- T_c matter?

Let me start with Fig. 54, emphasizing some features of the LHC (ALICE) data. The first one shows the suppression factor R_{AA} compared with theory based on pQCD expressions. The first obvious feature I want to point out is the pronounced dip in the data, clearly separating two distinct regimes. Although the magnitude is centrality dependent, its location at $p_t^{dip} \sim 6 GeV$ changes a little. (It also about the same as at RHIC, where the dip is minor.). The region above the dip $p_t > p_t^{dip}$ is well described by jet quenching models, while below the dip it is perhaps some tail of hydro-related phenomena, yet to be understood.

Now we proceed to angular distribution of jet quenching, fig.(b) on which v_2 (large p_t) is plotted. Already at the very beginning of RHIC era I noticed [124] a problem: direction-dependent in or out-of reaction plane by

as

$$R_{AA}^{in/out} = R_{AA}(1 \pm 2v_2) \quad (84)$$

apparently is incompatibly large to most theories of jet quenching. As one can see from the second Fig. 54, it is still very much true at LHC. Theory curves which describe so well R_{AA} , all the way down to the dip p_t^{dip} , lead to v_2 (at the dip) much smaller than needed! What is new here are LHC measurements at much higher $p_t > 30 \text{ GeV}$, demonstrating v_2 values which are consistent with the pQCD models. Yet it is still true that in the range $6 < p_t < 30 \text{ GeV}$ something significant is missing. (Steeply falling another contribution Fig. 54 (a) below the dip makes it unlikely to be important.)

A solution has been proposed by Liao and myself [125]: we found that one can get near the observed v_2 value if the jet quenching is strongly enhanced at the near- T_c matter. We motivated it by presence of magnetic monopole in the near- T_c region.

A model based on this idea can be reconciled with RHIC and LHC data. Let me jump to the recent paper [148] in which the corresponding model is well developed. In Fig.54 one finds fits of the R_{AA} and v_2 of the jets for models with and without magnetic component. In Fig.55 we show the $\hat{q}(T)$ of the model for a jet with 20 GeV.

XII. NEAR THE PHASE BOUNDARY: FLUCTUATIONS AND THE FREEZEOUTS

A. Chemical freezeouts

Statistical equilibration is a famous success story, and it hardly needs to be emphasized here. Let me just show ALICE data with thermal fits in Fig.56, presented at CPOD 2014 by A. Kalweit.

Note that even light nuclei – d, t, He^3 and their antiparticles are also included. One may wonder how d , with its 2 MeV binding energy, can be found in an environment with ambient temperature $T \sim 160 \text{ MeV}$. It is literally finding a snowflake jumping out of a hot oven. Shouldn't d be instantly destroyed in it? The answer to this and similar questions is well known: thermodynamics does not care about d lifetime. As it is destroyed with some rate, perhaps large, in equilibrium it is recreated by the inverse process with the same rate, so that its average population is conserved. What thermodynamics gives us is that average.

Note that one deviation is K^* : the model predicts more than observed. This is expected: it is short lived resonance which decays when the density is still non-negligible, the products can be re-scattered and their invariant mass moved out of the peak. Corrections to that can be made using any cascade codes.

Another deviation is for $p + \bar{p}$. Some argued that one should take into account possible annihilation on the way out, and again use available practical solution

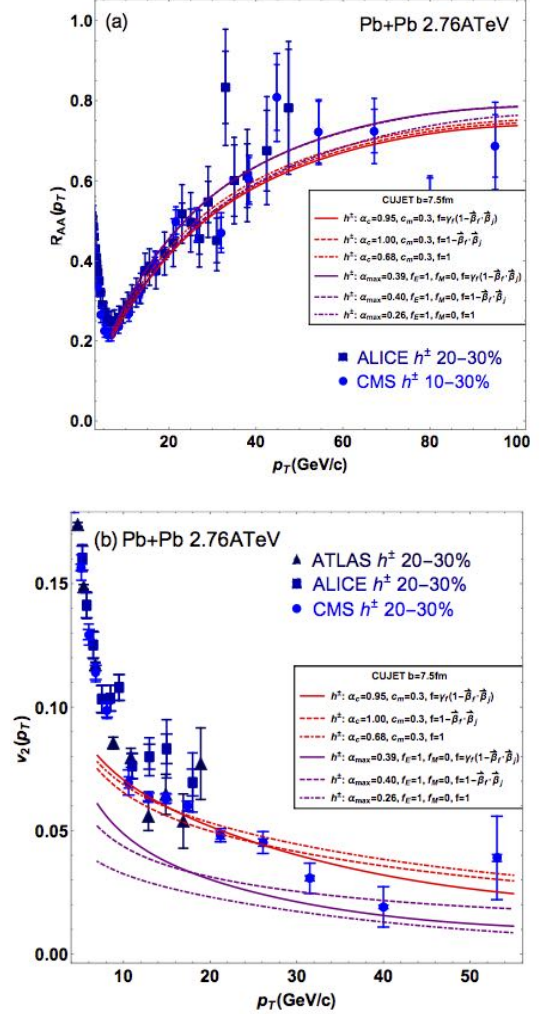


FIG. 54: (color online) From [148]: jet suppression and elliptic parameter v_2 , data versus models.

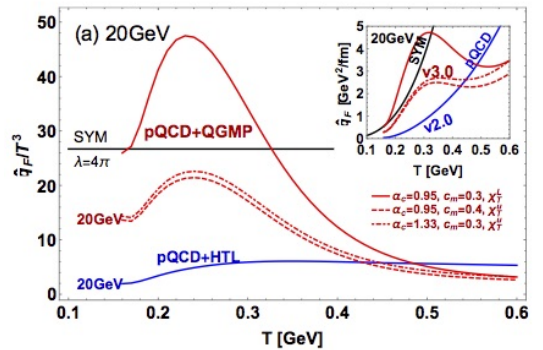


FIG. 55: (color online) the NTcE model with enhanced near- T_c quenching

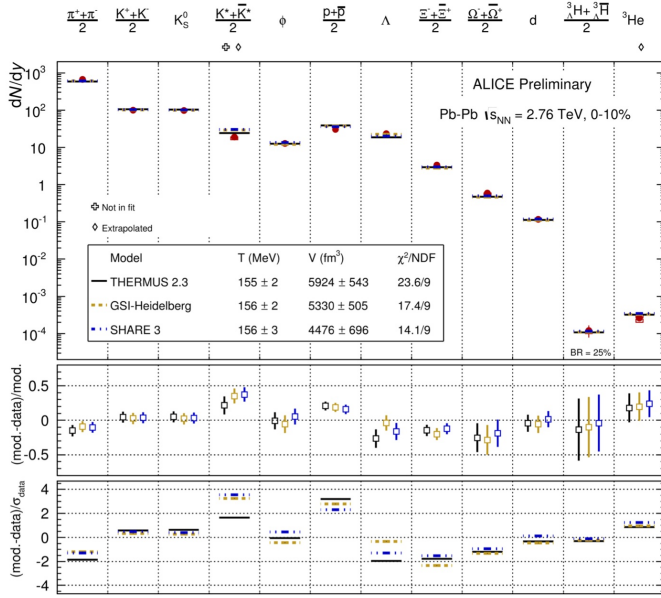


FIG. 56: Alice data on particle yields compared to thermal model [37]. The main fit parameters are indicated in the upper plot.

like UrQMD or similar code to calculate it. Here however comes an objection: all of them include annihilation $p + \bar{p} \rightarrow n\pi, n \sim 5$ but *not* the inverse reaction. This is an old story [153]: contrary to popular beliefs the inverse reactions are not suppressed, in fact at equilibrium their rate are exactly the same as the direct one. Using a cascade code which does not respect the detailed balance – and thus the very concept of thermal equilibrium – to calculate corrections to thermal model is just logical nonsense.

I would not show the freezeout points on the phase diagram, which has been done many times. Let me just remind that those seem to be remarkably close to the phase boundary, defined on the lattice. Why should this be the case? An answer suggested by Braun-Munzinger, Stachel and Wetterich [69] is also related with the multi-particle reaction rates. Since those depend on very high power of the temperature, they all should decoupled very close to critical line

$$\frac{|T_{ch} - T_c|}{T_c} \ll 1 \quad (85)$$

The concept of two separate freeze outs is based on separation of elastic and inelastic rates at low T , in magnitude.

New development is usage of event-by-event fluctuations. As it has been first pointed out in my paper [70], those in general provide information about multiple susceptibilities, or higher derivatives of the free energy over T or various chemical potentials.

This idea further was applied toward location of the critical point in [71], suggesting the low energy scan pro-

gram. The results of the RHIC scan are however still too fluent to be reviewed, even after QM14.

Let me instead comment on another development, on the interface of the lattice and heavy ion communities. Calculation of susceptibilities on the lattice, including the most difficult near- T_c region, reached significant maturity. Karsch stressed at many meetings, that higher susceptibilities now can be compared to the data and the freezeout curve be reconstructed, even without using the particle ratios. I will follow here [40] from which Fig.57 is taken: Fig(a) compares new set of freezeout parameters (points) compared to earlier one from the particle ratios. Fig.(b) shows that as μ grows a consistency between different ratios is getting worse. It is however generally believed that at chemical freezeout the Hadron Resonance Gas model is generally describing the QCD thermodynamics, expect perhaps in the vicinity of the QCD critical point.

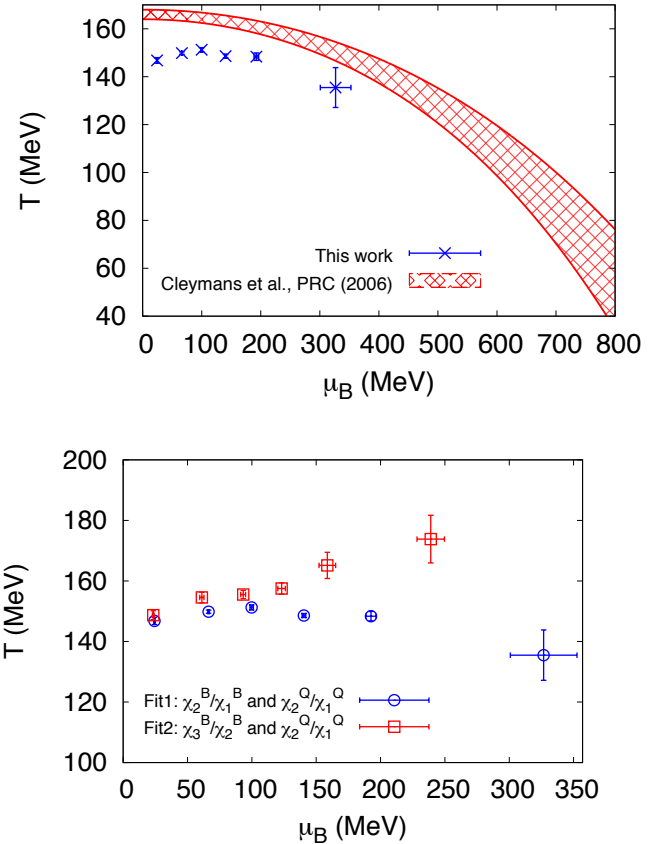


FIG. 57: (Color online) (a) Freeze-out parameters in the $(T - \mu_B)$ plane: comparison between the curve obtained in Cleymans et al (red band) and the values obtained in the present analysis from a combined fit for net-electric charge and net protons (blue symbols). (b) The freezeout parameters fitted from two different set of ratios, as shown in the plot

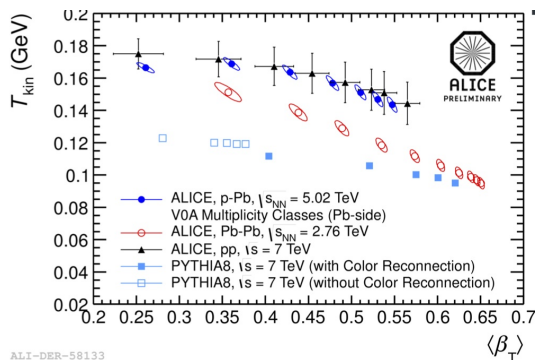


FIG. 58: (color online) The temperature of the kinetic freezeout versus mean velocity of the radial flow, fitted to ALICE spectra of the identified secondaries (π , K , p , Λ , Ξ , Ω).

B. From chemical to kinetic freezeouts

Separation in magnitude of the elastic and inelastic (low energy) hadronic reactions is the basis of the “two freezeouts” paradigm, with separate chemical T_{ch} and kinetic T_{kin} temperatures.

Its effectiveness became even more clear at LHC, which we illustrate by Fig.58 containing the “blast wave” fitted parameters to the ALICE spectra of . Unlike T_{ch} , the kinetic one T_{kin} strongly depends on centrality of PbPb collisions, decreasing to values below 0.1 GeV for the most central bins. Cooling from 0.16 to 0.1 GeV may not look so dramatic: but thermodynamical quantities in this region are proportional to high power of T and they do change strongly.

First, does one understand the dependences displayed in Fig.58 at all? The most central AA collisions produce the largest systems, which have the highest T at the early stages, and also the lowest T at the end. One popular way to explain it is to mention, that the energy conservation negatively correlates the flow velocity $\langle \beta_T \rangle$ and T_{kin} , so more “explosive” systems cool more.

While correct, this simple idea seems to be in contradiction to the pp, pA data also shown in Fig.58, and for which T_{ch} and T_{kin} are close. An explanation to that, discussed in the middle of this review, is that high multiplicity bins, displaying strong radial flow, achieve it via more extreme conditions at their early stage, by increasing the initial T_i . In other words, higher multiplicity in this case means large energy/particle, which reveals itself in the flow without cooling. (In AA collisions T_i also depends on centrality, but much weaker.)

The kinetics of the freezeout – that the rescattering probability on the way out should be about 1/2 – is of course central to defining T_{kin} . Cold fireballs created in central PbPb have thousands of particles and freezeout late, at times reaching 15 fm. The highest multiplicities observed in pp, pA have 10-20 times less particles, and freezeout time/size of 3 fm or so.

In summary, contrary to belief of many, in PbPb LHC

collisions one does have an extended phase of the collision, in which matter cools deep into the *hadronic phase*. This opens some interesting questions related to hadronic phase, which can now be addressed experimentally.

Let me mention only one issue here. Since between T_{ch} and T_{kin} the particle numbers are conserved, one should introduce new nonzero chemical potentials, not associated with conserved quantum numbers like charge and baryon number. In particular, there should be nonzero chemical potentials for pions.

Whether there are nontrivial fugacity factors at the kinetic freezeout can be directly observed in the pion spectra, because in this case Bose enhancement can be measured. This idea is at least 20 years old [58]: its experimental manifestation was displayed in the paper by me and Hung [59] is shown in Fig.59(a). (The reference SS collisions is much smaller system than PbPb, and thus its chemical and kinetic freeze outs should be close.) Fig.59(b) shows that the same effect shows up, now at LHC. The fit *without* chemical equilibrium, with nonzero pion μ on top, provides a better description to the spectra at small $p_t < 200$ MeV.

Interesting that the parameter of the fit in this last work gives $\mu_\pi \approx m_\pi$, so the authors speculated if the conditions for pion Bose-Einstein Condensation (BEC) were actually reached. If this indeed becomes true, it has been many times suggested previously that the femtoscopy parameter λ should show it, as it is sensitive to “degree of coherence” of the pion source. Recent femtoscopy data on 2 and 3 identical pions from ALICE, discussed in [155], can be indeed fitted with a coherent source. The fraction of coherent pions coming from this fit is as large as $23\% \pm 8\%$.

Do we actually witness BEC formation at LHC? In order to answer this question it is useful to recall BEC discovery in experiments with ultra cold atoms a decade ago. As the atomic system does evaporating cooling and its temperature decreases, the measurements of the momentum distribution (by switching off the trap) revealed appearance of new and much more narrow component. Unlike the usual thermal component, its width was independent of T , and related to the inverse spatial size of the BEC cloud.

This indeed sounds like what is observed in heavy ion collisions: as one goes to most central collisions and the kinetic freezeout T_{kin} get below 100 MeV, the p_t spectra do become enhanced at small momenta. The difference however is in the shape: we don’t see a new Gaussian, as in the atomic experiments, but thermal spectrum modified by μ .

The condensate should be a separate component, with μ being exactly m_π and independent on T . If BEC cloud contains about 1/4 of all pions, its diameter should be large, at least of the order of 2-3 fm. The corresponding width of momentum distribution, from uncertainty relation, should be as small as say $\langle p_t \rangle < 0.1$ GeV. Looking back to Fig.59(b) one however finds, that such soft secondaries seem to be *outside* of the acceptance. So,

even if BEC component is there, we so far cannot see it, neither with ALICE nor with any other LHC detectors! How then can we get their influence in the femtoscopy?

This issue can perhaps be clarified by a short dedicated run, in which the ALICE detector switches to smaller (say 1/2 of the current value) magnetic field, to improve the low p_t acceptance. (Yes, recalculating all the efficiencies is a lot of extra work, but perhaps it is worth clarifying this interesting issue.)

C. The search for the critical point and RHIC low energy scan

The main idea [71] is 15 years old and well known: critical point – if exists – should lead to large correlation

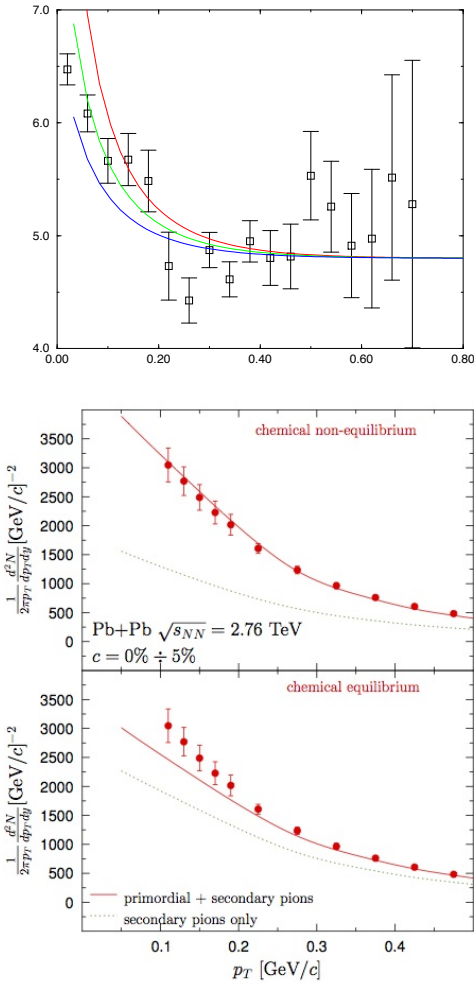


FIG. 59: (Color online) (a) Points show the ratio of PbPb to SS spectra, from NA44. Three curves are for pion chemical potential $\mu_\pi = 60, 80, 100 \text{ MeV}$, from [59]. (b) (From [60]) Dots are ALICE transverse momentum spectra of pions in the low- p_t region, compared to the model with (upper plot) and without (lower plot) pion chemical potential.

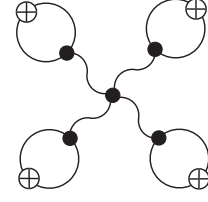


FIG. 60: The enhanced contribution to 4 particle correlator, from [152].

lengths and enhanced e-by-e fluctuations, similar to critical opalescence known in many cases. Mathematically speaking one may go for effects given by diagrams which have as many critical propagators as possible. Stephanov [152] pointed out that since the n -particle correlators may contain up to n such propagators, they are more sensitive to large correlation length: 3 particle correlators are $\sim \xi^6$, 4-particle ones $\sim \xi^8$, see Fig.60, and so on. The wavy line at zero 4-momentum is $\sim 1/m_\sigma^2 \sim \xi^2$: but the prediction is not just the power of the propagators because the coupling of critical modes by itself vanishes as certain power of ξ given by the critical indices. The quartic one in the diagram considered is $\sim 1/\xi$ so the total power is 7, not 8.

Let me first retell the same story in a simpler language. The critical field we here call σ should be viewed as some stochastic/fluctuating background field coupled to fluctuations in particle number (circles with crosses in the diagram above). One can view it being proportional to some stochastic potential $\Delta V(x)$ which enter the probability in the usual way $P \sim \exp(-\Delta V(x)/T)$, so that in its minima the probability is larger and more particles – e.g. 4 mentioned above – all gather there. The critical point is special in that the scale of the correlation length ξ of this potential increases, and thus more particles have a chance to get into the same fluctuations.

Which particles we speak about? In principle sigma is scalar-isoscalar, so any one of them. In our paper [71] and in [152] the simplest coupling was considered as an example, the $\sigma\pi\pi$ one, and so the particles were pions.

Let me now argue that using the nucleons should work even better. First, the powers of the baryon density $n_B = N_N - N_{\bar{N}}$ correlated together are the susceptibilities calculated on the lattice as derivatives over μ_B . Second, we know from the nucleon forces – e.g. the simplest version of the Walecka model – that σ is the main component of the attractive nuclear potential which binds the nuclei.

$$\Delta V = \frac{g_{\sigma NN}^2}{4\pi r} \exp(-m_\sigma r) \quad (86)$$

In vacuum the typical mass $m_\sigma \sim 600 \text{ MeV}$ and the inter-nucleon distance $r \sim 1.5 \text{ fm}$ are combined into small suppression factor $\sim \exp(-5) \ll 1$ explaining why the nuclear potential scale $\Delta V \sim -50 \text{ MeV}$ is much smaller

than the nucleon mass, in spite of strong coupling. (At smaller distance r the repulsive omega contribution dominates the attractive sigma one.)

Can it be so, that at the QCD critical point $m_\sigma \rightarrow 0$ and this small exponent disappears? If so, one should expect much deeper ΔV , perhaps even larger than the freezeout temperature T . Furthermore, if say $\xi = 2 fm$, the volume $4\pi\xi^3/3 \sim 40 fm^3$ is large enough to collect many nucleons, not just 3 or 4, as Stephanov suggested. So, such clustering of the nucleons should produce large nuclear fragments, a new cute signal of the critical point!

The argument, unfortunately, is rather naive. The critical mode which gets long-range is not just the σ field but – because we are at nonzero density – a certain combination with ω . Therefore the repulsive forces between nucleons should be getting longer range as well. To tell what happens we need a reliable theory or some dedicated experiments. Fortunately, we can do it in the coming low energy scan. Isoscalar sigma interacts with scalar – net baryon – density $n_s = N_N + N_{\bar{N}}$, while omega interacts with $n_B = N_N - N_{\bar{N}}$. The powers of these differ by the non-diagonal terms such as nucleon-antinucleon correlators $C^{m,n} = \langle N_N^m N_{\bar{N}}^n \rangle$ which can and should be measured. Perhaps restricting kinematics of all particles involved – rapidity and momenta differences – would further enhance the signal.

Let me now jump to the latest STAR data, presented at CPOD 2014 by Luo, and shown in Fig.61. The proton 4-point correlator has an interesting structure: a minimum at $\sqrt{s} = 20 - 30 GeV$ and perhaps a maximum at low energy (?). Antiprotons have a similar shape but with much smaller amplitude. Theory in fact predicts some oscillatory behavior of the kurtosis near the critical point: it can be that.

(However before getting excited by the new large signal – with large error bar – let me remind that it appeared as a result of particle ID improvement, from $0.4 < p_t < 0.8 GeV/c$ to now reaching $p_t = 2 GeV/c$. The newly open kinematic window should be sensitive to hydro flow, and potentially to its fluctuations.)

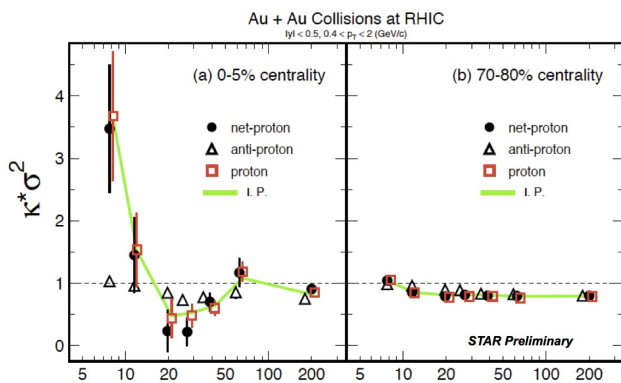


FIG. 61: The kurtosis – 4 particle correlator – in units of the width, as a function of the collision energy \sqrt{s}, GeV .

Also near critical point one expect significant modification of attractive (sigma-related) nuclear forces: can those affect the 4-proton (antiprotons) correlations in question?

Clearly more data at the low energies are needed to understand what is going on, and whether one does indeed discovered the QCD critical point or not.

XIII. SUMMARY AND DISCUSSION

A. Progress on the big questions

Before we go to summaries of the particular subjects, let me remind my list of “big questions” mentioned in the Introduction:

I. **Can one locate the “soft-to-hard” boundary**, where the transition from strong to weak coupling (perturbative) regimes take place?

II. **Can one locate the “micro-to-macro” boundary**, where the transition from single-participant to collective regime takes place?

III. **Can we experimentally identify signals of the QCD phase transition**, in particularly locate the QCD critical point?

Somewhat surprisingly, the sharpest observed transition which we discussed above is in the *profile of the pp elastic amplitude* shown in Fig.47(a). Although indirectly, rather sharp transition from black to gray is claimed to be related to the phase transition from the deconfined (gluonic) to confined (stringy) regimes of the Pomeron. At one hand, its sharpness is surprising because it is associated not with macroscopically large with quite small system – the Pomeron or a pair of strings. At the other, the analogy basically originates from the phase transition in gluodynamics (strings at early stage are considered excitable but not breakable, so no quarks yet), which is in fact a very strong first order transition.

Micro-to-macro transition in pA and pp collisions, as a function of multiplicity, is a debatable case. Data on the mean p_\perp and slopes shown in Fig.19 does indicate setting of the radial flow: but we know the radial flow can be “faked”. At the same time, the $v_2\{2\}$ as a function of multiplicity are rather flat. Its more-particle version $v_2\{n\}, n > 2$ are show rapid changes but better understanding of why it happens is still needed.

The theoretical justification of good agreement with hydro, inside the kinetics and/or hydrodynamics itself, is getting under control. A number of examples show rather effective cancellations of all higher-gradient corrections, leading to surprisingly accurate Navier-Stokes predictions, even in situations in which one hardly expected it to work.

The low energy scan at RHIC does show experimental evidences for “the softest point”. Yet attempts to locate the effects of the QCD critical point are intriguing but not yet fully successful. Dedicated measurements of event-by-event fluctuations at freezeout are already accurate

enough to put T, μ points on the phase diagram, but not yet good enough to discover/disprove the critical point.

B. Sounds

The first triumph of hydrodynamics, at the onset of RHIC program, was description of the “Little Bang” in great details: the radial and elliptic flows were obtained as a function of p_{\perp} , centrality, rapidity, particle type and collision energy. The second one, discussed above in detail, is even more spectacular description of higher azimuthal harmonics of the flow, with $m = 3 - 6$. As it has been repeatedly emphasized, those are basically sound harmonics, which should become even more obvious as m grows. The viscous damping of these modes actually agree with acoustic-inspired formulae very well.

Another phenomenon, well known for the Big Bang perturbations, is the “phase factor”. Common freezeout time for all flows does not imply the same phases, as their frequencies are m -dependent: and as the phases rotate one should see maxima/minima. The only experimental indication for that is enhancement of the triangular flow $m = 3$ over the damping curve, and even the elliptic one $m = 2$ for the ultra-central bin.

We emphasized that we only observed harmonics with $m < 7$ because the higher ones are damped too much by the freezeout time. Yet we are quite sure that at the initial time the Glauber model produced equally well harmonics up to $m = 20$ or so, and models like IP glasma predict harmonics by the hundreds. Perhaps one can invent other observable manifestations of those modes, such as Magneto-Sono-Luminescence process in which they are converted into electromagnetic signals.

The damping of harmonics with $m > 6$ is also an opportunity to observe the sources of sounds other than the initial state, in particular from inhomogeneities at the phase transition. (Those are important as seeds of the Big Bang acoustic cascade with possible observable production of the gravity waves).

Finally, even in equilibrium there must be fluctuations emitting sounds. Those in particular generate nontrivial “loop corrections” to hydrodynamics. Observation of “sound background” in hadronic matter is another challenge of the field.

C. The conflicting views of the initial state

Perhaps the most important conceptual controversy in the field remains the conflicting conclusions coming from weakly coupled and strongly coupled scenarios of the initial state and equilibration.

Significant progress in the theory of weakly coupled initial state is the adoption of the concept of *turbulent cascade*, with stationary and time-dependent self-similar solutions. Both classical glue simulation and gluon cascades came up with out-of-equilibrium attractors possess-

ing power spectra with certain indices, which are qualitatively different from the equilibrium. From practical perspective, these studies suggest that the stress tensor remains anisotropic for a long time. However more recent works indicate that nontrivial attractor solution is only approached if the coupling is unrealistically small.

Strongly coupled approaches, especially based on AdS/CFT and related models, view equilibration as a process dual to the *gravitational collapse* resulting in black hole production in the bulk. As soon as some trapped surface (a black hole) is there, the equilibration is very rapid: any kind of “debris” simply falls into it. Mathematically, the non-hydro modes have imaginary parts comparable to the real one, which numerically are quite large (50). So, in this scenario, equilibration is extremely rapid: there are no cascades or even gluon quasi-particles themselves, the only light propagating modes are sounds.

Whether the stress tensor remains anisotropic beyond the short initial period or not is still an open question. Theoretical efforts to combine hydrodynamics with out-of-equilibrium parameterization of the stress tensor were discussed above, and they will surely allow to model the situation at any realistic anisotropy. In order to decide which picture is correct one needs to think about experimental observables sensitive to the early stage. (My specific proposal – the dilepton polarization – has been discussed in section IX C.)

D. The smallest drops of sQGP

The major experimental discovery which came from the first years of LHC operation has been collective anisotropies in high multiplicity pA and pp collisions.

One point of view – admittedly advocated above – is that in those cases there are explosive QGP fireballs. While small then those produced in AA collisions, they are still “macroscopically large” and can be described hydrodynamically. Strong arguments for this are strong radial and elliptic flows in those systems.

The opposite point of view is that from the smallest to the highest multiplicity binds the pA and pp collisions produce microscopic systems which can be discussed dynamically, by the same models as used for minimally biased pp . The issue is reduced to “the shape of Pomeron” problem, and models based on pQCD (BFKL or color glass) or confining one (stringy Pomeron) need to be developed much further to see if such hopes are correct. High collectivity of angular anisotropies may still be a result of certain shape of the process. Experiments at RHIC with d and He^3 beams however disfavor such scenario, in my opinion.

Groups working on both scenarios now try to figure out the limits of their approaches, which is always a good thing. Inside hydrodynamics, for example, one study higher gradients and their effect. Inside the string-based picture we discussed a string-string interaction – ignored

for long time by event generators – leading to “spaghetti collapse” at certain density.

Meanwhile, phenomenologists describe the data. Hydrodynamical treatment of high multiplicity pA, pp events seem to be rather successful: but those require really small initial sizes and high temperatures of the fireball produced. But we do not really understand how such systems can be produced. In particular, the case of central pA collisions is contested between the IP-glasma model and a string-based initial state picture. So far one has very little theoretical control over the initial state of the high multiplicity pp : in anywhere glasma should be there. It is difficult to study it for statistical reasons, but since this is the highest density system we have by now, it should be pursued.

E. Heavy quarks and quarkonia

LHC data confirmed what has been already hinted by the RHIC data: significant fraction of the observed charmonia comes from *recombination* at the chemical freeze-out of charm quarks. The “surviving charmonia” fraction continue to be reduced. Such major change in charm quark behavior, from “heavy-like” to “light-quark-like” is clearly an important discovery.

Let me clarify this last statement. It remains true that c, b quarks are produced differently from the light ones, namely in the initial partonic processes. Yet their interaction with the ambient matter is strong. At large p_t we observe quenching $R_{AA}^{c,b}$ comparable to that of gluons/light quarks. At small p_t we observe an elliptic flow of open charm and changes in spectra.

Langevin/Fokker-Planck studies however suggest that c quarks are not moving with the flow. At early time c, b quarks are produced with large p_t and start decelerating, due to drag, while the matter is slowly accelerating due to pressure gradients: their velocities move toward each other, yet they do not match even by the end. As a result, charm radial/elliptic flows are *not* given by the Cooper-Fry expression. The recombinant charmonia are perhaps an exception: whether those actually co-move with the flow still needs to be established.

On the theory front, Langevin/Fokker-Planck studies has induced new conceptual developments. In particular, we discussed new set of solutions of those for charmonia, the quasi-equilibrium attractors with constant particle flux. Those states, not the original bound states like $J/\psi, \psi'$ etc, provide a convenient basis for evaluation of the speed of relaxation and out-of-equilibrium corrections to current charm hadronization models.

F. Jets

The theory of hard processes – jets, charm/bottom production – were based on factorization theorems and

a concept of structure functions. It is a solid foundation, but a very restrictive one. When one asks questions about say jets in high multiplicity bins of pp collisions, one soon realizes the “corresponding structure functions” do not exist: that concept has only been defined for the “untouched proton” in inclusive setting. Universal structure functions, measured rather than calculated, had served us since 1970’s, but now they cannot be used anymore. If certain fluctuation of a nucleon is selected, new models and measurements are needed.

Of course, there are practical limits: hard processes costs several orders of magnitude, and central pA costs also about factor 20-100 down the probability. Yet high LHC luminosity plus specialized triggers should be enough to get to some of those issues in the near future.

Jet quenching in central pA remains to be understood. Scaling arguments, like the ones we used for hydro in smaller-but-hotter systems, can and should be developed and confronted with data.

We argued above that in AA collisions jet quenching parameter \hat{q} seem to be strongly enhanced at the near- T_c region. Small systems evolution and freezeout is very different: this should play a role in jet quenching.

Acknowledgements. This paper is a summary from multiple conversations with colleagues, at seminars, workshops and conferences. They are too many to attempt to name them here (see long list of references below), but still I need to thank them for patiently teaching me about this or that idea or experimental findings. This work was supported in part by the U.S. Department of Energy, Office of Science, under Contract No. DE-FG-88ER40388.

Appendix A: Bjorken flow

The idea of rapidity-independent “scaling” distribution of secondaries originates from Feynman’s early discussion of the parton model, around 1970. The existence of rapidity-independent hydro solution was perhaps first noticed by Landau, who used rapidity variable in his classic paper, as a somewhat trivial case. The space-time picture connected with such scaling regime was discussed in refs [158, 159] before Bjorken’s famous paper [160] in which the solution was spelled out explicitly.

It is instructive first to describe it in the original Cartesian coordinates. There is no dependence on transverse coordinates x, y , only on time t and longitudinal coordinate z . The 1+1d equations $\partial_\mu T^{\mu\nu} = 0$ can be re-written in the following way

$$\frac{\partial}{\partial t}(s \cosh y) + \frac{\partial}{\partial z}(s \sinh y) = 0 \quad (\text{A1})$$

$$\frac{\partial}{\partial t}(T \sinh y) + \frac{\partial}{\partial z}(T \cosh y) = 0 \quad (\text{A2})$$

where $u_\mu = (\cosh(y), \sinh(y), 0, 0)$, and T, s are the temperature and the energy density. The first equation manifests the entropy conservation.

The central point is the 1-d-Hubble ansatz for the 4-velocity

$$u_\mu = (t, 0, 0, z)/\tau \quad (\text{A3})$$

where $\tau^2 = t^2 - z^2$ is the proper time. Note that all volume elements are expanded linearly with time and move along straight lines from the collision point. The spatial $\eta = \tanh^{-1}(z/t)$ and the momentum rapidities $y = \tanh^{-1}v$ are just equal to each other. Exactly as in the Big Bang, for each "observer" (the volume element) the picture is just the same, with the pressure from the left compensated by that from the right. The history is also the same for all volume elements, if it is expressed in its own proper time τ . Thus one has $s(\tau), T(\tau)$. Using this ansatz, the entropy conservation becomes an ordinary differential equation in proper time τ

$$\frac{ds(\tau)}{d\tau} + \frac{s}{\tau} = 0 \quad (\text{A4})$$

with an obvious solution

$$s = \frac{\text{const}}{\tau} \quad (\text{A5})$$

So far all dissipative phenomena were ignored. Including first dissipative terms into our equations one finds the following source for the entropy current

$$\frac{1}{\epsilon + p} \frac{d\epsilon}{d\tau} = \frac{1}{s} \frac{ds}{d\tau} = -\frac{1}{\tau} \left(1 - \frac{(4/3)\eta + \xi}{(\epsilon + p)\tau} \right) \quad (\text{A6})$$

with shear and bulk viscosities η, ξ , which tells us that one has to abandon ideal hydrodynamics at sufficiently early time.

Alternatively, one can start with curved coordinates τ, η from the beginning, and look for η -independent solution. Those are co-moving coordinates, in those $u_\mu = (1, 0, 0, 0)$ but the equations obtain extra term from Christoffel symbols.

Appendix B: Gubser flow

The Gubser flow [21, 68] is a solution which keeps the boost-invariance and the axial symmetry in the transverse plane of the Bjorken flow, but replaces the translational invariance in the transverse plane by symmetry under special conformal transformation. Therefore, one restriction is that the matter is required to be conformal, with the EOS $\epsilon = 3p$. Another is that the colliding systems has to be of a particular shape, corresponding to conformal map of the sphere onto the transverse plane.

The ideal hydro solution has three parameters: One is dimensional q , it defines the size of the system (and is

roughly corresponding to the radii of the colliding nuclei). The other two are dimensionless, f^* characterizes the number of degrees of freedom in the matter, and $\hat{\epsilon}_0$ the amount of entropy in the system.

The original setting uses the coordinates we used above, the proper time -spatial rapidity - transverse radius - azimuthal angle $(\bar{\tau}, \eta, \bar{r}, \phi)$ with the metric

$$ds^2 = -d\bar{\tau}^2 + \bar{\tau}^2 d\eta^2 + d\bar{r}^2 + \bar{r}^2 d\phi^2, \quad (\text{B1})$$

The dimensionless coordinates $\bar{\tau} = q\tau, \bar{r} = qr$ are rescaled versions of the actual coordinates.

Looking for solutions independent on both "angles" η, ϕ and using transverse rapidity

$$u_\mu = (-\cosh \kappa(\tau, r), 0, \sinh \kappa(\tau, r), 0) \quad (\text{B2})$$

Gubser obtained the following solution

$$v_\perp = \tanh \kappa(\tau, r) = \left(\frac{2q^2 \tau r}{1 + q^2 \tau^2 + q^2 r^2} \right) \quad (\text{B3})$$

$$\epsilon = \frac{\hat{\epsilon}_0 (2q)^{8/3}}{\tau^{4/3} (1 + 2q^2(\tau^2 + r^2) + q^4(\tau^2 - r^2)^2)^{4/3}} \quad (\text{B4})$$

where $\hat{\epsilon}_0$ is the second parameter. In [68] Gubser and Yarom re-derived the same solution by going into the co-moving frame. In order to do so they rescaled the metric

$$ds^2 = \tau^2 d\hat{s}^2 \quad (\text{B5})$$

and performed a coordinate transformation from the τ, r to a new set ρ, θ given by:

$$\sinh \rho = -\frac{1 - q^2 \tau^2 + q^2 r^2}{2q\tau} \quad (\text{B6})$$

$$\tan \theta = \frac{2qr}{1 + q^2 \tau^2 - q^2 r^2} \quad (\text{B7})$$

In the new coordinates the rescaled metric reads:

$$d\hat{s}^2 = -d\rho^2 + \cosh^2 \rho (d\theta^2 + \sin^2 \theta d\phi^2) + d\eta^2 \quad (\text{B8})$$

and we will use ρ as the "new time" coordinate and θ as a new "space" coordinate. In the new coordinates the fluid is at rest.

The relation between the velocity in Minkowski space in the (τ, r, ϕ, η) coordinates and the one in the rescaled metric in $(\rho, \theta, \phi, \eta)$ coordinates corresponds to:

$$u_\mu = \tau \frac{\partial \hat{x}^\nu}{\partial \hat{x}^\mu} \hat{u}_\nu, \quad (\text{B9})$$

while the energy density transforms as: $\epsilon = \tau^{-4} \hat{\epsilon}$.

The temperature (in the rescaled frame, $\hat{T} = \tau f_*^{1/4} T$, with $f_* = \epsilon/T^4 = 11$ as in [21]) is now dependent only on the new time ρ , in the case with nonzero viscosity the solution is

$$\hat{T} = \frac{\hat{T}_0}{(\cosh \rho)^{2/3}} + \frac{H_0 \sinh^3 \rho}{9(\cosh \rho)^{2/3}} {}_2F_1 \left(\frac{3}{2}, \frac{7}{6}; \frac{5}{2}, -\sinh^2 \rho \right) \quad (\text{B10})$$

where H_0 is a dimensionless constant made out of the shear viscosity and the temperature, $\eta = H_0 T^3$ and ${}_2F_1$ is the hypergeometric function. In the inviscid case the solution is just the first term of expression (B10), and of course it also conserves the entropy in this case. The picture of the explosion is obtained by transformation from this expression back to τ, r coordinates.

Small perturbations to the Gubser flow obey linearized equations which have also been derived in [68]. We start with the zero viscosity case, so that the background temperature (now to be called T_0) will be given by just the first term in (B10). The perturbations over the previous solution are defined by

$$\hat{T} = \hat{T}_0(1 + \delta) \quad (\text{B11})$$

$$u_\mu = u_{0\mu} + u_{1\mu} \quad (\text{B12})$$

with

$$\hat{u}_{0\mu} = (-1, 0, 0, 0) \quad (\text{B13})$$

$$\hat{u}_{1\mu} = (0, u_\theta(\rho, \theta, \phi), u_\phi(\rho, \theta, \phi), 0) \quad (\text{B14})$$

$$\delta = \delta(\rho, \theta, \phi) \quad (\text{B15})$$

Plugging expressions (B11),(B12) into the hydrodynamic equations and only keeping linear terms in the perturbation, one can get a system of coupled 1-st order differential equations. Furthermore, if one ignores the viscosity terms, one may exclude velocity and get the following (second order) closed equation for the temperature perturbation.

$$\frac{\partial^2 \delta}{\partial \rho^2} - \frac{1}{3 \cosh^2 \rho} \left(\frac{\partial^2 \delta}{\partial \theta^2} + \frac{1}{\tan \theta} \frac{\partial \delta}{\partial \theta} + \frac{1}{\sin^2 \theta} \frac{\partial^2 \delta}{\partial \phi^2} \right) + \frac{4}{3} \tanh \rho \frac{\partial \delta}{\partial \rho} = 0 \quad (\text{B16})$$

(Since the initial perturbations are assumed to be rapidity-independent, we also ignored this coordinate here.)

It has a number of remarkable properties: all 4 coordinates can be separated $\delta(\rho, \theta, \phi) = R(\rho)\Theta(\theta)\Phi(\phi)$ and a general solution is given by

$$\begin{aligned} R(\rho) &= \frac{C_1}{(\cosh \rho)^{2/3}} P_{-\frac{1}{2} + \frac{1}{6}\sqrt{12\lambda+1}}^{2/3}(\tanh \rho) \\ &\quad + \frac{C_2}{(\cosh \rho)^{2/3}} Q_{-\frac{1}{2} + \frac{1}{6}\sqrt{12\lambda+1}}^{2/3}(\tanh \rho) \\ \Theta(\theta) &= C_3 P_l^m(\cos \theta) + C_4 Q_l^m(\cos \theta) \\ \Phi(\phi) &= C_5 e^{im\phi} + C_6 e^{-im\phi} \end{aligned} \quad (\text{B17})$$

where $\lambda = l(l+1)$ and P and Q are associated Legendre polynomials. The part of the solution depending on θ and ϕ can be combined in order to form spherical harmonics $Y_{lm}(\theta, \phi)$, such that $\delta(\rho, \theta, \phi) \propto R_l(\rho)Y_{lm}(\theta, \phi)$. This property should have been anticipated, as one of the main ideas of Gubser has been to introduce a coordinate which together with ϕ make a map on a 2-d sphere.

Gubser setting was used as a theoretical laboratory ever since. A complete Green function has been constructed [36], leading to pictures of sound circles we discussed at the beginning of this review. Generalization to perturbations by the quenching jets, with the sounds propagating in the rapidity direction, was done in [49]. For the second order (the Israel-Stuart version) of the hydrodynamics in it has been done in [156, 157]. Recently the Boltzmann equation in tau-approximation has also been solved in it, see [53] discussed in section IV C.

There are also a number of phenomenological applications. Without going into those, let me just comment that those are limited by the fact that at large r the power tail of the solution is completely inadequate for heavy ion collisions. So to say, Gubser solution is like an explosion in atmosphere, while the real ones are in vacuum. As a result, in applications one basically has to amputate the unphysical regions.

-
- [1] E. V. Shuryak, Sov. Phys. JETP **47**, 212 (1978) [Zh. Eksp. Teor. Fiz. **74**, 408 (1978)].
 - [2] E. V. Shuryak, Phys. Rept. **61**, 71 (1980).
 - [3] D. J. Gross, R. D. Pisarski and L. G. Yaffe, Rev. Mod. Phys. **53**, 43 (1981).
 - [4] E. V. Shuryak, The QCD vacuum, hadrons and superdense matter (second edition, World scientific, 2004).
 - [5] T. Schafer and E. V. Shuryak, Rev. Mod. Phys. **70**, 323 (1998) [hep-ph/9610451].
 - [6] For recent extensive discussion of the topological solitons in gauge theory see talks at the workshop's webpage, <http://scgp.stonybrook.edu/archives/13417>
 - [7] For recent extensive discussion of the resurgence theory, transseries and solitons/saddle solutions see <http://scgp.stonybrook.edu/archives/10828>
 - [8] J. Liao and E. Shuryak, Phys. Rev. C **75**, 054907 (2007) [hep-ph/0611131].
 - [9] Y. Hidaka and R. D. Pisarski, Phys. Rev. D **78**, 071501 (2008) [arXiv:0803.0453 [hep-ph]].
 - [10] A. D'Alessandro, M. D'Elia and E. V. Shuryak, Phys. Rev. D **81**, 094501 (2010) [arXiv:1002.4161 [hep-lat]].
 - [11] J. Liao and E. Shuryak, Phys. Rev. Lett. **101**, 162302 (2008) [arXiv:0804.0255 [hep-ph]].
 - [12] C. Ratti and E. Shuryak, Phys. Rev. D **80**, 034004 (2009) [arXiv:0811.4174 [hep-ph]].
 - [13] J. Liao and E. Shuryak, Phys. Rev. D **82**, 094007 (2010) [arXiv:0804.4890 [hep-ph]].
 - [14] J. M. Maldacena, Int. J. Theor. Phys. **38**, 1113 (1999) [Adv. Theor. Math. Phys. **2**, 231 (1998)] [hep-th/9711200].
 - [15] M. Tannebaum, Nucl. Phys. A 931 (2014) c877, PHENIX Collab. S. S. Adler, et al., PRC 89, 044905 (2014)

- [16] D. Teaney, J. Lauret and E. V. Shuryak, Phys. Rev. Lett. **86**, 4783 (2001) [nucl-th/0011058].
- [17] D. Teaney, J. Lauret and E. V. Shuryak, nucl-th/0110037.
- [18] T. Hirano, U. W. Heinz, D. Kharzeev, R. Lacey and Y. Nara, Phys. Lett. B **636**, 299 (2006) [nucl-th/0511046].
- [19] J. P. Blaizot and J. Y. Ollitrault, Adv. Ser. Direct. High Energy Phys. **6**, 393 (1990).
- [20] D. Teaney, Phys. Rev. C **68**, 034913 (2003) [nucl-th/0301099].
- [21] S. S. Gubser, arXiv:1006.0006 [hep-th].
- [22] S. S. Gubser and A. Yarom, arXiv:1012.1314 [hep-th].
- [23] B. Schenke and R. Venugopalan, arXiv:1405.3605 [nucl-th].
- [24] Rajeev S. Bhalerao and Jean-Yves Ollitrault, Phys. Lett. B **641**, 260264 (2006), arXiv:nucl-th/0607009 [nucl-th].
- [25] J. B. Rose, J. F. Paquet, G. S. Denicol, M. Luzum, B. Schenke, S. Jeon and C. Gale, arXiv:1408.0024 [nucl-th].
- [26] Jan Fiete Grosse-Oetringhaus (ALICE), QM2014, Nucl. Phys. A **931**(2014) 22.
- [27] R. Granier de Cassagnac (CMS) Nucl. Phys. A **931** (2014) c22
- [28] B. A. Gelman, E. V. Shuryak and I. Zahed, Phys. Rev. C **74**, 044908 (2006) [nucl-th/0601029].
- [29] B. A. Gelman, E. V. Shuryak and I. Zahed, Phys. Rev. C **74**, 044909 (2006) [nucl-th/0605046].
- [30] G. Basar and D. Teaney, arXiv:1312.6770 [nucl-th].
- [31] D. Teaney and L. Yan, Phys. Rev. C **86**, 044908 (2012) [arXiv:1206.1905 [nucl-th]].
- [32] J. Jia (for the ATLAS Collaboration), arXiv:1107.1468.
- [33] K. Aamodt et al (ALICE Collaboration) arXiv:1105.3865, Phys. Rev. Lett. **107**, 032301 (2011)
- [34] U. Heinz and R. Snellings, Ann. Rev. Nucl. Part. Sci. **63**, 123 (2013) [arXiv:1301.2826 [nucl-th]].
- [35] R. A. Lacey, Y. Gu, X. Gong, D. Reynolds, N. N. Ajitanand, J. M. Alexander, A. Mwai and A. Taranenko, arXiv:1301.0165 [nucl-ex].
- [36] P. Staig and E. Shuryak, Phys. Rev. C **84**, 044912 (2011) [arXiv:1105.0676 [nucl-th]].
- [37] A. Andronic, P. Braun-Munzinger, K. Redlich and J. Stachel, PoS CPOD **07**, 044 (2007) [arXiv:0710.1851 [nucl-th]].
- [38] V. Khachatryan *et al.* [CMS Collaboration], arXiv:1410.1804 [nucl-ex].
- [39] T. Iritani, G. Cossu and S. Hashimoto, PoS LATTICE **2013**, 376 (2014) [arXiv:1311.0218 [hep-lat]].
- [40] P. Alba, W. Alberico, R. Bellwied, M. Bluhm, V. M. Sarti, M. Nahrgang and C. Ratti, arXiv:1403.4903 [hep-ph].
- [41] S. Chatrchyan *et al.* [CMS Collaboration], EPJC **74** (2014) 2847 [arXiv:1307.3442 [hep-ex]].
- [42] P. Bozek, Phys. Rev. C **85**, 014911
- [43] P. Bozek and W. Broniowski, Phys. Lett. B **739** (2014) 308
- [44] J.L. Nagle, A. Adare, S. Beckman, T. Koblesky, J. Orjuela Koop, D. McGlinchey, P. Romatschke, J. Carlson, J.E. Lynn, and M. McCumber, PRL **113**, 112301
- [45] V.E. Zakharov, V.S. Lvov, G. Falkovich, "Kolmogorov spectra of turbulence I. Wave turbulence.", Springer Verlag. ISBN 3-540-54533-6.
- [46] C. Young, J. I. Kapusta, C. Gale, S. Jeon and B. Schenke, arXiv:1407.1077 [nucl-th].
- [47] P. Staig and E. Shuryak, Phys. Rev. C **84**, 034908 (2011) [arXiv:1008.3139 [nucl-th]].
- [48] E. Shuryak and P. Staig, Phys. Rev. C **88**, no. 6, 064905 (2013) [arXiv:1306.2938 [nucl-th]].
- [49] E. Shuryak and P. Staig, Phys. Rev. C **88**, no. 5, 054903 (2013) [arXiv:1307.2568].
- [50] A. Mazeliauskas and D. Teaney, Phys. Rev. C **91**, no. 4, 044902 (2015) [arXiv:1501.03138 [nucl-th]].
- [51] M. Martinez and M. Strickland, Phys. Rev. C **81**, 024906 (2010) [arXiv:0909.0264 [hep-ph]].
- [52] W. Florkowski and R. Ryblewski, Phys. Rev. C **83**, 034907 (2011), 1007.0130.
- [53] G. S. Denicol, U. W. Heinz, M. Martinez, J. Noronha and M. Strickland, Phys. Rev. D **90**, no. 12, 125026 (2014) [arXiv:1408.7048 [hep-ph]].
- [54] M. Lublinsky and E. Shuryak, Phys. Rev. D **80**, 065026 (2009) [arXiv:0905.4069 [hep-ph]].
- [55] W. Florkowski, R. Ryblewski, NPA, **931** (2014) 343347
- [56] R. A. Janik and R. B. Peschanski, Phys. Rev. D **73**, 045013 (2006) [hep-th/0512162].
- [57] M. P. Heller, R. A. Janik and P. Witaszczyk, Phys. Rev. D **85**, 126002 (2012) [arXiv:1203.0755 [hep-th]].
- [58] H. Bebie, P. Gerber, J.L. Goity, H. Leutwyler. Nucl. Phys. B **378**:95-130, 1992
- [59] C. M. Hung and E. V. Shuryak, Phys. Rev. C **57**, 1891 (1998) [hep-ph/9709264].
- [60] V. Begun, W. Florkowski and M. Rybczynski, arXiv:1312.1487 [nucl-th].
- [61] D. Kharzeev, Y. V. Kovchegov and K. Tuchin, Phys. Lett. B **599**, 23 (2004) [hep-ph/0405045].
- [62] [ATLAS Collaboration], Measurement of the centrality dependence of the charged particle pseudorapidity distribution in proton-lead collisions ATLAS-CONF-2013-096 <https://cds.cern.ch/record/1599773>
- [63] J. D. Bjorken, S. J. Brodsky and A. Scharff Goldhaber, Phys. Lett. B **726**, 344 (2013) [arXiv:1308.1435 [hep-ph]].
- [64] G. R. Farrar and J. D. Allen, EPJ Web Conf. **53**, 07007 (2013) [arXiv:1307.2322 [hep-ph]].
- [65] T. Kalaydzhyan and E. Shuryak, arXiv:1407.3270 [hep-ph].
- [66] P. K. Kovtun and A. O. Starinets, Phys. Rev. D **72**, 086009 (2005) [hep-th/0506184].
- [67] P. M. Chesler and L. G. Yaffe, JHEP **1407**, 086 (2014) [arXiv:1309.1439 [hep-th]].
- [68] S. S. Gubser and A. Yarom, Nucl. Phys. B **846**, 469 (2011) [arXiv:1012.1314 [hep-th]].
- [69] P. Braun-Munzinger, J. Stachel and C. Wetterich, Phys. Lett. B **596**, 61 (2004) [nucl-th/0311005].
- [70] E. V. Shuryak, Phys. Lett. B **423**, 9 (1998) [hep-ph/9704456].
- [71] M. A. Stephanov, K. Rajagopal and E. V. Shuryak, Phys. Rev. D **60**, 114028 (1999) [hep-ph/9903292].
- [72] M. Lublinsky and E. Shuryak, Phys. Rev. C **84**, 061901 (2011) [arXiv:1108.3972 [hep-ph]].
- [73] T. Kalaydzhyan and E. Shuryak, arXiv:1402.7363 [hep-ph].
- [74] M. He, R. J. Fries and R. Rapp, Phys. Rev. C **86**, 014903 (2012) [arXiv:1106.6006 [nucl-th]].
- [75] E. Witten, Phys. Rev. D **30**, 272 (1984).
- [76] M. Hindmarsh, S. J. Huber, K. Rummukainen and D. J. Weir, Phys. Rev. Lett. **112**, 041301 (2014) [arXiv:1304.2433 [hep-ph]].
- [77] T. Kalaydzhyan and E. Shuryak, arXiv:1412.5147 [hep-

- ph].
- [78] L. D. McLerran and R. Venugopalan, Phys. Rev. D **49**, 3352 (1994) [hep-ph/9311205].
- [79] R. Baier, A. H. Mueller, D. Schiff and D. T. Son, Phys. Lett. B **502**, 51 (2001) [hep-ph/0009237].
- [80] T. Epelbaum, Nuclear Physics A 931 (2014) 337342
- [81] , J.Berges, B.Schenke, S.Schlichting , R.Venugopalan, Nuclear Physics A 931 (2014) 348353
- [82] T.Lappi, A.Dumitru and Y.Nara, Nuclear Physics A 931 (2014) c354
- [83] A. Kurkela and Y. Zhu, arXiv:1506.06647 [hep-ph].
- [84] E. V. Shuryak, Phys. Lett. B **78**, 150 (1978) [Sov. J. Nucl. Phys. **28**, 408 (1978)] [Yad. Fiz. **28**, 796 (1978)].
- [85] M. Chiu, T. K. Hemmick, V. Khachatryan, A. Leonidov, J. Liao and L. McLerran, Nucl. Phys. A **900**, 16 (2013) [arXiv:1202.3679 [nucl-th]].
- [86] E. V. Shuryak and L. Xiong, Phys. Rev. Lett. **70**, 2241 (1993) [hep-ph/9301218].
- [87] G. Basar, D. E. Kharzeev and E. V. Shuryak, arXiv:1402.2286 [hep-ph].
- [88] K. Tuchin, Phys. Rev. C **88**, 024911 (2013) [arXiv:1305.5806 [hep-ph]].
- [89] E. Shuryak, arXiv:1203.1012 [nucl-th].
- [90] E. Shuryak and I. Zahed, Phys. Rev. C **88**, no. 4, 044915 (2013) [arXiv:1301.4470 [hep-ph]].
- [91] T. Kalaydzhyan and E. Shuryak, arXiv:1404.1888 [hep-ph].
- [92] Collective string interactions in AdS/QCD models and high multiplicity pA collisions, I.Iatrakis, A.Ramamurti and E.Shuryak, in progress
- [93] P. A. R. Ade *et al.* [Planck Collaboration], arXiv:1303.5075 [astro-ph.CO].
- [94] S. Floerchinger and U. A. Wiedemann, JHEP **1111**, 100 (2011) [arXiv:1108.5535 [nucl-th]].
- [95] L. P. Csernai, F. Becattini and D. J. Wang, J. Phys. Conf. Ser. **509**, 012054 (2014).
- [96] P. Kovtun, J. Phys. A **45**, 473001 (2012) [arXiv:1205.5040 [hep-th]].
- [97] P. Kovtun, G. D. Moore and P. Romatschke, Phys. Rev. D **84**, 025006 (2011) [arXiv:1104.1586 [hep-ph]].
- [98] L. D. Landau, Izv. Akad. Nauk Ser. Fiz. **17**, 51 (1953).
- [99] E. V. Shuryak and O. V. Zhirov, Phys. Lett. B **89**, 253 (1979).
- [100] T. C. Brooks *et al.* [MiniMax Collaboration], (Private communication via J.D.Bjorken)
- [101] V. Khachatryan *et al.* [CMS Collaboration], JHEP **1009**, 091 (2010) [arXiv:1009.4122 [hep-ex]].
- [102] S. Chatrchyan *et al.* [CMS Collaboration], Phys. Lett. B **718**, 795 (2013) [arXiv:1210.5482 [nucl-ex]].
- [103] S. Chatrchyan *et al.* [CMS Collaboration], Eur. Phys. J. C **72**, 2164 (2012) [arXiv:1207.4724 [hep-ex]].
- [104] B. Abelev *et al.* [ALICE Collaboration], Phys. Lett. B **719**, 29 (2013) [arXiv:1212.2001 [nucl-ex]].
- [105] A. Adare *et al.* [PHENIX Collaboration], Phys. Rev. Lett. **111**, 212301 (2013) [arXiv:1303.1794 [nucl-ex]].
- [106] G. Goldhaber, S. Goldhaber, W. Y. Lee and A. Pais, Phys. Rev. **120**, 300 (1960).
- [107] G. I. Kopylov and M. I. Podgoretsky, Sov. J. Nucl. Phys. **18**, 336 (1974) [Yad. Fiz. **18**, 656 (1973)].
- [108] E. V. Shuryak, Yad. Fiz. **18**, 1302 (1973).
- [109] S. Pratt, Phys. Rev. Lett. **102**, 232301 (2009) [arXiv:0811.3363 [nucl-th]].
- [110] A. N. Makhlin and Y. M. Sinyukov, Z. Phys. C **39**, 69 (1988).
- [111] P. Bozek, arXiv:1408.1264 [nucl-th].
- [112] K. Aamodt *et al.* [ALICE Collaboration], Phys. Rev. D **84**, 112004 (2011) [arXiv:1101.3665 [hep-ex]].
- [113] Y.Hirono and E.Shuryak, Femtoscopic signature of strong radial flow in high-multiplicity pp collisions, in progress
- [114] E. Shuryak, S. J. Sin and I. Zahed, J. Korean Phys. Soc. **50**, 384 (2007) [hep-th/0511199].
- [115] T. Matsui and H. Satz, Phys. Lett. B **178**, 416 (1986).
- [116] N. Brambilla, M. A. Escobedo, J. Ghiglieri and A. Vairo, JHEP **1305**, 130 (2013) [arXiv:1303.6097 [hep-ph]].
- [117] A. Mocsy, P. Petreczky and M. Strickland, Int. J. Mod. Phys. A **28**, 1340012 (2013) [arXiv:1302.2180 [hep-ph]].
- [118] O. Kaczmarek and F. Zantow, PoS LAT **2005**, 192 (2006) [hep-lat/0510094].
- [119] D. E. Kharzeev, Phys. Rev. D **90**, 074007 (2014) [arXiv:1409.2496 [hep-ph]].
- [120] C. Young and E. Shuryak, Phys. Rev. C **79**, 034907 (2009) [arXiv:0803.2866 [nucl-th]].
- [121] P. Romatschke, arXiv:1504.02529 [nucl-th].
- [122] J. Liao and E. Shuryak, Phys. Rev. D **82**, 094007 (2010) [arXiv:0804.4890 [hep-ph]].
- [123] J. -P. Blaizot, Y. Mehtar-Tani and M. A. C. Torres, arXiv:1407.0326 [hep-ph].
- [124] E. V. Shuryak, Phys. Rev. C **66**, 027902 (2002) [nucl-th/0112042].
- [125] J. Liao and E. Shuryak, Phys. Rev. Lett. **102**, 202302 (2009) [arXiv:0810.4116 [nucl-th]].
- [126] X. Zhang and J. Liao, arXiv:1311.5463 [nucl-th].
- [127] J. Xu, J. Liao and M. Gyulassy, arXiv:1508.00552 [hep-ph].
- [128] E. Shuryak, Phys. Rev. C **86**, 024907 (2012) [arXiv:1203.6614 [hep-ph]].
- [129] S. Lin and E. Shuryak, Phys. Rev. D **78**, 125018 (2008) [arXiv:0808.0910 [hep-th]].
- [130] V. Balasubramanian, A. Bernamonti, J. de Boer, N. Copland, B. Craps, E. Keski-Vakkuri, B. Muller and A. Schafer *et al.*, Phys. Rev. D **84**, 026010 (2011) [arXiv:1103.2683 [hep-th]].
- [131] S. Lin and E. Shuryak, Phys. Rev. D **77**, 085013 (2008) [hep-ph/0610168].
- [132] S. Lin and E. Shuryak, Phys. Rev. D **77**, 085014 (2008) [arXiv:0711.0736 [hep-th]].
- [133] S. S. Gubser, S. S. Pufu and A. Yarom, Phys. Rev. D **78**, 066014 (2008) [arXiv:0805.1551 [hep-th]].
- [134] S. Lin and E. Shuryak, Phys. Rev. D **79**, 124015 (2009) [arXiv:0902.1508 [hep-th]].
- [135] S. S. Gubser, S. S. Pufu and A. Yarom, JHEP **0911**, 050 (2009) [arXiv:0902.4062 [hep-th]].
- [136] S. Lin and E. Shuryak, Phys. Rev. D **83**, 045025 (2011) [arXiv:1011.1918 [hep-th]].
- [137] U. Gursoy and E. Kiritsis, JHEP **0802**, 032 (2008) [arXiv:0707.1324 [hep-th]].
- [138] U. Gursoy, E. Kiritsis and F. Nitti, JHEP **0802**, 019 (2008) [arXiv:0707.1349 [hep-th]].
- [139] D. Aren, I. Iatrakis, M. Jrvinen and E. Kiritsis, JHEP **1311**, 068 (2013) [arXiv:1309.2286 [hep-ph]].
- [140] Ioannis Iatrakis, Adith Ramamurti and Edward Shuryak, QCD strings and their interaction in the AdS/QCD, in progress
- [141] E. A. Kuraev, L. N. Lipatov and V. S. Fadin, Sov. Phys. JETP **45**, 199 (1978) Ya. Ya. Balitsky and L. N. Lipatov, Sov. J. Nucl. Phys. **28**, 22 (1978)
- [142] A. Stoffers and I. Zahed, Phys. Rev. D **87**, 075023

- (2013) [arXiv:1205.3223 [hep-ph]].
- [143] G. Basar, D. E. Kharzeev, H. U. Yee and I. Zahed, *Phys. Rev. D* **85**, 105005 (2012) [arXiv:1202.0831 [hep-th]].
- [144] E. Shuryak and I. Zahed, *Phys. Rev. D* **89**, 094001 (2014) [arXiv:1311.0836 [hep-ph]].
- [145] B. Svetitsky, *Phys. Rev. D* **37**, 2484 (1988)
- [146] G. D. Moore and D. Teaney, *Phys. Rev. C* **71**, 064904 (2005) [hep-ph/0412346].
- [147] M. Strickland, arXiv:1410.5786 [nucl-th].
- [148] J. Xu, J. Liao and M. Gyulassy, arXiv:1508.00552 [hep-ph].
- [149] A. Andronic, *Nucl. Phys. A* **931** (2014) c135.
- [150] A. Beraudo, *Nucl. Phys. A* **931** (2014) c145.
- [151] R. J. Fries, B. Muller, C. Nonaka and S. A. Bass, *Phys. Rev. C* **68**, 044902 (2003) [nucl-th/0306027].
- [152] M. A. Stephanov, *Phys. Rev. Lett.* **102**, 032301 (2009) [arXiv:0809.3450 [hep-ph]].
- [153] R. Rapp and E. V. Shuryak, nucl-th/0202059.
- [154] Y. Qian and I. Zahed, arXiv:1411.3653 [hep-ph].
- [155] C. Loizides [ALICE collaboration], talk at The 2nd International Conference on the initial stages..., Napa, Dec. 2014
- [156] H. Marrochio, J. Noronha, G. S. Denicol, M. Luzum, S. Jeon and C. Gale, *Phys. Rev. C* **91**, no. 1, 014903 (2015) [arXiv:1307.6130 [nucl-th]].
- [157] L. G. Pang, Y. Hatta, X. N. Wang and B. W. Xiao, *Phys. Rev. D* **91**, no. 7, 074027 (2015) [arXiv:1411.7767 [hep-ph]].
- [158] C. B. Chin, E. C. G. Sudarshan and K. H. Wang, *Phys. Rev* **012**(1975)902
- [159] M. I. Gorenstein, V. A. Zhdanov and Yu. M. Sinjukov, *ZhETF* **74**(1978)833
- [160] J. Bjorken, *Phys. Rev. D* **27**(1983)140
- [161] P. Danielewicz, M. Gyulassy, *Phys. Rev. D* **31**:53-62, 1985
- [162] A certain anisotropy of the momentum distribution in hydro cells is created by the viscosity. Since QGP is a very good liquid with small viscosity it is a quite small effect, and its effect on the observed v_2 has the opposite sign. Let me also remind that all calculations in early 1990's were originally done at zero viscosity, and yet they predicted v_2 very well.
- [163] Note that we use not gravitational but particle physics units, in which $c=1$ but the Newton constant $G_N = 1/M_p^2$.
- [164] Even ϵ_2 is the same as others, as we now for simplicity focus on central collisions. Note further that of one select the so called super-central collisions, like below 0.1 or 0.01%, larger multiplicity relates to larger N and all v_n do decrease as $O(N^{-1/2})$.
- [165] Dividing the cost of LHC, $\sim 10^{10}$ \$ by the number of recorded pp events $\sim 10^{10}$ one finds that they cost about a dollar each. These high multiplicity pp events we speak about thus cost about a million dollar each, and one needs thousands of them to report a correlation function!
- [166] Like wave functions of the α -decaying nuclei, when energy is complex the wave function grows in space and is not normalizable— thus the name. Physicists called them quasistationary states.
- [167] Up to a timescale issue, which potential to use, F or V or their combination?